PHOTO-DEGRADATION OF CAFFEINE IN AQUEOUS SYSTEM USING HETEROGENEOUS MIXED OXIDE CATALYSTS

by

VUYOLWETHU OWETHU NDABANKULU

Submitted in fulfillment of the academic requirements for the degree of
Master of Science in the Chemistry, School of Chemistry & Physics
College of Agriculture, Engineering and Science
University of KwaZulu-Natal
Durban

May 2017

As the candidate's supervisor, I have approved this dissertation for submission

Supervisor: **Prof. Sreekantha B. Jonnalagadda**

Signed:..... Date: .....

ABSTRACT

The presence of undesirable organics in water systems and air is one of the biggest problems in the world. Pharmaceutical compounds (PC) are a class of organic contaminates that have been widely detected in water systems all over the world. Wastewater treatment plants are not designed to remediate all the organic substances. As a result, residual levels of these substances are detected even after treatment. PC have been found in surface water, ground water and drinking water at low concentrations ranging in the ppb levels. The application of advanced oxidation processes (AOPs) a combination of two or more oxidation techniques is one of the approaches availed in resolving this problem and use catalyst to accelerate the efficacy of an oxidising species is one of the AOPs.

In this work four lanthanides (La) (cerium, dysprosium, lutetium, and samarium) with different loadings (0.1, 0.5, 1.0 wt %) were doped in TiO_2 using a sol gel method in order to synthesise mesoporous lanthanide doped TiO_2 compounds. Synthesis of the materials was done in room temperature. Titania precursor was used as a starting material and also for each lanthanide, metal precursor was used. The prepared materials were then characterized using different analytical and spectroscopic techniques. Scanning electron microscope (SEM) and High resolution transmission electron microscope (HRTEM) were used to investigate the surface morphology and particle nature. Quantitative analysis of the metal dopants was performed with (SEM-EDX). The crystalline nature of the materials was evaluated using powder X-ray diffraction (PXRD). Structural changes of the as prepared TiO_2 material were examined by using Raman spectroscopy. Photoluminescence (PL) was used in determining the effectiveness of charge transfer, migration, and trapping of charge carriers. To investigate photon absorption and band gap energy, ultra-valet / Visible diffused reflectance (UV-Vis DRS) was used. The textural properties were investigated using Nitrogen sorption-desorption analysis and the BET surface area was obtained. Fourier Transmission Infrared (FTIR) spectroscopy was used to identify the presence of functional groups in a catalyst. All the characterization of the prepared materials was compared to that of the commercial catalyst (Degussa P25) anatase TiO_2.

The activity of the catalysts was tested in degradation of chosen pharmaceutical (caffeine) in presence of ozone and under visible light irradiation conditions. The effect of pH of the solution on the degradation on pollutant in presence of an external oxidant (Ozone) was investigated in presence of catalysts. Degradation products were determined with liquid chromatograph-mass spectroscopy (LC-MS).

In a typical experiment, photo-catalytic experiments were carried out in a simple open quartz reactor under visible light irradiation. A double beam UV-VIS spectrophotometer was used to monitor degradation and LC-MS was used to identify degradation intermediates and products. Photocatalysed ozonation experiments showed higher degradation efficiency compared to photocatalytic experiments in absence of ozone. The dose of ozone played a vital role as it enhanced the generation of OH radicals.

Keywords: Photocatalysis, Nanomaterials, Reactive species, Photocatalytic ozonation, Organic pollutants, pH, Surfactant concentration, Dopants, Sol-gel method.

DECLARATIONS

DECLARATION 1 - PLAGIARISM

I, **Vuyolwethu Owethu Ndabankulu,** declare that

1. The research reported in this dissertation, except where otherwise indicated is my original research.
2. This dissertation has not been submitted for any degree or examination at any other university.
3. This dissertation does not contain other person's data, pictures, graphs, or other information, unless specifically acknowledged as being sourced from other persons.
4. This dissertation does not contain other persons writing, unless specifically acknowledged as being sourced from other researchers. Where other written sources have been quoted, then:
    a. Their words have been re-written but the general information attributed to them has been referenced
    b. Where their exact words have been used, then their writing has been placed in italics and inside quotation marks, and referenced.
5. This dissertation does not contain text, graphics or tables copied and pasted from the Internet, unless specifically acknowledged, and the source being detailed in the thesis and in the References sections.

Signed: .....

CONFERENCE PARTICIPATION

1. Ndabankulu V.O, Maddila S, Jonnalagadda S.B. "Photocatalytic degradation of caffeine using visible light and TiO_2 – doped with Ce". (Oral presentation at the **42nd National Convention of the South African Chemical Institute Conference** 29 Nov. - 4th December, 2015 at ***Elangeni Hotel, Durban***.

2. Ndabankulu V.O, Jonnalagadda S.B. "Synthesis and characterization of lanthanide doped TiO2- nanoparticles and their photocatalytic activity under visible light (Poster presentation at the **College of Agriculture, Engineering and Science Research** day, 29th November 2016, ***Howard college Campus, UKZN***.

ACKNOWLEDGEMENTS

I would like to thank almighty Lord and savior Jesus Christ for his love, grace protection and his faithfulness in my life and academics. My great appreciation go to my kind supervisor Prof. S.B Jonnalagadda for his guidance, patience, understanding and encouragement through the cause of my studies. I am thankful to him for providing me with funding throughout my study from his NRF grant holder bursary. My sincere gratitude goes to the School of Chemistry and Physics, College of Agriculture Engineering and Science, University of KwaZulu-Natal, and staff for providing an enabling environment to carry out my research.

To my parents (Mr. B.P. Ndabankulu and Mrs. N.G Ndabankulu) and my awesome siblings (Sibusisiwe, Nosakhiwo, Momelezi, Sekelwa, Odwa and Mfezeko), I would like to express my heart felt appreciation for the love, encouragement, and moral support, you have given me.

I would like to thank my friends and colleagues, from the entire Physchem research group, Nokubonga, Nhlanhla, Sebenzile, Surya, Ekemena, Bhekumuzi, Darrel for your wise advice and words of support.

To my dear friends, Siphesihle, Sinqobile, Sboniso, Ngcebo, Sfiso, Nyameka, Denis, I thank God for bringing you into my life. I am thankful for the love and emotional support that they provided, giving me the courage to carry on, when my energy was down.

Exceptional and unreserved gratitude to Dr. Suresh Maddila, for everything that he has taught me, for his patience, understanding and emotional support, for which I am truly grateful.

List of abbreviations

Abbreviation	Full Name
AOPs	Advanced oxidation processes
BET	Brunauer-Emmett-Teller theory
FT-IR	Fourier transform infrared spectroscopy
HPLC	High performance liquid chromatography
HRTEM	High resolution transmission electron microscope
LC-MS	Liquid chromatography-Mass spectroscopy
Min	Minutes
nm	Nanometres
PL	Photoluminescence
PZC	Point of zero charge
Raman	Raman spectroscopy
SEM	Scanning electron microscope
TEM	Transmission electron microscope
TIP	Titanium (IV) isopropoxide
UV	Ultraviolet
UVDRS	UV-Vis diffused reflectance spectroscopy
UV/Vis spectroscopy	Ultraviolet-visible light spectroscopy
WWTP	Wastewater treatment plant
Wt%	Weight percentage

XRD	X-ray diffraction pattern

Table of Contents

CHAPTER ONE

Introduction

1 Background

Pharmaceuticals are the chemical substances used in treating, preventing and curing diseases. Pharmaceuticals (PC) are biologically active compounds designed to interact with specific pathways and processes in humans and animals. Some of PCs properties include, hydrophilic, high polarity, low volatility and highly stable, this ensures that they can remain in the human system for a prolonged period [1, 2]. These substances have helped and enabled a prolonged life of humans and animals. Thousands of PC are produced worldwide and their purpose is to improve health and hygiene of humans. Because of their abundance, pharmaceuticals, illicit drugs and veterinary medicines are increasingly recognised as ubiquitous contaminants in freshwater ecosystems. They belong in the class of micro organic pollutants known as emerging contaminants. This class also includes surfactants, plasticizers, herbicides, and personal care products (PPC) [3-6]. They are characterised by their stability these substances are excreted unchanged, conjugated with other inactivating compounds or as a mixture of metabolites, which then make their way into wastewater treatment plants, ground water and surface water [7-9].

Pharmaceutically active compounds such as ibuprofen, caffeine, ketoprofen and propoxyphene, anti-depressants (fluoxetine paroxetine and sertraline), antibiotics (amoxicillin, azithromycin, penicillin and, and hormones) are widely used. Other most commonly consumed human pharmaceuticals are anti-inflammatory drugs / analgesics, antibiotics, lipid regulators, beta blockers, steroids and related hormones. They were first detected in the environment in the 1960s and the potential risk was first raised in 1999 [10-12]. Initially, although they were noticed, there was little or no toxicological studies carried for both humans and other living organisms.

The increasing growth in the world's population has led to a rapid increase in the number of infection cases reported. Due to this increase in the population the application and use of pharmaceuticals has also increased. The continuous use of these substances is associated with contamination of water either through the sewage systems or through runoff from treatment plants. It is because of this reason that there is a rise in level of these compounds in the environment and especially in fresh water supply. Wastewater treatment plants (WWTPs) are not equipped to treat these types of contaminants. Thus, many of PC occur at different concentrations in the environment, where they may exert ecotoxicological effects even at

relatively low concentrations [13-16]. While most pharmaceuticals are relatively soluble in water and non-bioaccumulative, the continuous release of PC into the environment downstream of WWTPs, resident biota can be chronically exposed [17, 18]. Hence, the scientific public has made efforts to increase the studies concerning human and aquatic risk assessment associated with pharmaceuticals in the environment.

There is limited data and minimal understanding of the environmental occurrence, fate, transport, and exposure of PC and their metabolites. This is despite their abundant usage. Lack of suitable analytical method for detection of such compounds in very low concentrations and their complex environmental matrix. Because there is a continuous introduction of these substances in the environment, even those compounds that have low persistence can cause adverse effect [19, 20]. Understanding the fate of PC and their metabolites in the environment is one the crucial tasks that faces many environmental scientists currently. By understanding the mechanism with which such compounds interact with the biotic systems one can comprehend the problems that are associated with the presence of such substances in the aquatic systems.

1.1 Pharmaceuticals in the environment

In the past levels of PCs in the environment were insignificant, this was up until 1990s. It was considered because they are produced and used in small quantities; the release of active products into the environment was expected to be very small. PCs are designed to target a metabolic or molecular pathway, when they enter the environment they may exert similar or comparable pathways to the aquatic organisms such as vertebrate and invertebrates [21-24]. Some if not most pharmaceuticals present threats for aquatic organism and microorganisms. In the past few years, there has been an increase in the studies of the occurrences of emerging contaminants in the coastal areas and in the marine environment. Pharmaceuticals may reach the aquatic environment through different pathways i.e. from domestic wastewater from urban areas, effluent from pharmaceutical manufacturing industries, hospital disposal, and the disposal of unused medicine [25]. As already mentioned above, many of these compounds are disposed without being metabolised this means that biologically active forms are mixed with water bodies. Like most of organic pollutants, pharmaceuticals are known to bioaccumulate in the living organisms. Food chain in the aquatic environment is affected even at relatively low concentration of PC since they accumulate [26]. One of the most concerning things about pharmaceutic is that they are created such that they interact with known biological targets with a specific mode of action. They highly interact with biological systems and are resistant to

inactivation before leaving the intended target function. Flow-driven transport processes like advection and dispersion, drive the concentration of PCs in water systems. The degradation and photolysis, partitioning to the sediments, uptake by biota, biological entities, volatilisation or transformation through other biotic mechanisms such as hydrolysis are also important. Environmental pH plays a role, since these compounds tend to bio-accumulate in non-ionised medium.

Emission of pharmaceuticals into the environment may sometimes depend on the wastewater treatment process, the content or usage pattern which varies from region to region, and it may depend on the flow of the waste stream [27]. Upon entering the water systems, PC and their metabolites become potential hazard to aquatic organisms and human beings even at low levels in the environment. Some adverse effects to aquatic organisms include feminisation of male fish, impairment of gills, and livers in fish, decrease in plankton diversity and development of pathogenic resistance and inflammatory reaction in liver; especially when exposed to diclofenac [28, 29].

Pharmaceuticals are used by humans and animals for medical purposes, when evaluated individually, PC show no significant toxicity to living organisms, but some have demonstrated to inhabit growth of aquatic organisms such as algae. Diclofenac was reported to be the reason behind the decline in the vulture population in Pakistan. Some reports have shown that diclofenac, carbamazepine and metoprolol show chronic and cytological effect in fish (*oncorhynch mykiss* and *cyprinus carpio*)[30]. Shin et al. performed an experiment aimed to determine the toxicity of hospital pharmaceutical exposure to four aquatic organisms (two vertebrates and two invertebrates). They reported that no significant toxicity response was observed from (*D.magna*) but a high acute toxicity was for two vertebrates (*C. Carpio and P.Paria*) and *Nidenticulate*. They further tested the synergistic effect of PC in water systems, they exposed 19 different pharmaceuticals to these organisms individually, and observed that nothing happened to the organisms. However, when all 19 PCs were combined, all organisms were killed. This proved that there is a synergistic effect of PC in water and their interactions with aquatic organisms.

2 Advanced oxidation processes

In the past decades, extensive research has been conducted to address the problem of degradation of non-biodegradable and refractory compounds. Advanced oxidation processes (AOPs), a combination of two or more oxidation techniques have attracted significant attention in wastewater treatment systems. They mostly operate at ambient temperature and pressure, which is cost effective [31, 32]. AOPs are preferred over the use chemical oxidation processes,

which are based on the use of chlorine, hydrogen peroxide or ozone. Chemical oxidation processes have low oxidation potential compared to AOPs and cannot completely degrade and mineralize all types of organic pollutants. AOPs can mineralize refractory organic pollutants without the risk of generating secondary toxic pollutants with better efficiency [33]. AOPs are characterized by *in-situ* production of highly reactive hydroxy radicals (•OH). This has proven to be highly advantageous compared to chemical oxidation processes because the generated hydroxyl radicals are non-selective, which give good degradation and mineralization efficiency. Hydroxyl radicals are classified as of the most powerful oxidants with high reactive potential in the table. Hydroxyl radicals re characterized by extracting hydrogen atoms from a saturated hydrocarbon chain and an electrophilic addition to unsaturated bond such as aromatic hydrocarbons. Hydroxyl radicals attack regions with high electron density, which leads to its addition to an unsaturated bond of aromatic compounds.

2.1 Types of AOPs

In AOPs, hydroxyl radicals are generated by coupling chemical and/ physical systems such as, Fenton system, (H_2O_2 / Fe^{2+} or Fe^{3+}), H_2O_2 / catalyst, H_2O_2 / O_3 (peroxone). All these processes are associated with application of radiation (light) i.e. UV-irradiation, vacuum-UV irradiation, ultrasound, or pulse radiolysis, hydrodynamic induced cavitation [34].

2.2 Photo-catalysis

Heterogeneous catalysis aided with metal oxide has attracted a lot of attention in wastewater treatment applications due to their effectiveness in degradation of organic substances [35, 36]. Photocatalysis permits the use of visible light for degradation of highly toxic and dangerous organic molecules in the environment; it is also used in the production of hydrogen and solar energy into electrical power [37-40]. Some of the metal oxides used in these catalysts are semiconductors, which are UV/ visible light assisted catalysts. Unlike metals, which have filled electronic state, semiconductors have a region that exist between the filled valence band and an empty conducting band, this region is called the band gap. Heterogeneous photocatalysis is a system where photochemical reaction occurs on the surface of the catalyst. It can be divided into two categories, depending on the initial excitation process. If the initial excitation takes place on the adsorbent molecule, the interaction with the catalyst is in the ground state and this type is called catalysed photoreaction. Whereas if the process is reversed and the initial excitation occurs on the catalyst and transfers an excited electron into a ground state molecule then the process is called sensitised photoreaction [41-45]. This is one of the most researched topics currently; this is due to its major applications which lead to self-

cleaning surface and generation of hydrogen using green energy such as sunlight[46]. The process leads to redox reactions until finally the overall degradation of the organic substance.

This process occurs through interaction of organic substance with photo-generated electron, hole or by interaction with reactive oxygen species or $[OH]^-$ radicals [47-49]. Photo-catalysis play a very big role in conversion of solar energy into chemical fuel, electricity and decomposition of organic pollutants. It is understood that all the reaction occurs on the surface of the semiconductor. Photocatalysis occurs in three basic steps, (1) first is the absorption of the incident light by the semiconductor, if the absorbed light is larger than the bandgap of the material it can excite the electrons from the valence band (VB) into conducting band (CB) and thereby generating an electron hole. (2) This then leads to the release of photon or heat, which is due to the recombination of the photo-generated electrons and holes. Sometimes there is also a possibility of the migration of the photo-generated holes to move into the surface of the semiconductor. (3) The third step is the reduction reaction between the photo-generated electron and the organic species. This happens on the surface of the semiconductor, holes then generate strong oxidising species like OH radicals [50-53]. The valence band is composed of the 2p orbitals of oxygen hybridized with the 3d orbitals of titanium, while the conduction band is only the 3d orbitals of titanium. Molecular oxygen scavenges the photo-generated electron (e^-) from the surface of catalyst to form superoxide (O_2^-) this occurs because the conducting bend of TiO_2 is of similar energy as reduction potential of O_2 [47, 54].

$$\text{Metal oxide} + h\nu \rightarrow \text{metal oxide}\ (h^+_{VB} + e^-_{CB}) \quad (1)$$

$$h^+_{VB} + H_2O \rightarrow H^+ + OH^\bullet \quad (2)$$

$$h^+_{VB} + OH^- \rightarrow OH^\bullet \quad (3)$$

$$e^-_{CB} + O_2 \rightarrow O^{2-} \quad (4)$$

Figure.1 shows photo-generation of oxidising species in a process that takes place on the surface of the photocatalytic semiconductor TiO_2 under light illumination, where HO_2^- is the hydroperoxide radical that is formed, when a proton reacts with the superoxide radical [55].

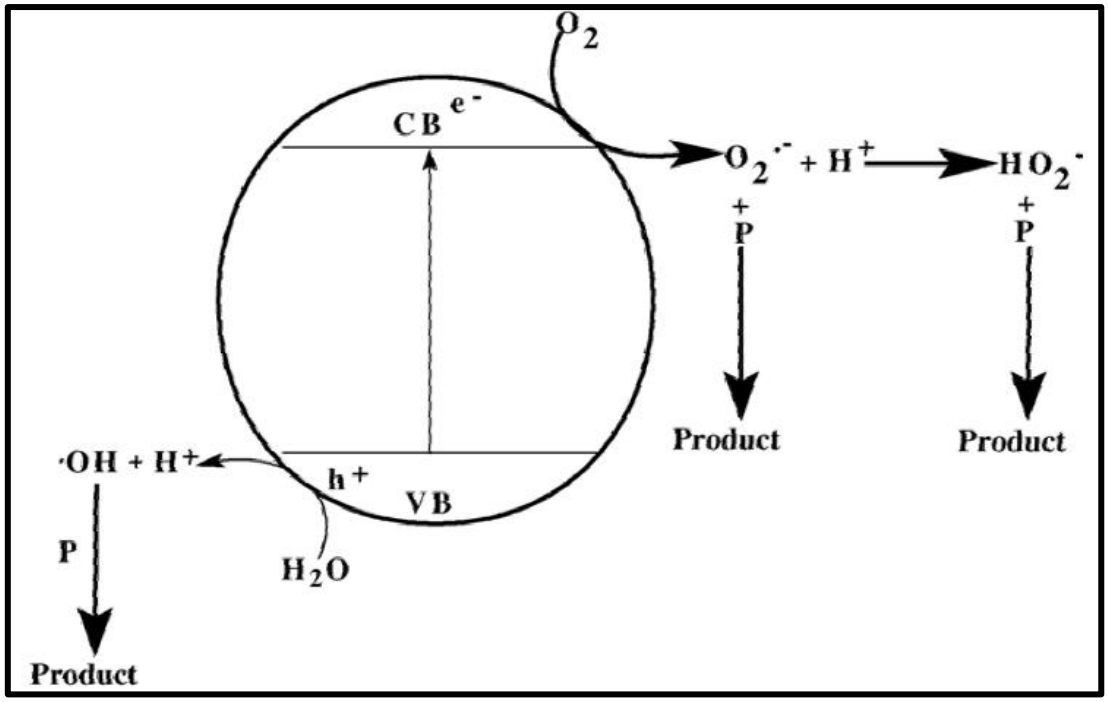

Figure 1: photocatalytic oxidation of organic pollutant using TiO_2 under light [57]

However, it is always worthwhile to look at molecule that is adsorbed energy level rather only looking at the redox potential of the photocatalyst to establish if hole generation or electron transfer will be possible in the given situation. Nano-size semiconductors have been found to have a very wide range of applications from commercial and technological applications including optical, environmental and electronics [56-58]. **Figure.2** shows the schematic process that occur during the photocatalytic process under the interaction of light in time scale.

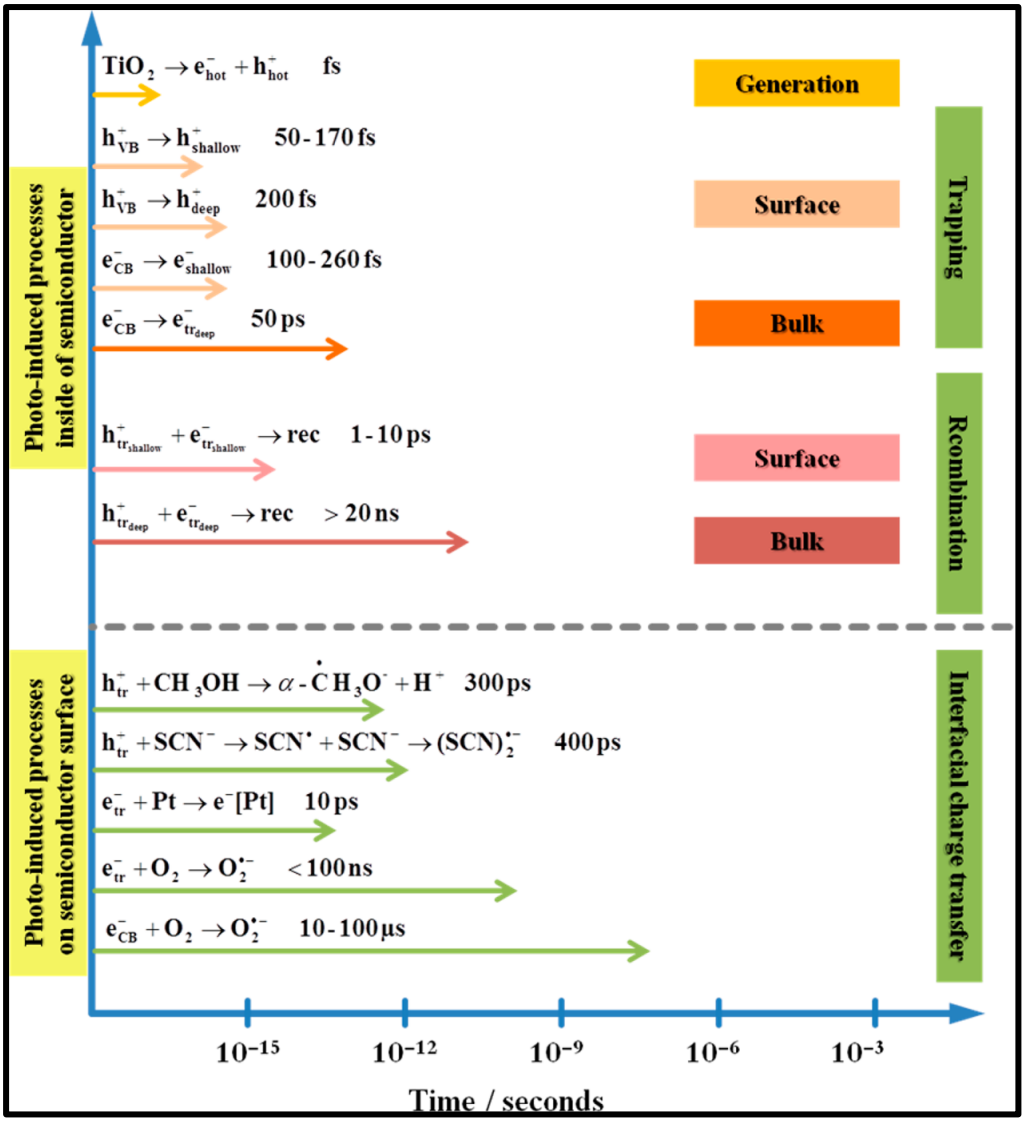

Figure 2: Photocatalytic reactions induced in TiO_2 and the corresponding time scales [58].

Nanoparticles with very high surface area have shown to be very important in carrying photocatalytic reactions on the surface of the semiconductor. Recently, there has been a search for material possessing required criteria for a good photocatalyst. The ideal material should consist a bandgap between (1.6 - 2eV), with high efficiency for the absorption of visible light and high carrier mobility [59, 60]. Different metal oxides, such as TiO_2, ZnO_2, and CeO_2 etc. have been used in the synthesis of these photocatalytic semiconductors. These metal oxides offer better stability in water and are found to be less expensive than valence semiconductors. Semiconductor facilitated photocatalysis offers potentially facile and inexpensive method for removing organic pollutants from wastewater. Mesoporous nano-sized particle Titania (TiO_2) is one of the widely-used materials for photocatalytic reaction. This is because Titania has proven very versatile, with different forms and it exists in three different crystalline phases, which are anatase, rutile and brookite. While anatase and rutile are monoclinic and brookite is

orthorhombic [61-64]. The structure of anatase and rutile can be described in terms of chains of TiO_6 octahedra, the crystal structure tends to differ in terms of distortion of the octahedral. The octahedron in rutile is irregular and shows a slight of orthorhombic distortion, whereas in the case of anatase the octahedron is significantly distorted such that its symmetry is lower than orthorhombic. Another difference is that in anatase phase, each Ti^{4+} is in contact with 8 neighbouring oxygen, whereas in rutile each Ti^{4+} is in contact with 10 neighbouring O^{2-}[65-67]. Rutile is denser (4.25 g/cm^2) than anatase (3.89 g/cm^2). Because of this difference in density, it is possible to transform anatase to rutile because it is less stable. The transformation occurs between 450 to 1200 ºC. **Figure.3** illustrates the crystalline structures of titania in different phases. For the superior physical and chemical properties, due to their special structural features, more attention has been intensive on controllable assembly of TiO_2 with desired morphologies such as nanoparticles.

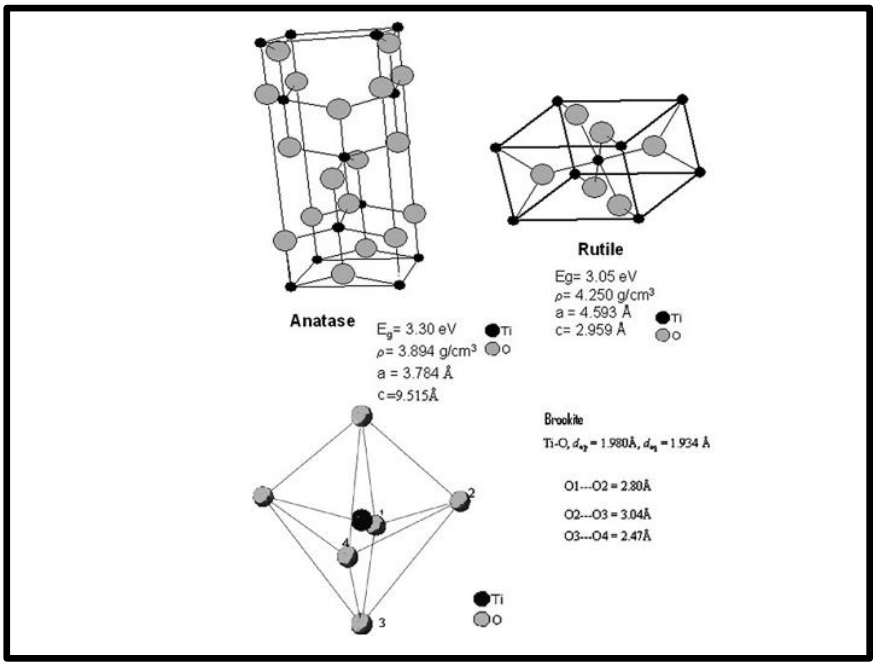

Figure 3: Crystalline structures of TiO_2 [68]

Anatase is the active photocatalytic phase based on its chemical properties, charge carrier dynamics and the activity of photocatalytic degradation of organic compounds. Other reason, for wider use of anatase over rutile is the larger band gap of anatase (3.2eV) compared with rutile, which has a band gap of (3.02 eV) [69, 70]. Synthesising mesoporous nanoparticles does not guarantee the effectiveness of the photocatalyst, there are other factors such as surface area, excitation of the photo-generated electron and the recombination of the hole and the photo-generated electron. Some of the disadvantages of TiO_2 is that it only absorbs UV light

at λ = 388 nm,[39] this is due to the large band gap of E_g 3.2 eV that is exhibited by anatase. To ensure that TiO_2 has all these properties the photo-catalyst under UV/ visible illumination is usually doped with cations or anionic doping, some of treatments that have been applied are surface chelation, surface derivatization, and platinization [71].

2.2.1 Effect of doing TiO_2

Doping of TiO_2 is one of the important approaches in band gap engineering to change the optical response of semiconductor photocatalyst. Efficiency of photocatalytic process is defined as number of events that occur per photon absorbed. The objective of doping is to induce a red shift, or the introduction of intra-band gap states, which results in more visible light absorption. Charge recombination is among factors that decrease efficiency of the process [72, 73]. It has been reported that to monitor photocatalytic activity, it is very important to ensure efficient charge separation. In determining the efficiency, the combination of all pathways is considered. Different tactics are applied to improve charge separation. Carrier traps are used to trap the electron and hole at the surface, which leads to more activity taking place by charge transfer. Doping is the addition of an impurity into the crystal structure of the material to alter the chemical, electrical and physical properties of that material. To extend the absorption band of TiO_2 to visible light region, metal and / non-metals doping is introduced to the crystal lattice of TiO_2. Metal ion doping and surface modification are considered as the most useful methods for reducing recombination rate [74, 75]. However, when the metal ion is merged into TiO_2 by doping the impurity energy levels that are formed in the bend gap can also lead to an increase in recombination rate between the electron and hole, which are photo-generated. It was noticed that in addition to all the methods mentioned above to improve efficiency, the reaction conditions such as temperature, pH, reactant and product concentrations and the light energy also play a very critical role [38, 76]. Some of the drawbacks that are associated with using metal ions as dopants are the thermal instability of TiO_2, the use of expensive metal implantation and electron trapping by metal centres [49, 77]. It is considered that metal ion of the surface or in the crystal lattice of TiO_2 accelerates the transportation of electrons produced by photoexcitation to the outer surface. Choi et al. reported that trivalent and pentavalent metal dopants are disadvantageous for photocatalytic reactions. These dopants have caused other effects such as increased the recombination process, which then leads to negligible increase in photoactivity [75]. Amongst many strategies used to improve the efficiency of the photo-catalyst, to modification of the crystal structure and the morphology are the well-used techniques. Initially, it was considered that for TiO_2, anatase is the best crystal

structure due to its high bend gap compared to rutile. From studying the crystal structure of Degussa p25 TiO_2, it has been seen that a combination of anatase and rutile crystal phases results in improved charge separation, which results in excellent photocatalytic activity. It shows that metal ions with higher valence than Ti^{4+} have better activity.

2.2.1.1 Metal Ion doping

Transition metal and rare earth metal have been extensively studies for the transformation and reduction of the large anatase band gap to be active under visible light. Since, electron-hole trapping is in competition with charge recombination, the rate of trapping will then be enhanced by reducing the charge recombination process. Introducing metal ion onto the surface of TiO_2 is effective in retarding the process [41, 43, 78].

In the band structure of TiO_2, O2p orbitals contribute to the filled VB, while Ti 3d, 4s, 4p orbitals contribute to the unoccupied CB. The lower position of CB is dominated by Ti 3d orbitals [71, 79, 80]. When metal ion is introduced onto the lattice structure of TiO_2, the impurity energy levels are generated on TiO_2.

$$M^{n+} + h\nu \rightarrow M^{(n+1)} + e^{-}_{CB} \quad (5)$$

$$M^{n+} + h\nu \rightarrow M^{(n-1)} + h^{+}_{VB} \quad (6)$$

Where M/M^{+} are metal and metal ion dopants.

Electron trapping: $M^{n+} + h\nu \rightarrow M^{(n-1)+}$

Hole trapping: $M^{n+} + h\nu \rightarrow M^{(n+1)-}$

For efficient photocatalysis, the energy level of $M^{n+}/ M^{(n-1)+}$ should less negative than the conducting band edge, and $M^{n+}/ M^{(n+1)-}$ should be less positive than that of the valence band edge. Photocatalytic reactions can only take place, if the trapped electron and hole are transferred to the surface of the photocatalyst [81-83]. Thus, the reason why metal should be doped close to the surface of TiO_2 is for better charge transfer. Studies show that transition metal ions increase the formation of Ti^{3+} ions, which leads to an enhanced photocatalytic activity, since more Ti^{3+} states might cause oxygen defects thereby facilitating the efficient adsorption of oxygen on the titania surface. Chromium is one of the frequently used transition metal dopants because of the excitation of the 3d electrons of Cr^{3+} to the conduction band CB of TiO_2, doping TiO_2 with Cr exhibits a good ability of absorbing visible light to induce the photocatalytic activity [84-86]. Doping with Fe was found to be more efficient in photo-degradation of methyl orange than undoped TiO_2 and P25, Authors suggested Fe ion was

needed to increase the space charge region potential. Authors mentioned that as the Fe^{+} concentration is increased, the space charge region became narrower [87, 88].

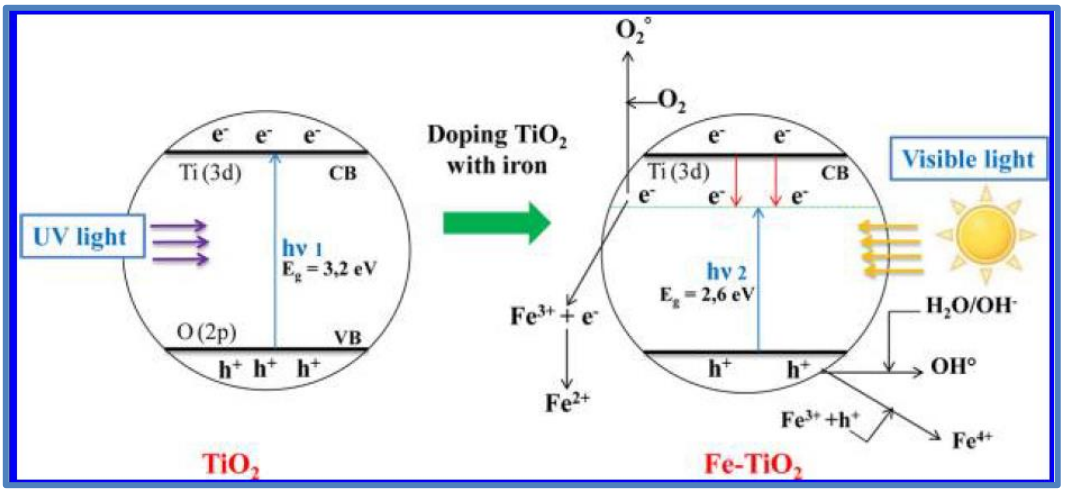

Figure 4: Comparison between undoped and doped TiO_2 with iron [35].

Doping with rare earth metals have better photocatalytic enhancement when compared to doping with transition metal ions. Doping TiO_2 nanoparticles with cerium ions has been found to generate additional electronic states in the bandgap of TiO_2. The new state is above the valence band and acting by capturing the photogenerated holes, therefore decreasing the recombination rate of photogenerated electrons and holes (**figure.4**). Electrons from these new generated electronic states can be photoexcited directly into the conduction band of TiO_2, which leads to a better visible light absorption and enhancing the photocatalytic degradation [89-91]. There are some unavoidable drawbacks with doping cerium in TiO_2, such as the reduction in the number of surface groups and possible partial blockages [92]. Photocatalytic degradation of organic molecules is influenced by the type of transition metal used when doping and the microstructural characteristics of the catalyst and its concentration. Studies indicate that the concentration of the metal is crucial, since an increase in the concentration of the metal dopant does not necessary increase photocatalytic activity. The further increase in dopant concentration could increase the recombination of the charge carriers, therefore lowering the photo activity of TiO_2. Photocatalytic activities of a cation doped TiO_2 sometimes decrease even under UV irradiation. The metal–doped materials have been shown to suffer from thermal instability, and the metals centers act as electron traps, which reassure the recombination of the photo generated charge carrier [93].

Lanthanides have been used as TiO_2 dopants for some time now. Though they appear to reduce the band gap and charge recombination rate, there are still problems associated with

using these metals. One of the most obvious problem is the large ionic radii in replacing Ti^{4+} ions in TiO_2 lattice. When doping using lanthanides, it is suggested that they do not enter the TiO_2 matrix due to their large (3+) ions, but instead they form a rare-earth oxide $[Re]_2O_3$, these oxides are then uniformly adsorbed onto the surface of TiO_2 [94, 95]. One of the most interesting feature exhibited by rare earth metals are the 4f orbitals. Another important feature is their 3+ oxidation state. Unlike transition metals, which also have 4f orbitals, the nature of these orbitals in lanthanides is such that they are shielded by filled $5p^6 6s^2$ sub-shell. Lanthanides can form metal complexes with different Lewis bases, by using the 4f orbitals and the functional group of the base [96]. The electron configuration of lanthanides also leads to formation of different optical properties and redox coupling (Ln^{n+} /$Ln^{(n-1)}$) can form oxygen vacancies. After calcining the catalyst, a tetrahedral complex is formed, when Ti^{4+} ions replace rare earth ions from the oxide. Because Ti^{4+} has small ionic radii compared to 3^+ of the rare-earth ion, during the exchange process a charge imbalance is formed, hydroxide (OH^-) ions are then adsorbed onto the doped TiO_2 [97]. This then leads to the formation of Ti – O – Ln structure, this then result in the appearance of a new electronic state in the TiO_2 band. This new electronic state is crucial, because an excited electron from the valence band of TiO_2 is absorbed by the inter band transition state which leads to retarding recombination process [98]. The 4f energy levels plays another important role since it can act as an electron pair scavenger. Some lanthanides contain half-filled electron configurations like Gadolinium (Gd^{3+})[99]. It is known that half-filled electron configurations are more stable. Violain et al. synthesised different lanthanide doped TiO_2 and reported that Gd showed a greater red-shift than most lanthanide metal ions used [100]. High photocatalytic efficiency is reported using Gd doped TiO_2. Some authors suggest that this is caused by the half-filled electron configuration, which leads to higher ability to transfer charge into the interface, while others suggests that it caused by reduction in band gap [96, 101].

Cruz et al., have showed that doping TiO_2 with Sm^{3+} exhibits a great red-shift, when compared with bare TiO_2 synthesised using a similar method. This was also tested by degrading deluron under visible light, again the Sm-TiO_2 catalyst performed better in both anatase and rutile phases compared to the bare TiO_2. These results were then attributed to the reduction in band gap, because it leads to the absorption of photons in the visible range [102]. Xiao et al. reported that Sm^{3+} ions were responsible for the red shift and reduction in the band gap, due to band narrowing. They also reported that red shift related to the concentration of the metal loading, because a greater reduction in the band gap was observed in the highest metal dopant [103]. Even Samarium doped TiO_2 showed a reduced in band gap compared to bare TiO_2, bare

TiO_2 is shown to exhibit more oxygen vacancies and structural defects, this was seen on their photoluminescence.

2.2.1.2 Non-metal doping

Doping with non-metal has been found to improve photocatalytic activity; anionic dopants such as (N, S, C, F, etc.) can shift the absorption edge from short wavelength into longer wavelength thereby increasing the photo-response into visible spectrum. One advantage of using anion doping is that unlike metal ions, anions are less likely to form recombination centre in high concentration, which will reduce photoactivity of the catalyst. Therefore, non-metals are more efficient in improving photoactivity. There are some limitations with doping with anions, i.e. though doping with S has been reported to narrow the band gap. It is not ideal due to its large ionic radius and it cannot be incorporated into the lattice structure of TiO_2. Hence, the insertion of cationic sulphur S^{6+} is chemically favourable over the ionic form S^{2-} lattice [104, 105]. Dopants P and C are less effective as the introduced states were so deep that photo-generated charge carriers were difficult to be transferred to the surface of the catalyst.

Nitrogen is an ideal non-metal dopant because it can be introduced in TiO_2 structure easily, due to its comparable atomic size with oxygen. It is highly stable and has a small ionisation energy [106, 107]. There are two ways with which N_2 can be introduced in TiO_2 lattice, (i) by substitutional element, whereby nitrogen atom is substitute oxygen atom from TiO_2 lattice. (ii) Or it can be interstitial lattice sites. Using X-ray photoelectron spectroscopy, (which is dependent on the distinct N 1s binding energy) one can determine which of the processes occurred [108, 109].

2.2.1.3 Effect of metal co-doping TiO_2

Low concentration co-doping with cations and anions is an effective solution to enhance the visible light absorption efficiency and reduces the recombination of the photo-generated charge carriers [110, 111]. Co-doping was found to show higher activity than that of a single ion doping, but this requires elements with synergistic effects with each other since they are co-dependent. Co-doping can be performed with various elemental combination such as, metal ion – metal ion pair, metal ion – non-metal ion, non-metal with other non-metal and it can also be done by doping TiO_2 with other semiconductors. Doping with In_2O_3 has been proven an efficient sensitizer to extend the absorption spectra of oxide semiconductor photocatalysts from the UV region to the visible region [112, 113]. When titania is in contact with other semiconductors that have higher conduction band position than that of it, a new electronic state is formed at the interface, which can trap electrons in the conduction and restrict

holes in valence bands thereby extending the time of the photogenerated charge carriers.

There are two views that are assumed when dealing with co-doping, the first approach is that both elements/ions are introduced in the lattice structure of TiO_2 which assists in promoting better photocatalytic activity. The second is that one element (metal ion or non-metal ion) is substituted in the lattice structure and the other ion sits on the surface of the catalyst. Jinlong et al., have mentioned that co-doping N-F shows higher activity than using single element. Cong et al., tested the effect of doping Fe^{3+} compared to co-doping Fe – N in degradation of rhodamine B, they suggested that Fe^{3+} ions act as trap retarder, slowing down the charge recombination process. They concluded that co-doping TiO_2 showed better activity when it came to degradation of rhodamine B [114].

2.2.2 Synthesis of mesoporous TiO_2 nanoparticles

Templated mesoporous transition metal oxides are made in a similar way as silica. However, special attention needs to be given to the higher reactivity of the transition metal precursors in comparison to the silica sources [115, 116]. To synthesise mesoporous nanoparticles there are many commonly used methods, (1) the hydrothermal method, (2) solvothermal and (3) sol gel method etc [117-122]. Sol gel method is the most commonly used method of synthesis of TiO_2 nanoparticles. The method requires the use of metal alkoxide (precursor of TiO_2), such as titanium isopropoxide, titanium butoxide, etc. As the starting reagent. The metal alkoxide is the hydrolysed by water, this step of the reaction is catalysed by acid, base or the use of organic surfactants (block copolymers) [123-125]. Surfactants are divided into two groups non-ionic and ionic depending on the shape and size of the nanoparticles required. Hydroxy (Ti – OH) and ethyl (Ti – OEt) groups are then formed as intermediates of the hydrolysis step. Surfactants are mostly used to control the shape and size of nanoparticles formed during the hydrolysis step. Review on the topic shows that uncontrolled synthesis of this material lack some of the properties such as uniform shape and size, and formation of agglomerates [126-129].

2.2.2.1 Sol gel method

It has been published that there are many factors affecting the crystallisation and characteristic of the final product, such as the concentration of the precursor concentration used in the starting material, whereas the morphology and stability are greatly affected by the water: titania ratio. Hydrolysis reaction occurs simultaneously with polycondensation reaction, which takes place when water is mixed with titania precursor, ploycondensation prompts polymerisation forming higher molecular weight product.

Hydrolysis reaction

$$Ti(OR)_n + H_2O \rightarrow Ti(OH)(OR)_{n-1} + ROH \quad (7)$$

$$Ti(OH)(OR)_{n-1} + H_2O \rightarrow Ti(OH)_2(OR)_{n-2} + ROH \quad (8)$$

Reaction for equation 8 continues to form Ti $(OH)_n$

Poly-condensation reactions

$$-Ti-OH + HO-Ti- \rightarrow -Ti-O-Ti- + H_2O \quad (9)$$

$$-Ti-OR + HO-Ti- \rightarrow -Ti-O-Ti- + ROH \quad (10)$$

Sol gel method is one of the most effective methods used in preparation of Nano-sized material. The doping metal ion into the crystalline structure of the semiconductor photocatalyst allows direct interaction between the metal ion and the catalyst and this is achieved during the sol formation [127, 130, 131]. The incorporation of a metal in the sol during the gelation process allows the metal to have a direct interaction with the support therefore, the material will have special photocatalytic properties [132]. These reactions are followed by a thermal treatment (400 – 700°C) to remove the organic part and to crystallize either anatase or rutile TiO_2. Calcining predictably cause a decline in surface area due to crystal growth and sintering, loss of surface hydroxyl groups, and even induce phase transformation.

2.2.3 Characterisation of TiO_2 nanoparticles

As mentioned above, method of synthesis of TiO_2 nanoparticles plays a crucial role in determining properties, which are responsible for their chemical purity and crystal form. The method is also responsible for various particle features such as crystallinity, shape of particles, surface area and pore volume. These properties are also dependent on defect states in the crystal lattice structure, since defects affects photoactivity. Catalytic performance of any catalyst is largely dependent on the surface properties because catalytic reactions usually take place on the surface. The crystalline phase in the surface region is typically different from that in the bulk for some metal oxides, such as TiO_2 or ZrO_2 [133-135].

The surface and electronic properties of mesoporous TiO_2 nanoparticles strongly depend on the presence of adsorbed molecules on the surface, as adsorbates disturb the distribution of electron trap sites, thereby affecting electron conductivity [136]. Some of the techniques used in characterising TiO_2 nanoparticles are mentioned below.

2.2.3.1 Photoluminescence

Photoluminescence spectroscopy is a non-destructive, contactless method of determining the electronic structure of materials. Light is directly irradiated onto the sample; it

is then absorbed by the sample and sends excess energy into to the material, this process is called photo-excitation [137, 138]. The energy is absorbed by the material does not stay excited for a long time, and it is then released through emission or during a process called luminance.

Photoluminescence (PL) is used to determine the effectiveness of trapping, migration and transfer of charge carriers. It is also used to examine the role of the e^-/h^+ pair in a semiconductor. PL spectroscopy of TiO_2 can in addition be used in investigating the energy level that provides information between anatase and rutile. PL of TiO_2 strongly depends on the surface conditions, and therefore information about surface conditions can be obtained by PL spectroscopy.

Tang.et.al. did an experiment on determining the low temperature PL for single crystal of TiO_2 doped with aluminium, anatase TiO_2 crystals had a broad emission band at 2.3 eV, which was said to be attributed to the combination of self – trapped excitons[70]. Room temperature PL was conducted by Kernazhitsky et al. and the authors observed that the PL peak positions were similar in both anatase and rutile samples the only difference was in the intensities of the peak. They concluded that sharp peaks at 2.17 – 2.81 eV was attributed to excitonic recombination via oxygen vacancies in both anatase and rutile TiO_2[139]. Using results from literature one can differentiate between the PL spectra of anatase and rutile, it is well mentioned that UV emission peaks is generally attributed to band to band transitions. The peak which is attributed to band edges is found in 3.26 eV for anatase and at 3.03 eV for rutile.

2.2.3.2 Powder X-Ray diffraction

X-Ray diffraction (XRD) is an analytical technique that is used for phase identification of crystalline materials and gives information about the nature of the unit cell. A solid material can be described as crystalline, so when radiation interacts with crystalline substance diffraction pattern is produced. In 1919 W Hull suggested that all crystalline substances give a pattern, the same substance always gives the same pattern and a mixture of substances each generate its pattern independently of others [140, 141]. Diffraction patterns are seen when an electromagnetic radiation imposes on periodic structure that has geometric distinctions on length scale of the wavelength of light. Because of these reasons, XRD pattern is considered as a fingerprint of a substance [142, 143].

X-ray radiation is passed through a crystalline material; diffraction patterns are produced. Diffraction takes place when X-ray that passes through a crystal bends at various angles. X-ray diffraction involves the measurement of X-ray intensity that is being scattered from electron bound atom [144].

The angle of diffraction is dependent on the distance between the adjacent layers of atoms in the crystal structure. Using Bragg's law, the distances between the planes of the atoms can be measured. Bragg's law explains the formation of constructive interference that give rise to diffraction patterns. Bragg postulated that when X-ray radiation is incident on the surface of atom (crystal), it forms an angle of incident (θ), radiation will then be reflected with the same scattering (θ). This occurs when the path difference (d) is equal to a whole number (n) of wavelength (λ), a constructive interference will occur [145-149]. Bragg's equation describes X-ray diffraction in terms reflection of X-ray by lattice planes. Lattice planes are crystallographic planes that are characterised by index triplet also known as Miller indices (hkl). Parallel planes having the same indices are spaced equally and separated by distance (d_{hkl}) [150-152]. Using XRD, one can determine lattice parameters, phase purity, crystallinity of the sample, percentage composition and crystal structure.

2.2.3.3 Raman Spectroscopy

Raman spectroscopy is named after Sir Chandrasekhara Venkata Raman, who inverted the technique alongside with K.S Krishnan in 1928 [153, 154]. It is an analytical technique, which is used for both quantitative and qualitative analysis. It belongs to a family of spectral measurements made on molecular media that is based on inelastic scattering of monochromatic radiation. Raman spectroscopy is based on Raman Effect, (a small fraction of frequency of scattered light is different from frequency of monochromatic incident light), it is also based on scattering of incident light through its interaction with vibrating molecules. It enquiries the molecular vibrations [155-157]. Photons are scattered when monochromatic radiation (laser source) is irradiates the material, when this happens, most fraction of the scattered radiations tends to have the same wavelength as the source, this type of scattering is said to be elastic scattering known as Rayleigh scattering [158-162]. When there is a change in wavelength of photons, this is known as inelastic scattering. Raman scattering is a non-parametric process.

There is an energy exchange between photon and molecule, which results in energy of the photon can either be higher or lower than that of the incident radiation. If a molecule gains energy during Raman scattering, the scattered photon will then shift to longer wavelength producing stokes lines, whereas if energy is lost photons will shift to shorter wavelength producing anti-stokes lines [163]. From this, the magnitude of Raman shift is independent of wavelength of the incident radiation, but Raman scattering is dependent on the wavelength of the incident radiation.

Like infrared spectroscopy, Raman spectroscopy is used as a fingerprint of a molecule. Molecular fingerprint is generated from the atomic arrangement, bond strength of the molecule and vibrational frequency of the molecule. Each molecule has several vibrational modes, but not all vibrational modes are Raman active. Only those that are Raman active can produce Raman spectrum. Polarizability of a molecule plays a major role in Raman spectroscopy. Raman transitions depends on the rate of change of polarizability with respect to the molecular geometry. This suggests that Raman scattering is only possible for some symmetries of molecular vibrations, is forms the basis of selection rule for Raman scattering [164-166].

2.2.3.4 Nitrogen sorption – desorption studies

Gas adsorption analysis is commonly used in ordered organic-inorganic nanocomposite materials, characterisation that allows the determination of specific area, pore volume and pore size distribution and surface property studies [167, 168]. The method involves exposing solid material to gases or vapour at different conditions and evaluating the weight or sample volume. This is possible because, the internal structure of porous materials is highly complex, the exact form of the wide space structure can influence several features which then affect the way the material functions [169].

Nitrogen sorption at 77 K is a well-known standard tool which allows the analysis of porous materials in the range of 0.5 – 50 nm. N_2 adsorption follows certain procedure, at relative low pressures, pores are filled because of large adsorption potential. Micropores are filled at different relative pressure (0.02, 0.05, 0.2) depending on the nature of the material [170-172]. The quantity of molecules adsorbed on the external surface is negligible compared to that in micropores. Multilayer is formed after the nitrogen molecule monolayer is formed. Capillary condensation for small mesopores occurs when relative pressure and pore width agree with Kelvin equation [173-175]. When the relative pressure is increased, capillary condensation occurs at relatively large meso and macropores. Capillary condensation starts occurring on same parts of the surface for heterogeneous surface. This leads to the adsorbed and capillary – condensed phases to coexist in the pores [176, 177].

The reverse of the adsorption process gives the desorption branch of the isotherm; this leads to release in liquid adsorbate and decreasing the equilibrium relative pressure.

2.2.3.5 Infrared spectroscopy

Infrared spectroscopy is an analytical technique used in characterisation of biological, organic and inorganic materials. Like UV/Vis spectroscopy, it is an absorption technique, whereby infrared radiation in the wavelength range of (1 – 100 μm). An IR spectrum is

generated when passing infrared radiation through a sample. When this happens some of the radiation is absorbed (incident radiation) at different energies [178, 179]. IR spectroscopy has been used since 1940s. Studies can be done in samples of all types, liquids, powder, pastes, fibres, gasses, and even surfaces can be analysed [180, 181].

2.3 Ozonation

Ozone (O_3) is a powerful oxidant that is generally produced by an electric discharge method using oxygen gas or air as source. Ozone is an unstable gas that decompose in gaseous phase to oxygen (O_2). At normal or lower temperatures, decomposition is relatively slow and at high temperatures, decomposition is faster. Because of this, decrease in ozone concentration is accelerated by heat [182-184]. The decomposition of ozone in water can be described by the reaction illustrated in **figure 5**.

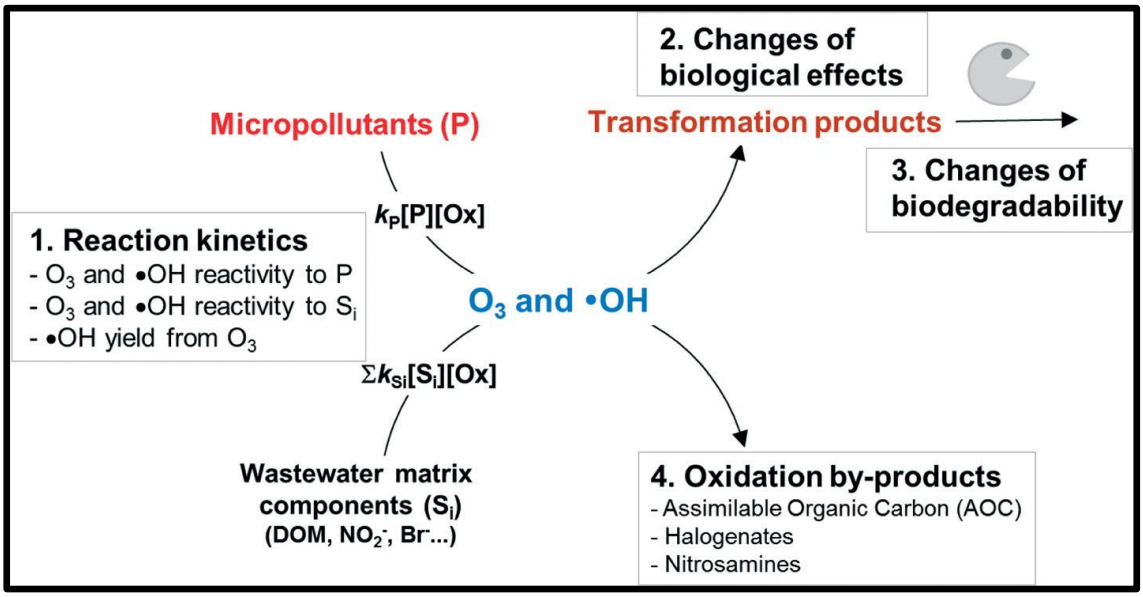

Figure 5: Ozonation of organic pollutants and its kinetics

Ozone is applied for odour control, disinfection and removal of colour, taste, and oxidation micro-pollutants. The use of ozone in degradation and mineralisation of organic pollutants in water is a well-established method. This is due to the production of active oxygen species such as OH radicals that are produced during the process. Many research articles have been published using this degradation of organic substances like dye, pharmaceuticals, etc [185-189].

Reaction of organic molecule with ozone can be divided into two reactions. (i) this occurs at low pH, where molecular ozone directly attacks the substrate at the same time radicals from decomposition of ozone react non-selectively with substrate. Free OH radicals are

produced in aqueous media by altering the pH of the solution. (ii) Ozone is applied water treatment systems; it is used in pre-treatment stage because of its capability of selective of substrate. It reacts with organic compounds, but does not break single bonded functional groups, such as C – C, C – O, O – H at high rates, however, can react with simple ions that can be oxidised like, S^{2-} to form, oxyanions like SO_3^{2-}, SO_4^{2-} [190-193]. These are thought to be fast reactions, since they react by just encountering ozone.

The effectiveness of ozonation reaction is dependent on the concentration of the oxidant (O_3 and ·OH) and the second order rate constant with respect to the oxidants. The rate constant is highly influenced by the electronic properties of the organic pollutant. Recent publications point out that, ozone reacts readily with organic pollutants that contain activated aromatics rings, C=C and NH_2 groups. Ozone with these groups have high rate constants. While it reacts relatively slow with inactivated aromatic rings, halogens, NO_2 and COO groups [194-197]. Ozone react by converting unsaturated organic compounds into saturated compounds by facilitating with bond breaking, which leads to ring opening.

This means that there is a high reactivity towards pharmaceuticals and fast kinetics are to be expected. For highly ionisable substrates such as amines and phenols, the rate constant increases with increasing pH of the solution. This is due to enhanced reactivity of ozone with deprotonated form of these groups.

Reaction of ozone with organic compounds usually leads to the formation of carboxylic acids and aldehydes or both. This is because both these groups are refractory groups (they do not react with ozone) [198, 199]. Oxidising using ozone alone gives low total organic carbon (TOC) and chemical oxygen demand (COD) removal because of refractory organic molecules produced in aqueous system. Derek etal., reported the kinetics of degrading Carbamazepine using molecular ozone, and reported that degradation rate constant followed first order kinetics at natural pH = 8 [186].

2.3.1 Catalytic Ozonation

Recent research has shown that there is limitation with application of ozone only in remediation of water systems, such the low ability to degrade some organic groups, such as COOH. One of the solutions of this problem is the use of ozone combined with the catalyst. The catalyst can be in the same phase as the pollutant, in this case homogeneous catalyst is used. The most used catalysts are the transition metal ions like Fe^{3+}, Cu^{2+}, Fe^{2+} [200, 201], the decomposition of ozone using metal ions leads to the formation of hydroxyl radicals. Typical reaction is shown below:

$$Fe^{2+} + O_3 \rightarrow FeO^{2-} + O_2 \quad (11)$$

$$FeO^{2-} + H_2O \rightarrow Fe^{3+} + OH^{\cdot} + OH^{-} \quad (12)$$

It is important to note that these reactions can only occur at low concentrations of Fe^{2+}, because at higher concentrations there is no formation of hydroxyl radicals.

$$FeO^{2-} + Fe^{2+} + H^{+} \rightarrow 2Fe^{3+} + H_2O \quad (13)$$

Heterogeneous catalyst is the one that is mostly applied. In this instant, the catalyst is of different phase as the solute. Metal oxides catalyst are the mostly used catalyst for catalytic ozonation of micro-pollutants. This is because transition metal oxides have a variable electronic structure [202, 203].

Degradation using metal oxides catalysts is known to occur in two ways. (i) Ozone decompose on the catalyst surface thus generating hydroxyl radicals, which are non-selective. (ii) in the other way ozone is oxidant. Ozone directly attack the metal – organic complex. As mentioned above, this method was developed to overcome some of the disadvantages that are associated with conventional ozonation such as inability to oxidise and mineralise some of organic pollutants such as natural occurring organics. The most important limitation is the accumulation of refractory biodegradable by-products and partial mineralisation. Maddila et.al reported on dechlorination of chloronitrophenol using Ce-V loaded metal oxides and ozone. The authors showed that combining ozone with metal oxide catalyst displays high degradation efficiency than using ozone alone [204]. Chetty et al., studied the efficient conversion of 1,2-dichlorobenzene through catalytic ozonation process using vanadium pentoxide loaded metal oxide as an catalyst and they reported that catalytic ozonation had high selectivity on oxidation products, which was attributed to the presence of metal oxide catalyst [205].

2.3.2 Photocatalytic ozonation

Photocatalytic ozonation is an emerging technology that combines two AOPs, with the main advantage being higher $^{\bullet}OH$ yield due to the more power oxidant character of ozone. Combing photocatalytic process with ozone has proven to have higher efficiency than either of the two methods [206]. In this process, ozone traps electrons from the conducting band of TiO_2, thereby retarding recombination of photo-induced electrons and hole, which enhance the efficiency of photocatalysis. The produced ozone species (ozonide, $O_3^{\bullet-}$) is a good source of hydroxyl radicals [207].

$$\text{Metal oxide} + h\nu \rightarrow \text{metal oxide}\ (h^{+}_{VB} + e^{-}_{CB}) \quad (1)$$

$$O_3 + e^{-} \rightarrow O_3^{\bullet-} \quad (14)$$

$$O_3^{\bullet-} + H^{+} \rightarrow HO_3^{\bullet} \quad (15)$$

$HO_3^{\bullet} \rightarrow O_2 + HO^{\bullet}$ (16)

$O_3 + h\nu \rightarrow H_2O_2$ (17)

$H_2O_2 + h\nu \rightarrow 2HO^{\bullet}$ (18)

$h_{VB}^{+} + \text{org pollutant} \rightarrow \text{product}$ (19)

$HO^{\bullet} + \text{org pollutant} \rightarrow \text{product}$ (20)

Equations 14 to 20 shows generation of active radicals in the photocatalytic ozonation of organic pollutant in aqueous system.

Photocatalytic ozonation kinetics can be described by Langmuir– Hinshelwood (L–H) mechanism, where the rate of oxidation of organic pollutant is given by $(-\frac{C_p}{dt})$, where C_p is the initial concentration of the organic pollutant in water. k_{ads} and k_{ox} are adsorption/desorption constants on TiO_2 and oxidation constant.

$$-\frac{C_p}{dt} = k_{O_3}.C_{O_3}.C_p + k_{OH}.C_{OH}.C_p + \frac{k_{OX}.k_{Ads.}C_p}{1+k_{Ads}.C_p} \quad (21)$$

C_{O_3} and C_{OH} are ozone and hydroxyl concentrations in water with their constants.

3 Objectives of the study

- To synthesise and characterise the recyclable heterogeneous catalysts that display enhanced catalytic and/or photocatalytic activity
- Study the mechanism of oxidation of selected aromatic compounds using ozone and advanced oxidation processes
- Systematic study into the effect of reaction parameters on the catalytic activity and substrate degradation.
- Studies on oxidative degradation of selected organic substrates under mild reaction conditions.

4 Aim

- Determine the effect of modification of material TiO_2 in improving its catalytic activity and stability
- To study the UV/Ozonation process for degradation of selected organic substrates using newly developed catalyst materials.

Objectives were achieved by:

- Ozonation of caffeine in presence and absence of heterogeneous catalysts (Ce-TiO_2) and studies on the effect of ozone concentration and other parameters in substrate degradation. Determination of point of zero charge of the material in order to optimise reaction conditions.
- Investigating the effect of dopant weight percentage on the prepared materials, and photocatalytic degradation of caffeine in aqueous solution at different pH and propose a reasonable mechanism for intermediate and product formation.
- Comparing the effect of lanthanide dopants on the prepared TiO_2 material by sol gel method using the same weight percentage. Investigations on the photocatalytic performance of the materials under visible light in degradation of caffeine and the generation of OH radicals.

References

[1] J. Radjenovic, M. Petrovic, D. Barceló, Analysis of pharmaceuticals in wastewater and removal using a membrane bioreactor, Analytical and Bioanalytical Chemistry, 387 (2007) 1365-1377.

[2] L. You, V.T. Nguyen, A. Pal, H. Chen, Y. He, M. Reinhard, K.Y.-H. Gin, Investigation of pharmaceuticals, personal care products and endocrine disrupting chemicals in a tropical urban catchment and the influence of environmental factors, Science of The Total Environment, 536 (2015) 955-963.

[3] C. Ávila, V. Matamoros, C. Reyes-Contreras, B. Piña, M. Casado, L. Mita, C. Rivetti, C. Barata, J. García, J.M. Bayona, Attenuation of emerging organic contaminants in a hybrid constructed wetland system under different hydraulic loading rates and their associated toxicological effects in wastewater, Science of The Total Environment, 470–471 (2014) 1272-1280.

[4] Y. Li, G. Zhu, W.J. Ng, S.K. Tan, A review on removing pharmaceutical contaminants from wastewater by constructed wetlands: Design, performance and mechanism, Science of The Total Environment, 468–469 (2014) 908-932.

[5] D. Taylor, T. Senac, Human pharmaceutical products in the environment – The "problem" in perspective, Chemosphere, 115 (2014) 95-99.

[6] C. Gadipelly, A. Pérez-González, G.D. Yadav, I. Ortiz, R. Ibáñez, V.K. Rathod, K.V. Marathe, Pharmaceutical industry wastewater: Review of the technologies for water treatment and reuse, Industrial & Engineering Chemistry Research, 53 (2014) 11571-11592.

[7] D.R. Baker, B. Kasprzyk-Hordern, Spatial and temporal occurrence of pharmaceuticals and illicit drugs in the aqueous environment and during wastewater treatment: New developments, Science of The Total Environment, 454–455 (2013) 442-456.

[8] D.R. Baker, V. Očenášková, M. Kvicalova, B. Kasprzyk-Hordern, Drugs of abuse in wastewater and suspended particulate matter — Further developments in sewage epidemiology, Environment International, 48 (2012) 28-38.

[9] S. Teixeira, R. Gurke, H. Eckert, K. Kühn, J. Fauler, G. Cuniberti, Photocatalytic degradation of pharmaceuticals present in conventional treated wastewater by nanoparticle suspensions, Journal of Environmental Chemical Engineering, 4 (2016) 287-292.

[10] C.S. Wong, S.L. MacLeod, JEM Spotlight: Recent advances in analysis of pharmaceuticals in the aquatic environment, Journal of Environmental Monitoring, 11 (2009) 923-936.

[11] P.C. Rua-Gomez, W. Puttmann, Impact of wastewater treatment plant discharge of lidocaine, tramadol, venlafaxine and their metabolites on the quality of surface waters and groundwater, Journal of Environmental Monitoring, 14 (2012) 1391-1399.

[12] C. Vatovec, P. Phillips, E. Van Wagoner, T.-M. Scott, E. Furlong, Investigating dynamic sources of pharmaceuticals: Demographic and seasonal use are more important than down-the-drain disposal in wastewater effluent in a University City setting, Science of The Total Environment, 572 (2016) 906-914.

[13] S.R. de Solla, È.A.M. Gilroy, J.S. Klinck, L.E. King, R. McInnis, J. Struger, S.M. Backus, P.L. Gillis, Bioaccumulation of pharmaceuticals and personal care products in the unionid mussel Lasmigona costata in a river receiving wastewater effluent, Chemosphere, 146 (2016) 486-496.

[14] K.M.S. Hansen, A. Spiliotopoulou, R.K. Chhetri, M. Escolà Casas, K. Bester, H.R. Andersen, Ozonation for source treatment of pharmaceuticals in hospital wastewater – Ozone lifetime and required ozone dose, Chemical Engineering Journal, 290 (2016) 507-514.

[15] M. Escolà Casas, R.K. Chhetri, G. Ooi, K.M.S. Hansen, K. Litty, M. Christensson, C. Kragelund, H.R. Andersen, K. Bester, Biodegradation of pharmaceuticals in hospital wastewater by a hybrid biofilm and activated sludge system (Hybas), Science of The Total Environment, 530–531 (2015) 383-392.

[16] Y. Yu, Q. Huang, Z. Wang, K. Zhang, C. Tang, J. Cui, J. Feng, X. Peng, Occurrence and behavior of pharmaceuticals, steroid hormones, and endocrine-disrupting personal care products in wastewater and the recipient river water of the Pearl River Delta, South China, Journal of Environmental Monitoring, 13 (2011) 871-878.

[17] S. Zorita, B. Boyd, S. Jonsson, E. Yilmaz, C. Svensson, L. Mathiasson, S. Bergstrom, Selective determination of acidic pharmaceuticals in wastewater using molecularly imprinted solid-phase extraction, Analytica Chimica Acta, 626 (2009) 147-154.

[18] D. Simazaki, R. Kubota, T. Suzuki, M. Akiba, T. Nishimura, S. Kunikane, Occurrence of selected pharmaceuticals at drinking water purification plants in Japan and implications for human health, Water Research, 76 (2015) 187-200.

[19] T. Mackuľak, M. Mosný, J. Škubák, R. Grabic, L. Birošová, Fate of psychoactive compounds in wastewater treatment plant and the possibility of their degradation using aquatic plants, Environmental Toxicology and Pharmacology, 39 (2015) 969-973.

[20] B. Ferrari, R. Mons, B. Vollat, B. Fraysse, N. Paxēaus, R.L. Giudice, A. Pollio, J. Garric, Environmental risk assessment of six human pharmaceuticals: Are the current environmental risk assessment procedures sufficient for the protection of the aquatic environment, Environmental Toxicology and Chemistry, 23 (2004) 1344-1354.

[21] C. Bouissou-Schurtz, P. Houeto, M. Guerbet, M. Bachelot, C. Casellas, A.-C. Mauclaire, P. Panetier, C. Delval, D. Masset, Ecological risk assessment of the presence of pharmaceutical residues in a French national water survey, Regulatory Toxicology and Pharmacology, 69 (2014) 296-303.

[22] P. Houeto, A. Carton, M. Guerbet, A.-C. Mauclaire, C. Gatignol, P. Lechat, D. Masset, Assessment of the health risks related to the presence of drug residues in water for human consumption: Application to carbamazepine, Regulatory Toxicology and Pharmacology, 62 (2012) 41-48.

[23] K.E. Arnold, A.R. Brown, G.T. Ankley, J.P. Sumpter, Medicating the environment: assessing risks of pharmaceuticals to wildlife and ecosystems, Philosophical Transactions of the Royal Society B: Biological Sciences, 369 (2014) 20130569.

[24] K.J. Groh, R.N. Carvalho, J.K. Chipman, N.D. Denslow, M. Halder, C.A. Murphy, D. Roelofs, A. Rolaki, K. Schirmer, K.H. Watanabe, Development and application of the adverse outcome pathway framework for understanding and predicting chronic toxicity: II. A focus on growth impairment in fish, Chemosphere, 120 (2015) 778-792.

[25] G.Z. Kyzas, J. Fu, N.K. Lazaridis, D.N. Bikiaris, K.A. Matis, New approaches on the removal of pharmaceuticals from wastewaters with adsorbent materials, Journal of Molecular Liquids, 209 (2015) 87-93.

[26] S.-W. Li, A.Y.-C. Lin, Increased acute toxicity to fish caused by pharmaceuticals in hospital effluents in a pharmaceutical mixture and after solar irradiation, Chemosphere, 139 (2015) 190-196.

[27] A. Butkovskyi, L. Hernandez Leal, H.H.M. Rijnaarts, G. Zeeman, Fate of pharmaceuticals in full-scale source separated sanitation system, Water Research, 85 (2015) 384-392.

[28] B.T. Ferrari, N. Paxéus, R.L. Giudice, A. Pollio, J. Garric, Ecotoxicological impact of pharmaceuticals found in treated wastewaters: study of carbamazepine, clofibric acid, and diclofenac, Ecotoxicology and Environmental Safety, 55 (2003) 359-370.

[29] B. Ferrari, amp, x, N. Paxéus, R.L. Giudice, A. Pollio, J. Garric, Erratum to "Ecotoxicological impact of pharmaceuticals found in treated wastewaters: study of carbamazepine, clofibric acid, and diclofenac" Ecotoxicology and Environmental Safety, 56 (2003) 450-455.

[30] M. Saravanan, S. Karthika, A. Malarvizhi, M. Ramesh, Ecotoxicological impacts of clofibric acid and diclofenac in common carp (Cyprinus carpio) fingerlings: Hematological, biochemical, ionoregulatory and enzymological responses, Journal of Hazardous Materials, 195 (2011) 188-194.

[31] Y. Deng, R. Zhao, Advanced Oxidation Processes (AOPs) in Wastewater Treatment, Current Pollution Reports, 1 (2015) 167-176.

[32] S. Parsons, Advanced oxidation processes for water and wastewater treatment, IWA publishing, 5 (2004) 159-165.

[33] M. Swaminathan, M. Muruganandham, M. Sillanpaa, Advanced oxidation processes for wastewater treatment, International Journal of Photoenergy, 13 (2013) 152-163.

[34] A.M. Jr., S.C. Oliveira, M.E. Osugi, V.S. Ferreira, F.H. Quina, R.F. Dantas, S.L. Oliveira, G.A. Casagrande, F.J. Anaissi, V.O. Silva, R.P. Cavalcante, F. Gozzi, D.D. Ramos, A.P.P.d. Rosa, A.P.F. Santos, D.C.d. Castro, J.A. Nogueira, Application of Different Advanced Oxidation Processes for the Degradation of Organic Pollutants, Environmental Sciences, 6 (2013) 141-166.

[35] B.K. Mutuma, G.N. Shao, W.D. Kim, H.T. Kim, Sol–gel synthesis of mesoporous anatase–brookite and anatase–brookite–rutile TiO2 nanoparticles and their photocatalytic properties, Journal of Colloid and Interface Science, 442 (2015) 1-7.

[36] M.A. Fox, M.T. Dulay, Heterogeneous photocatalysis, Chemical Reviews, 93 (1993) 341-357.

[37] J. Zhang, Y. Wu, M. Xing, S.A.K. Leghari, S. Sajjad, Development of modified N doped TiO2 photocatalyst with metals, nonmetals and metal oxides, Energy & Environmental Science, 3 (2010) 715-726.

[38] S. Ikeda, N. Sugiyama, B. Pal, G. Marci, L. Palmisano, H. Noguchi, K. Uosaki, B. Ohtani,Photocatalytic activity of transition-metal-loaded titanium(IV) oxide powders suspended in aqueous solutions: Correlation with electron-hole recombination kinetics, Physical Chemistry Chemical Physics, 3 (2001) 267-273.

[39] T. Peng, D. Zhao, K. Dai, W. Shi, K. Hirao, Synthesis of Titanium Dioxide Nanoparticles with Mesoporous Anatase Wall and High Photocatalytic Activity, The Journal of Physical Chemistry B, 109 (2005) 4947-4952.

[40] A. Fujishima, H. Honda, TiO_2 photoelectrochemistry and photocatalysis. Nature, 238 (1972) 37-38.

[41] K. Ozawa, M. Emori, S. Yamamoto, R. Yukawa, S. Yamamoto, R. Hobara, K. Fujikawa, H. Sakama, I. Matsuda, Electron–hole recombination time at TiO_2 single-crystal surfaces: Influence of surface band bending, The Journal of Physical Chemistry Letters, 5 (2014) 1953-1957.

[42] A.L. Linsebigler, G. Lu, J.T. Yates, Photocatalysis on TiO_2 surfaces: principles, mechanisms, and selected results, Chemical Reviews, 95 (1995) 735-758.

[43] A. Fujishima, T.N. Rao, D.A. Tryk, Titanium dioxide photocatalysis, Journal of Photochemistry and Photobiology C: Photochemistry Reviews, 1 (2000) 1-21.

[44] M. Schiavello, Some working principles of heterogeneous photocatalysis by semiconductors, Electrochimica Acta, 38 (1993) 11-14.

[45] M.A. Rauf, S.S. Ashraf, Fundamental principles and application of heterogeneous photocatalytic degradation of dyes in solution, Chemical Engineering Journal, 151 (2009) 10-18.

[46] U.I. Gaya, Principles of Heterogeneous Photocatalysis, Heterogeneous photocatalysis using inorganic semiconductor solids, Springer Netherlands, Dordrecht, (2014), 1-41.

[47] C.S. Turchi, D.F. Ollis, Photocatalytic degradation of organic water contaminants: Mechanisms involving hydroxyl radical attack, Journal of Catalysis, 122 (1990) 178-192.

[48] J. Zhao, C. Chen, W. Ma, Photocatalytic degradation of organic pollutants under visible light irradiation, Topics in Catalysis, 35 (2005) 269-278.

[49] A.B. Djurisic, Y.H. Leung, A.M. Ching Ng, Strategies for improving the efficiency of semiconductor metal oxide photocatalysis, Materials Horizons, 1 (2014) 400-410.

[50] C. Burda, X. Chen, R. Narayanan, M.A. El-Sayed, Chemistry and Properties of Nanocrystals of Different Shapes. Chemical Reviews, 105 (2005) 1025-1102.

[51] X.F. Gao, H.B. Li, W.T. Sun, Q. Chen, F.Q. Tang, L.M. Peng, Removal of emerging pollutants by Ru/TiO_2-catalyzed permanganate oxidation, The Journal of Physical Chemistry C, 113 (2009) 7531-7535.

[52] L. Du, A. Furube, K. Hara, R. Katoh, M. Tachiya, Photocatalytic oxidation of small molecule hydrocarbons over Pt/TiO_2 nanocatalysts Journal of Photochemistry and Photobiology C: Photochemistry Reviews, 15 (2013) 21-30.

[53] Y. Li, H. Wang, Q. Feng, G. Zhou, Z.S. Wang, Gold nanoparticles inlaid TiO_2 photoanodes: a superior candidate for high-efficiency dye-sensitized solar cells Energy Environmental. Science, 6 (2013) 2156-2165.

[54] L.R. Sheppard, S. Hager, J. Holik, R. Liu, S. Macartney, R. Wuhrer, Tantalum Segregation in Ta-Doped TiO_2 and the related impact on charge separation during illumination, The Journal of Physical Chemistry C, 119 (2015) 392-400.

[55] M.M. Khan, S.F. Adil, A. Al-Mayouf, Metal oxides as photocatalysts, Journal of Saudi Chemical Society, 19 (2015) 462-464.

[56] U.I. Gaya, A.H. Abdullah, Heterogeneous photocatalytic degradation of organic contaminants over titanium dioxide: A review of fundamentals, progress and problems, Journal of Photochemistry and Photobiology C: Photochemistry Reviews, 9 (2008) 1-12.

[57] D. Chatterjee, S. Dasgupta, Visible light induced photocatalytic degradation of organic pollutants, Journal of Photochemistry and Photobiology C: Photochemistry Reviews, 6 (2005) 186-205.

[58] K. Rajeshwar, M.E. Osugi, W. Chanmanee, C.R. Chenthamarakshan, M.V.B. Zanoni, P. Kajitvichyanukul, R. Krishnan-Ayer, Heterogeneous photocatalytic treatment of organic dyes in air and aqueous media, Journal of Photochemistry and Photobiology C: Photochemistry Reviews, 9 (2008) 171-192.

[59] M.M. Khin, A.S. Nair, V.J. Babu, R. Murugan, S. Ramakrishna, A review on nanomaterials for environmental remediation, Energy & Environmental Science, 5 (2012) 8075-8109.

[60] D.J. Martin, G. Liu, S.J.A. Moniz, Y. Bi, A.M. Beale, J. Ye, J. Tang, Efficient visible driven photocatalyst, silver phosphate: performance, understanding and perspective, Chemical Society Reviews, 44 (2015) 7808-7828.

[61] A.K. Tripathi, M.K. Singh, M.C. Mathpal, S.K. Mishra, A. Agarwal, Study of structural transformation in TiO_2 nanoparticles and its optical properties, Journal of Alloys and Compounds, 549 (2013) 114-120.

[62] S. Bagheri, N. Muhd Julkapli, S. Bee Abd Hamid, Titanium dioxide as a catalyst support in heterogeneous catalysis, The Scientific World Journal, 2014 (2014) 21.

[63] G. Thennarasu, A. Sivasamy, Enhanced visible photocatalytic activity of cotton ball like nano structured Cu doped ZnO for the degradation of organic pollutant, Ecotoxicology and Environmental Safety, 134, Part 2 (2016) 412-420.

[64] C. Jia, P. Yang, H.-S. Chen, J. Wang, Template-free synthesis of mesoporous anatase titania hollow spheres and their enhanced photocatalysis, Cryst Eng Comm, 17 (2015) 2940-2948.

[65] C.K. Song, J. Baek, T.Y. Kim, S. Yu, J.W. Han, J. Yi, Exploring crystal phase and morphology in the TiO_2 supporting materials used for visible-light driven plasmonic photocatalyst, Applied Catalysis B: Environmental, 198 (2016) 91-99.

[66] J. Li, G. Lu, G. Wu, D. Mao, Y. Guo, Y. Wang, Y. Guo, Effect of TiO_2 crystal structure on the catalytic performance of Co_3O_4/TiO_2 catalyst for low-temperature CO oxidation, Catalysis Science & Technology, 4 (2014) 1268-1275.

[67] J.-W. Lee, T.-Y. Lee, P.J. Yoo, M. Gratzel, S. Mhaisalkar, N.-G. Park, Rutile TiO_2-based perovskite solar cells, Journal of Materials Chemistry A, 2 (2014) 9251-9259.

[68] D.P. Macwan, P.N. Dave, S. Chaturvedi, A review on nano-TiO_2 sol-gel type syntheses and its applications, The Journal of Materials Science, 46 (2011) 3669-3686.

[69] H. Berger, H. Tang, F. Lévy, Growth and Raman spectroscopic characterization of TiO_2 anatase single crystals, Journal of Crystal Growth, 130 (1993) 108-112.

[70] H. Tang, H. Berger, P.E. Schmid, F. Lévy, G. Burri, Photoluminescence in TiO_2 anatase single crystals, Solid State Communications, 87 (1993) 847-850.

[71] Y. Ma, X. Wang, Y. Jia, X. Chen, H. Han, C. Li, Titanium Dioxide-based nanomaterials for photocatalytic fuel generations, Chemical Reviews, 114 (2014) 9987-10043.

[72] M. Myilsamy, V. Murugesan, M. Mahalakshmi, Indium and cerium co-doped mesoporous TiO_2 nanocomposites with enhanced visible light photocatalytic activity, Applied Catalysis A: General, 492 (2015) 212-222.

[73] L. Hu, Y. Zhang, S. Zhang, B. Li, A transparent TiO_2-C/TiO_2-graphene free-standing film with enhanced visible light photocatalysis, RSC Advances, 6 (2016) 43098-43103.

[74] E.O. Oseghe, P.G. Ndungu, S.B. Jonnalagadda, Synthesis of mesoporous Mn/TiO_2 nanocomposites and investigating the photocatalytic properties in aqueous systems, Environmental Science and Pollution Research, 22 (2015) 211-222.

[75] W. Choi, A. Termin, M.R. Hoffmann, The role of metal ion dopants in quantum-sized TiO_2: Correlation between photoreactivity and charge carrier recombination dynamics, The Journal of Physical Chemistry, 98 (1994) 13669-13679.

[76] C. Siriwong, N. Wetchakun, B. Inceesungvorn, D. Channei, T. Samerjai, S. Phanichphant, Doped-metal oxide nanoparticles for use as photocatalysts, Progress in Crystal Growth and Characterization of Materials, 58 (2012) 145-163.

[77] J. Fang, F. Wang, K. Qian, H. Bao, Z. Jiang, W. Huang, Bifunctional N-doped mesoporous TiO_2 photocatalysts, The Journal of Physical Chemistry C, 112 (2008) 18150-18156.

[78] A. Wold, Photocatalytic properties of titanium dioxide (TiO_2), Chemistry of Materials, 5 (1993) 280-283.

[79] A.M.T. Silva, C.G. Silva, G. Drazic, J.L. Faria, Ce-doped TiO_2 for photocatalytic degradation of chlorophenol, Catal. Today, 144 (2009) 13-18.

[80] E.M. Samsudin, S.B.A. Hamid, J.C. Juan, W.J. Basirun, G. Centi, Enhancement of the intrinsic photocatalytic activity of TiO_2 in the degradation of 1,3,5-triazine herbicides by doping with N.F, The Chemical Engineering Journal, 280 (2015) 330-343.

[81] J. Schneider, M. Matsuoka, M. Takeuchi, J. Zhang, Y. Horiuchi, M. Anpo, D.W. Bahnemann, Understanding TiO_2 photocatalysis: Mechanisms and Materials, Chemical Reviews, 114 (2014) 9919-9986.

[82] T.H. Tan, J. Scott, Y.H. Ng, R.A. Taylor, K.-F. Aguey-Zinsou, R. Amal, Understanding plasmon and band gap photoexcitation effects on the thermal-catalytic oxidation of ethanol by TiO_2-Supported Gold, ACS Catalysis, 6 (2016) 1870-1879.

[83] J.M. Notestein, E. Iglesia, A. Katz, Photoluminescence and charge-transfer complexes of calixarenes grafted on TiO_2 nanoparticles, Chemistry of Materials, 19 (2007) 4998-5005.

[84] Y.-H. Peng, G.-F. Huang, W.-Q. Huang, Visible-light absorption and photocatalytic activity of Cr-doped TiO_2 nanocrystal films, Advanced Powder Technology, 23 (2012) 8-12.

[85] A. Ghicov, B. Schmidt, J. Kunze, P. Schmuki, Photoresponse in the visible range from Cr doped TiO_2 nanotubes, Chemical Physics Letters, 433 (2007) 323-326.

[86] H. Zhu, J. Tao, X. Dong, Preparation and photoelectrochemical activity of Cr-doped TiO_2 nanorods with nanocavities, The Journal of Physical Chemistry C, 114 (2010) 2873-2879.

[87] N. Nasralla, M. Yeganeh, Y. Astuti, S. Piticharoenphun, N. Shahtahmasebi, A. Kompany, M. Karimipour, B.G. Mendis, N.R.J. Poolton, L. Šiller, Structural and spectroscopic study of Fe-doped TiO_2 nanoparticles prepared by sol–gel method, Scientia Iranica, 20 (2013) 1018-1022.

[88] M. Crişan, M. Răileanu, N. Drăgan, D. Crişan, A. Ianculescu, I. Niţoi, P. Oancea, S. Şomăcescu, N. Stănică, B. Vasile, C. Stan, Sol–gel iron-doped TiO_2 nanopowders with photocatalytic activity, Applied Catalysis A: General, 504 (2015) 130-142.

[89] A.-W. Xu, Y. Gao, H.-Q. Liu, The preparation, characterization, and their photocatalytic activities of rare-earth-doped TiO_2 nanoparticles, Journal of Catalysis, 207 (2002) 151-157.

[90] J. Liqiang, S. Xiaojun, X. Baifu, W. Baiqi, C. Weimin, F. Honggang, The preparation and characterization of La doped TiO_2 nanoparticles and their photocatalytic activity, Journal of Solid State Chemistry, 177 (2004) 3375-3382.

[91] S. Jeon, P.V. Braun, Hydrothermal synthesis of Er-doped luminescent TiO_2 nanoparticles, Chemistry of Materials, 15 (2003) 1256-1263.

[92] M. Tsega, F.B. Dejene, Structural and optical properties of Ce-Doped TiO_2 nanoparticles using the sol-gel process, ECS Journal of Solid State Science and Technology, 5 (2016) R17-R20.

[93] M. Khairy, W. Zakaria, Effect of metal-doping of TiO_2 nanoparticles on their photocatalytic activities toward removal of organic dyes, Egyptian Journal of Petroleum, 23 (2014) 419-426.

[94] J. Wang, Y. Yu, S. Li, L. Guo, E. Wang, Y. Cao, Doping Behavior of Zr^{4+} Ions in Zr^{4+}-Doped TiO_2 Nanoparticles, The Journal of Physical Chemistry C, 117 (2013) 27120-27126.

[95] P.M. Martins, V. Gomez, A.C. Lopes, C.J. Tavares, G. Botelho, S. Irusta, S. Lanceros-Mendez, Improving photocatalytic performance and recyclability by development of Er-doped and Er/Pr-codoped TiO_2/Poly(vinylidene difluoride)–Trifluoroethylene composite membranes, The Journal of Physical Chemistry C, 118 (2014) 27944-27953.

[96] A.S. Weber, A.M. Grady, R.T. Koodali, Lanthanide modified semiconductor photocatalysts, Catalysis Science & Technology, 2 (2012) 683-693.

[97] S. Bingham, W.A. Daoud, Recent advances in making nano-sized TiO_2 visible-light active through rare-earth metal doping, Journal of Materials Chemistry, 21 (2011) 2041-2050.

[98] G. Zhang, G. Liu, L. Wang, J.T.S. Irvine, Inorganic perovskite photocatalysts for solar energy utilization, Chemical Society Reviews, 45 (2016) 5951-5984.

[99] J. Xu, Y. Ao, D. Fu, C. Yuan, Synthesis of Gd-doped TiO_2 nanoparticles under mild condition and their photocatalytic activity, Colloids and Surfaces A: Physicochemical and Engineering Aspects, 334 (2009) 107-111.

[100] V. Mendez, K. Guillois, S. Daniele, A. Tuel, V. Caps, Aerobic methylcyclohexane-promoted epoxidation of stilbene over gold nanoparticles supported on Gd-doped titania, Dalton Transactions, 39 (2010) 8457-8463.

[101] J. Choi, P. Sudhagar, P. Lakshmipathiraj, J.W. Lee, A. Devadoss, S. Lee, T. Song, S. Hong, S. Eito, C. Terashima, T.H. Han, J.K. Kang, A. Fujishima, Y.S. Kang, U. Paik, Three-dimensional Gd-doped TiO_2 fibrous photoelectrodes for efficient visible light-driven photocatalytic performance, RSC Advances, 4 (2014) 11750-11757.

[102] D. de la Cruz, J.C. Arévalo, G. Torres, R.G.B. Margulis, C. Ornelas, A. Aguilar-Elguézabal, TiO_2 doped with Sm^{3+} by sol–gel: Synthesis, characterization and photocatalytic activity of diuron under solar light, Catalysis Today, 166 (2011) 152-158.

[103] Q. Xiao, Z. Si, Z. Yu, G. Qiu, Sol–gel auto-combustion synthesis of samarium-doped TiO_2 nanoparticles and their photocatalytic activity under visible light irradiation, Materials Science and Engineering: B, 137 (2007) 189-194.

[104] E.M. Rockafellow, L.K. Stewart, W.S. Jenks, Is sulfur-doped TiO_2 an effective visible light photocatalyst for remediation?, Applied Catalysis B: Environmental, 91 (2009) 554-562.

[105] T. Ohno, M. Akiyoshi, T. Umebayashi, K. Asai, T. Mitsui, M. Matsumura, Preparation of S-doped TiO_2 photocatalysts and their photocatalytic activities under visible light, Applied Catalysis A: General, 265 (2004) 115-121.

[106] J. Zhang, Y. Wu, M. Xing, S.A.K. Leghari, S. Sajjad, Development of modified N doped TiO_2 photocatalyst with metals, nonmetals and metal oxides, Energy Environmental Science., 3 (2010) 715-726.

[107] X. Zhang, K. Udagawa, Z. Liu, S. Nishimoto, C. Xu, Y. Liu, H. Sakai, M. Abe, T. Murakami, A. Fujishma, Photocatalytic and photoelectrochemical studies on N-doped TiO_2 photocatalyst, Journal of Photochemistry and Photobiology A: Chemistry, 202 (2009) 39-47.

[108] M. Ni, M.K.H. Leung, D.Y.C. Leung, K. Sumathy, A review and recent developments in photocatalytic water-splitting using for hydrogen production, Renewable and Sustainable Energy Reviews, 11 (2007) 401-425.

[109] A. Fujishima, X. Zhang, D.A. Tryk, TiO_2 photocatalysis and related surface phenomena, Surface Science Reports, 63 (2008) 515-582.

[110] H.M. Yadav, T.V. Kolekar, A.S. Barge, N.D. Thorat, S.D. Delekar, B.M. Kim, B.J. Kim, J.S. Kim, Enhanced visible light photocatalytic activity of Cr^{3+}-doped anatase TiO_2 nanoparticles synthesized by sol–gel method, Journal of Materials Science: Materials in Electronics, 27 (2016) 526-534.

[111] W. Raza, M.M. Haque, M. Muneer, D. Bahnemann, Synthesis of visible light driven TiO_2 coated carbon nanospheres for degradation of dyes, Arabian Journal of Chemistry.

[112] A.K. Guria, N. Pradhan, Doped or not doped: ionic impurities for influencing the phase and growth of semiconductor nanocrystals, Chemistry of Materials, 28 (2016) 5224-5237.

[113] D. Chen, Z. Jiang, J. Geng, Q. Wang, D. Yang, Carbon and nitrogen co-doped TiO_2 with enhanced visible-light photocatalytic activity, Industrial & Engineering Chemistry Research, 46 (2007) 2741-2746.

[114] X. Li, Z. Chen, Y. Shi, Y. Liu, Preparation of N, Fe co-doped TiO_2 with visible light response, Powder Technology, 207 (2011) 165-169.

[115] X. Deng, K. Chen, H. Tüysüz, Protocol for the nanocasting method: preparation of ordered mesoporous metal oxides, Chemistry of Materials, (2016).

[116] N. Linares, A.M. Silvestre-Albero, E. Serrano, J. Silvestre-Albero, J. Garcia-Martinez, Mesoporous materials for clean energy technologies, Chemical Society Reviews, 43 (2014) 7681-7717.

[117] T. Charinpanitkul, K. Faungnawakij, W. Tanthapanichakoon, Review of Recent research on nanoparticle production in thailand, Advanced Powder Technology, 19 (2008) 443-457.

[118] D. Fattakhova-Rohlfing, A. Zaleska, T. Bein, Three-dimensional titanium dioxide nanomaterials, Chemical Reviews, 114 (2014) 9487-9558.

[119] S. Mahshid, M. Askari, M.S. Ghamsari, Synthesis of TiO_2 nanoparticles by hydrolysis and peptization of titanium isopropoxide solution, Journal of Materials Processing Technology, 189 (2007) 296-300.

[120] L. Gu, A. Zhang, K. Hou, C. Dai, S. Zhang, M. Liu, C. Song, X. Guo, One-pot hydrothermal synthesis of mesoporous silica nanoparticles using formaldehyde as growth suppressant, Microporous and Mesoporous Materials, 152 (2012) 9-15.

[121] R. Ding, L. Qi, M. Jia, H. Wang, Simple hydrothermal synthesis of mesoporous spinel $NiCo_2O_4$ nanoparticles and their catalytic behavior in CH_3OH electro-oxidation and H_2O_2 electro-reduction, Catalysis Science & Technology, 3 (2013) 3207-3215.

[122] C. Guo, M. Ge, L. Liu, G. Gao, Y. Feng, Y. Wang, Directed synthesis of mesoporous TiO_2 Microspheres: Catalysts and their photocatalysis for bisphenol a degradation, Environmental Science & Technology, 44 (2010) 419-425.

[123] X. Chen, S.S. Mao, Titanium dioxide nanomaterials: Synthesis, Properties, modifications, and applications, Chemical Reviews, 107 (2007) 2891-2959.

[124] P. Pathak, M.J. Meziani, L. Castillo, Y.-P. Sun, Metal-coated nanoscale TiO_2 catalysts for enhanced CO_2 photoreduction, Green Chemistry, 7 (2005) 667-670.

[125] Z. Zhao, Method for preparing multifunctional TiO_2 nanoscale coating, Beijing Lion Trunk New Material Technology Co., Ltd., Peop. Rep. China. 4 (2016) 17-23.

[126] G.J. Owens, R.K. Singh, F. Foroutan, M. Alqaysi, C.-M. Han, C. Mahapatra, H.-W. Kim, J.C. Knowles, Sol–gel based materials for biomedical applications, Progress in Materials Science, 77 (2016) 1-79.

[127] M. Niederberger, Nonaqueous sol–gel routes to metal oxide nanoparticles, Accounts of Chemical Research, 40 (2007) 793-800.

[128] T. Zeng, Y. Chen, X. Su, Y. Li, Q. Feng, Hydrothermal steam induced crystallization synthesis of anatase TiO_2 nanoparticles with high photovoltaic response, Materials Letters, 119 (2014) 43-46.

[129] N.T.K. Thanh, N. Maclean, S. Mahiddine, Mechanisms of Nucleation and growth of nanoparticles in solution, Chemical Reviews, 114 (2014) 7610-7630.

[130] D.-H. Chen, X.-R. He, Synthesis of nickel ferrite nanoparticles by sol-gel method, Materials Research Bulletin, 36 (2001) 1369-1377.

[131] A. Hernández-Gordillo, A. Hernández-Arana, A. Campero, L.I. Vera-Robles, Biomimetic sol–gel synthesis of TiO_2 and SiO_2 nanostructures, Langmuir, 30 (2014) 4084-4093.

[132] J. Tang, F. Redl, Y. Zhu, T. Siegrist, L.E. Brus, M.L. Steigerwald, An organometallic synthesis of TiO_2 Nanoparticles, Nano Letters, 5 (2005) 543-548.

[133] S.M. M Zawawi, R. Yahya, A. Hassan, H.N.M.E. Mahmud, M.N. Daud, Structural and optical characterization of metal tungstates (MWO(4); M=Ni, Ba, Bi) synthesized by a sucrose-templated method, Chemistry Central Journal, 7 (2013) 80-80.

[134] S. Chaturvedi, P.N. Dave, N.K. Shah, Applications of nano-catalyst in new era, Journal of Saudi Chemical Society, 16 (2012) 307-325.

[135] M.M. Khan, S.A. Ansari, D. Pradhan, M.O. Ansari, D.H. Han, J. Lee, M.H. Cho, Band gap engineered TiO_2 nanoparticles for visible light induced photoelectrochemical and photocatalytic studies, The Journal of Materials Chemistry. A, 2 (2014) 637-644.

[136] M. Kapilashrami, Y. Zhang, Y.-S. Liu, A. Hagfeldt, J. Guo, Probing the optical property and electronic structure of TiO_2 nanomaterials for renewable energy applications, Chemical Reviews, 114 (2014) 9662-9707.

[137] B.L. Zhang, K. Raghavachari, Photoabsorption and photoluminescence of divalent defects in silicate and germanosilicate glasses: First-principles calculations, Physical Review B, 55 (1997) R15993-R15996.

[138] M. Anpo, M. Che, Applications of Photoluminescence techniques to the characterization of solid surfaces in relation to adsorption, catalysis, and photocatalysis, in: B.C.G. Werner O. Haag, K. Helmut (Eds.) Advances in Catalysis, Academic Press (1999) 119-257.

[139] L. Kernazhitsky, V. Shymanovska, T. Gavrilko, V. Naumov, L. Fedorenko, V. Kshnyakin, J. Baran, Photoluminescence of Cr-doped TiO_2 induced by intense UV laser excitation, Journal of Luminescence, 166 (2015) 253-258.

[140] J.M. Cole, Single-crystal X-ray diffraction studies of photo-induced molecular species, Chemical Society Reviews, 33 (2004) 501-513.

[141] S.V. Borisov, N.V. Podberezskaya, X-ray diffraction analysis: A brief history and achievements of the first century, Journal of Structural Chemistry, 53 (2012) 1-3.

[142] D.T. Crouse, X-ray diffraction and the discovery of the structure of DNA. A Tutorial and historical account of james watson and francis crick's use of x-ray diffraction in their discovery of the double helix structure of DNA, Journal of Chemical Education, 84 (2007) 803.

[143] C.R.S. Matos, M.J. Xavier, L.S. Barreto, N.B. Costa, I.F. Gimenez, Principal component analysis of x-ray diffraction patterns to yield morphological classification of brucite particles, Analytical Chemistry, 79 (2007) 2091-2095.

[144] H.S. Kaufman, I. Frankuchen, X-Ray Diffraction, Analytical Chemistry, 26 (1954) 31-34.

[145] O.E. Piro, Centennial of X-ray diffraction: development of an unpromising experiment with a wrong explanation, Crystallography Reviews, 22 (2016) 197-219.

[146] R.E. Dinnebier, S.J.L. Billinge, Principles of powder diffraction, Royal Society of Chemistry, 2008, 1-19.

[147] R.E. Dinnebier, S.J. Billinge, Principles of Powder Diffraction, Royal Society of Chemistry, 05 (2008) 1-19

[148] H.P. Klug, L.E. Alexander, X-ray diffraction procedures, Wiley New York (1954). 19-23

[149] R.E. Dinnebier, Powder diffraction: theory and practice, Royal Society of Chemistry 118 (2008). 1-19

[150] Y. Aray, A.B. Vidal, J. Rodriguez, M.E. Grillo, D. Vega, D.S. Coll, First Principles Study of Low Miller Index RuS2 Surfaces in Hydrotreating Conditions, The Journal of Physical Chemistry C, 113 (2009) 19545-19557.

[151] C.H.L. Kennard, L. Bretherton, Teaching aids illustrating the concept of Miller Index, Journal of Chemical Education, 56 (1979) 38.

[152] Conventions in Chemistry, The ACS Style Guide, American Chemical Society (2006) 255-286.

[153] G.S. Bumbrah, R.M. Sharma, Raman spectroscopy – Basic principle, instrumentation and selected applications for the characterization of drugs of abuse, Egyptian Journal of Forensic Sciences, 6 (2016) 209-215.

[154] R.S. Das, Y.K. Agrawal, Raman spectroscopy: Recent advancements, techniques and applications, Vibrational Spectroscopy, 57 (2011) 163-176.

[155] I. Pence, A. Mahadevan-Jansen, Clinical instrumentation and applications of Raman spectroscopy, Chemical Society Reviews, 45 (2016) 1958-1979.

[156] T.W. Collette, T.L. Williams, The role of Raman spectroscopy in the analytical chemistry of potable water, Journal of Environmental Monitoring, 4 (2002) 27-34.

[157] L.A. Austin, S. Osseiran, C.L. Evans, Raman technologies in cancer diagnostics, Analyst, 141 (2016) 476-503.

[158] M. Hu, J. Chen, M. Marquez, Y. Xia, G.V. Hartland, Correlated Rayleigh Scattering Spectroscopy and Scanning Electron Microscopy Studies of Au−Ag Bimetallic Nanoboxes and Nanocages, The Journal of Physical Chemistry C, 111 (2007) 12558-12565.

[159] R.J. Clarke, A. Oprysa, Fluorescence and Light Scattering, Journal of Chemical Education, 81 (2004) 705.

[160] F.C. Basilio, P.T. Campana, E.M. Therézio, N.M. Barbosa Neto, F. Serein-Spirau, R.A. Silva, O.N. Oliveira, A. Marletta, Ellipsometric Raman Spectroscopy, The Journal of Physical Chemistry C, 120 (2016) 25101-25109.

[161] S.A. Borman, Nonlinear Raman spectroscopy, Analytical Chemistry, 54 (1982) 1021A-1026A.

[162] D.A. Long, Introduction to Raman spectroscopy, RSC Anal. Spectrosc. Monogr., 9 (2005) 17-40.

[163] A.D. Buckingham, Solvent effects in vibrational spectroscopy, Transactions of the Faraday Society, 56 (1960) 753-760.

[164] J.-U. Lee, D. Yoon, H. Cheong, Estimation of young's modulus of graphene by raman spectroscopy, Nano Letters, 12 (2012) 4444-4448.

[165] B.Z. Chowdhry, J.P. Ryall, T.J. Dines, A.P. Mendham, infrared and raman spectroscopy of eugenol, isoeugenol, and methyl eugenol: conformational analysis and vibrational assignments from density functional theory calculations of the anharmonic fundamentals, The Journal of Physical Chemistry A, 119 (2015) 11280-11292.

[166] R.S. Tobias, Raman spectroscopy in inorganic chemistry. I. Theory, Journal of Chemical Education, 44 (1967) 2.

[167] M. Kruk, M. Jaroniec, Gas adsorption characterization of ordered organic−inorganic nanocomposite materials, Chemistry of Materials, 13 (2001) 3169-3183.

[168] M. Jaroniec, P.F. Fulvio, Standard nitrogen adsorption data for α-alumina and their use for characterization of mesoporous alumina-based materials, Adsorption, 19 (2013) 475-481.

[169] P.I. Ravikovitch, A.V. Neimark, Characterization of nanoporous materials from adsorption and desorption isotherms, Colloids and Surfaces A: Physicochemical and Engineering Aspects, 187–188 (2001) 11-21.

[170] K. Sing, The use of nitrogen adsorption for the characterisation of porous materials, Colloids and Surfaces A: Physicochemical and Engineering Aspects, 187–188 (2001) 3-9.

[171] K.S.W. Sing, Characterization of porous materials: past, present and future, Colloids and Surfaces A: Physicochemical and Engineering Aspects, 241 (2004) 3-7.

[172] T. Zelenka, Adsorption and desorption of nitrogen at 77 K on micro-and meso-porous materials: Study of transport kinetics, Microporous and Mesoporous Materials, 227 (2016) 202-209.

[173] A.V. Neimark, P.I. Ravikovitch, Capillary condensation in MMS and pore structure characterization, Microporous and Mesoporous Materials, 44–45 (2001) 697-707.

[174] M. Thommes, Physical adsorption characterization of nanoporous materials, Chemie Ingenieur Technik, 82 (2010) 1059-1073.

[175] J. Hwang, S. Kataoka, A. Endo, H. Daiguji, Adsorption and desorption of water in two-dimensional hexagonal mesoporous silica with different pore dimensions, The Journal of Physical Chemistry C, 119 (2015) 26171-26182.

[176] R.M. Barrer, N. McKenzie, J.S.S. Reay, Capillary condensation in single pores, Journal of Colloid Science, 11 (1956) 479-495.

[177] G. Mason, The effect of pore space connectivity on the hysteresis of capillary condensation in adsorption—desorption isotherms, Journal of Colloid and Interface Science, 88 (1982) 36-46.

[178] E. Ozensoy, E.I. Vovk, In-Situ vibrational spectroscopic studies on model catalyst surfaces at elevated pressures, Topics in Catalysis, 56 (2013) 1569-1592.

[179] H.W. Siesler, Y. Ozaki, S. Kawata, H.M. Heise, Near-infrared spectroscopy: principles, instruments, applications, John Wiley & Sons2008.

[180] H. Susi, D.M. Byler, Resolution-enhanced fourier transform infrared spectroscopy of enzymes, Methods in enzymology, 130 (1986) 290-311.

[181] G. Reich, Near-infrared spectroscopy and imaging: basic principles and pharmaceutical applications, Advanced drug delivery reviews, 57 (2005) 1109-1143.

[182] T. Batakliev, V. Georgiev, M. Anachkov, S. Rakovsky, G.E. Zaikov, Ozone decomposition, Interdisciplinary Toxicology, 7 (2014) 47-59.

[183] J.L. Sotelo, F.J. Beltran, F.J. Benitez, J. Beltran-Heredia, Ozone decomposition in water: kinetic study, Industrial & Engineering Chemistry Research, 26 (1987) 39-43.

[184] H. Tomiyasu, H. Fukutomi, G. Gordon, Kinetics and mechanism of ozone decomposition in basic aqueous solution, Inorganic Chemistry, 24 (1985) 2962-2966.

[185] M.M. Huber, S. Canonica, G.-Y. Park, U. von Gunten, Oxidation of pharmaceuticals during ozonation and advanced oxidation processes, Environmental Science & Technology, 37 (2003) 1016-1024.

[186] D.C. McDowell, M.M. Huber, M. Wagner, U. von Gunten, T.A. Ternes, Ozonation of carbamazepine in drinking water: identification and kinetic study of major oxidation products, Environmental Science & Technology, 39 (2005) 8014-8022.

[187] L. Yang, C. Hu, Y. Nie, J. Qu, Catalytic ozonation of selected pharmaceuticals over mesoporous alumina-supported manganese oxide, Environmental Science & Technology, 43 (2009) 2525-2529.

[188] O. Adedayo, S. Javadpour, C. Taylor, W.A. Anderson, M. Moo-Young, Decolourization and detoxification of methyl red by aerobic bacteria from a wastewater treatment plant, World Journal of Microbiology and Biotechnology, 20 (2004) 545-550.

[189] G. Muthuraman, T.T. Teng, Extraction of methyl red from industrial wastewater using xylene as an extractant, Progress in Natural Science, 19 (2009) 1215-1220.

[190] L.M.d. Silva, W.F. Jardim, Trends and strategies of ozone application in environmental problems, Química Nova, 29 (2006) 310-317.

[191] K. Turhan, S.A. Ozturkcan, Decolorization and degradation of reactive dye in aqueous solution by ozonation in a semi-batch bubble column reactor, Water, Air, & Soil Pollution, 224 (2012) 1353.

[192] M.B. Gilliard, C.A. Martín, A.E. Cassano, M.E. Lovato, Reaction kinetic model for 2,4-dichlorophenoxyacetic acid decomposition in aqueous media including direct photolysis, direct ozonation, ultraviolet C, and pH enhancement, Industrial & Engineering Chemistry Research, 52 (2013) 14034-14048.

[193] P.R. Gogate, A.B. Pandit, A review of imperative technologies for wastewater treatment I: oxidation technologies at ambient conditions, Advances in Environmental Research, 8 (2004) 501-551.

[194] J. Zazo, J. Casas, A. Mohedano, M. Gilarranz, J. Rodriguez, Chemical pathway and kinetics of phenol oxidation by Fenton's reagent, Environmental science & technology, 39 (2005) 9295-9302.

[195] T.M. Vogel, C.S. Criddle, P.L. McCarty, ES&T critical reviews: transformations of halogenated aliphatic compounds, Environmental Science & Technology, 21 (1987) 722-736.

[196] P.P.K. Kuo, E.S.K. Chian, B.J. Chang, Identification of end products resulting from ozonation and chlorination of organic compounds commonly found in water, Environmental Science & Technology, 11 (1977) 1177-1181.

[197] F. Keppler, R. Eiden, V. Niedan, J. Pracht, H. Schöler, Halocarbons produced by natural oxidation processes during degradation of organic matter, Nature, 403 (2000) 298-301.

[198] T.E. Agustina, H.M. Ang, V.K. Vareek, A review of synergistic effect of photocatalysis and ozonation on wastewater treatment, Journal of Photochemistry and Photobiology C: Photochemistry Reviews, 6 (2005) 264-273.

[199] Y. Lee, U. von Gunten, Advances in predicting organic contaminant abatement during ozonation of municipal wastewater effluent: reaction kinetics, transformation products, and changes of biological effects, Environmental Science: Water Research & Technology, 2 (2016) 421-442.

[200] M. Sui, L. Sheng, K. Lu, F. Tian, FeOOH catalytic ozonation of oxalic acid and the effect of phosphate binding on its catalytic activity, Applied Catalysis B: Environmental, 96 (2010) 94-100.

[201] J. Nawrocki, B. Kasprzyk-Hordern, The efficiency and mechanisms of catalytic ozonation, Applied Catalysis B: Environmental, 99 (2010) 27-42.

[202] B. Legube, N. Karpel Vel Leitner, Catalytic ozonation: a promising advanced oxidation technology for water treatment, Catalysis Today, 53 (1999) 61-72.

[203] B. Kasprzyk-Hordern, M. Ziółek, J. Nawrocki, Catalytic ozonation and methods of enhancing molecular ozone reactions in water treatment, Applied Catalysis B: Environmental, 46 (2003) 639-669.

[204] S. Maddila, V.D.B.C. Dasireddy, S.B. Jonnalagadda, Ce-V loaded metal oxides as catalysts for dechlorination of chloronitrophenol by ozone, Applied Catalysis B: Environmental, 150–151 (2014) 305-314.

[205] E.C. Chetty, V.B. Dasireddy, S. Maddila, S.B. Jonnalagadda, Efficient conversion of 1,2-dichlorobenzene to mucochloric acid with ozonation catalyzed by V_2O_5 loaded metal oxides, Applied Catalysis B: Environmental, 117–118 (2012) 18-28.

[206] O. Gimeno, F.J. Rivas, F.J. Beltrán, M. Carbajo, Photocatalytic ozonation of winery wastewaters, Journal of Agricultural and Food Chemistry, 55 (2007) 9944-9950.

[207] A. Hassani, A. Khataee, S. Karaca, M. Fathinia, Heterogeneous photocatalytic ozonation of ciprofloxacin using synthesized titanium dioxide nanoparticles on a montmorillonite support: parametric studies, mechanistic analysis and intermediates identification, RSC Advances, 6 (2016) 87569-87583.

CHAPTER TWO

Ozone facilitated degradation of caffeine using Ce-TiO_2 catalyst

Vuyolwethu O. Ndabankulu, Suresh Maddila and Sreekantha B Jonnalagadda*

*School of Chemistry & Physics, University of KwaZulu-Natal, Westville Campus, Chiltern Hills, Durban-4000, South Africa.

***Corresponding Author:** Prof. Sreekantha B. Jonnalagadda

School of Chemistry & Physics,

University of KwaZulu-Natal,

Durban 4000, South Africa.

Tel.: +27 31 2607325,

Fax: +27 31 2603091

E-mail: **jonnalagaddas@ukzn.ac.za**

Abstract

The ozone initiated oxidation of caffeine in an aqueous system catalyzed by different loadings of ceria doped on titania was investigated under various pH conditions. Nano-catalysts with different loadings of Ce on TiO_2 were synthesized by sol-gel route and characterized by SEM, TEM, BET, and P-XRD spectral techniques. The results showed that the material retained a highly ordered mesoporous structure and possessed large surface area. Catalyst activity was evaluated for degradation of caffeine. Effect of different oxidation methods based on their first-order rate constants were compared. The combination of catalyst Ce-TiO_2 and ozone aeration significantly enhanced the degradation of caffeine compared to uncatalysed ozone (O_3), through enhanced ozone decomposition into OH radicals in aqueous solution and the oxidation of caffeine ensued via the free radical mechanism. A kinetic study exhibited the degradation in Ce-TiO_2/O_3 followed the Langmuir–Hinshelwood equation. Using Liquid chromatography-mass spectroscopy (LC-MS), degradation products were analysed. One reaction intermediate and one final product were positively identified.

Key words: Ce-TiO_2, Heterogeneous catalyst, Ozone, Catalytic ozonation, Caffeine, Degradation.

1 Introduction

Environmental pollution and water contamination are some of the biggest concerns to the humanity in the past few decades. One of the sources the environmental and water pollution is contamination by organic pollutants. Waste generation is associated with an increase in population, which has led to an excess production of pharmaceuticals, pesticides, and personal care products (PCPs) which are the major contributors in the environment [1-3]. The problem that arise from over use of these substances is the fact that all these substances are very stable and highly resistant to degradation. Of all these organic pollutants, pharmaceuticals are the biggest contributors of water pollution. Polychlorinated aromatic pharmaceuticals are characteristic of being water insoluble, non-biodegradable, thermally stable, non-flammable and highly persistent in the environment etc. Due to their persistence, non-biodegradability, bioaccumulation and toxicity these chemicals possess a potential health risk to both humans and animals [4-7].

Application of advanced oxidation processes (AOPs) in wastewater treatment is one of the most widely used techniques in recent years. AOPs are efficient in promoting non-selective oxidation of wide range of organic pollutants in aqueous solution that is based on the

combination of two or more degradation techniques [8, 9]. Ozone is a powerful oxidant agent, which is used in degradation organic pollutants in wastewater treatment. However, there is a limitation with application of ozone only in removal of these pollutants [10]. Ozone aeration alone has proven to be less efficient in removal or refractory organic pollutants, because in some cases it leads to formation of more toxic by product. Coupling ozone with other oxidants or techniques such as O_3/H_2O_2, UV/O_3, catalyst/O_3 or catalyst/O_3/UV has shown to yield higher efficiency [11, 12]. Catalytic ozonation with metal oxides as catalysts has shown to enhance the removal of most organic pollutants in water systems. It was developed to overcome the limitations such as formation of unwanted and harmful by-products. Catalytic ozonation on metal oxide catalysts is generally accepted to occur in two ways: ozone decomposition on the catalyst surface generating hydroxyl radicals and direct ozone oxidation of surface metal-organic complexes [13-15].

Heterogeneous catalysts have attracted a wide-ranging attention for potential application in catalytic degradation of environmental organic pollutants. Mainly, heterogeneous catalysis is a green technology for water treatment to remove recalcitrant organic compounds. It has a potential to remove organic pollutants in wastewater even though it is little slow process. Among the catalysts that have been studied, crystalline titania was considered a promising support catalyst for degradation of pollutants due to its notable characteristics comprising good activity, high stability in aqueous systems and low cost. Doping of titania with metals could also substantially improve its catalytic activity. Transition metal doped titania is reported to show higher catalytic activity under ozonation. Cerium salts are commonly used as dopants and their usefulness is demonstrated through ease of handling, low-cost, high stability and non-hazardous properties. Unwanted environmental and economic features [17] frequently thwart their use in stoichiometric quantities. Lanthanide doped titania has drawn an ample attention due to their distinct 4f electronic configuration. Amongst them, ceria doping drawn additional interest, possibly due to the redox couple, Ce^{3+} or Ce^{4+} creates cerium oxide shift between CeO_2 under oxidizing and reducing conditions. Various electronic configurations of ($4f^15d^0$) could result in different optical properties and different catalytic properties. Ozonation in presence of catalyst produces hydroxyl radicals that are non-selective and powerful enough to oxidise even refractory organic pollutants and eventually form CO_2, inorganics and H_2O. It occurs when generated electrons or radicals are trapped by dissolved ozone there by retarding the charge carrier recombination process this then increase $^{\bullet}OH$ radicals generated. When ozone is trapped with catalyst, it also leads to formation of ozonide radicals ($O_3^{\bullet-}$) which leads to the production of more $^{\bullet}OH$ radicals [16-19].

Herein, different loadings of ceria doped on titania were synthesized via incipient sol-gel method. The ozone aeration in presence of catalyst exhibited higher efficiency for the degradation. This was mainly due to the multivalent oxidation states of Ce, high dispersion of metal oxide and the enhanced interfacial electron transfer process. The catalytic mechanism of caffeine degradation over Ce/TiO_2 with ozone was discussed.

2 Experimental Section

Titanium (IV) isopropoxide (TIP) (MW = 284.22 97 %) (Sigma-Aldrich). Non-ionic surfactant (Pluronic F-127) (Sigma-Aldrich), Caffeine (Sigma-Aldrich), Absolute ethanol, Cerium acetylacetonate hydrate (Sigma-Aldrich), Hydrochloric acid, Sodium hydroxide.

2.1 Catalyst preparation

Sol gel method was adopted for the synthesis different loadings of ceria (0.1, 0.5 and 1.0 wt %) on titania support. For a typical run, 60 ml of absolute ethanol was mixed with 2 g of Pluronic F-127 in a closed 400 ml Pyrex beaker and placed under magnetic stirring for 4 h. In the resultant clear solution, 6 ml of TIP was added drop wise and stirred further for 2 h. Cerium acetylacetonate hydrate was dissolved in 36 ml deionised water and added into the solution. The mixture was stirred for 24 h and stopped and the resulting mixture was aged overnight in the dark at room temperature. After aging the gel separated from the solvent, the solvent was the decanted. The gel was dried in an oven at 80 °C for 12 h and a yellowish solid was obtained. The solid was cooled at room temperature and ground to form a powder. The powder was then place into an alumina boat and transferred into a furnace. The material was calcined at 450 °C for 4 h (ramp rate = 2 °C/ min) to obtain a white powder TiO_2.

2.2 Instrumentation details

Surface morphology of the synthesised material were characterised by scanning electron microscope (ZEISS ULtralpus FEG-SEM). (JOEL JEM 1010) transmission electron microscope was used to obtain the physical structural characteristics. Bruker D2 phase Powder X-ray diffraction (PXRD) equipped with a CuK_α radiation ($\lambda = 0.15401$) was used to obtain diffractogram. The texture characterisation was determined using a micrometric flow 3030 instrument. All samples were degassed on micrometric flow prep (060) under nitrogen flow at 90 °C for 1 h then temperature was ramped to 200 °C for 12 h to allow the samples to degas before the textural analysis.

2.3 Catalytic Ozone experiments

Ozone and catalytic experiments were carried out in a simple open quartz reactor using with ozone generator. Before the start of each experiment, 0.05 g of the catalyst was added in

300 mL caffeine solution (5 mg/L). The solution was then mixed through ultrasonication for 10 min before equilibrating in the dark for 1 h. Then, ozone was generated from pure oxygen using Mighty Zone mzpvL-8000 Ozone generator. Ozone was bubbled through the solution at constant flow rate of 10 ml per minute at constant inlet of 5 mg/L. The steady ozone concentration in water was controlled by adjusting the electric current of the ozone generator at 0.2 A. Iodometric titration method was used to determine ozone concentration. Continuous stirring of the solution was maintained using a magnetic stirrer. A typical experiment was done over 120 min with samples collected every 20 min intervals. Sodium thiosulphate (0.1 M) was used to quench excess ozone before analysis. Further, 3 mL of the solution was taken, centrifuged and samples were analysed using UV/VIS spectrophotometer.

3 Results and discussion

3.1 Morphology analysis

Figure 1 shows the SEM and TEM micrographs of the as prepared materials. It can be seen in SEM (a) and TEM (b) images, the materials show agglomerated, and irregular shaped particles with inter particle voids, which were observed to be formed from aggregates of the agglomerated particles consisting of Ce and Ti in their oxide. EDX mapping was used to confirm quantitatively the composition and distribution of the dopant on the as prepared material. The result obtained from EDX mapping displayed the presence of a well distributed dopant Ce on the surface of TiO_2

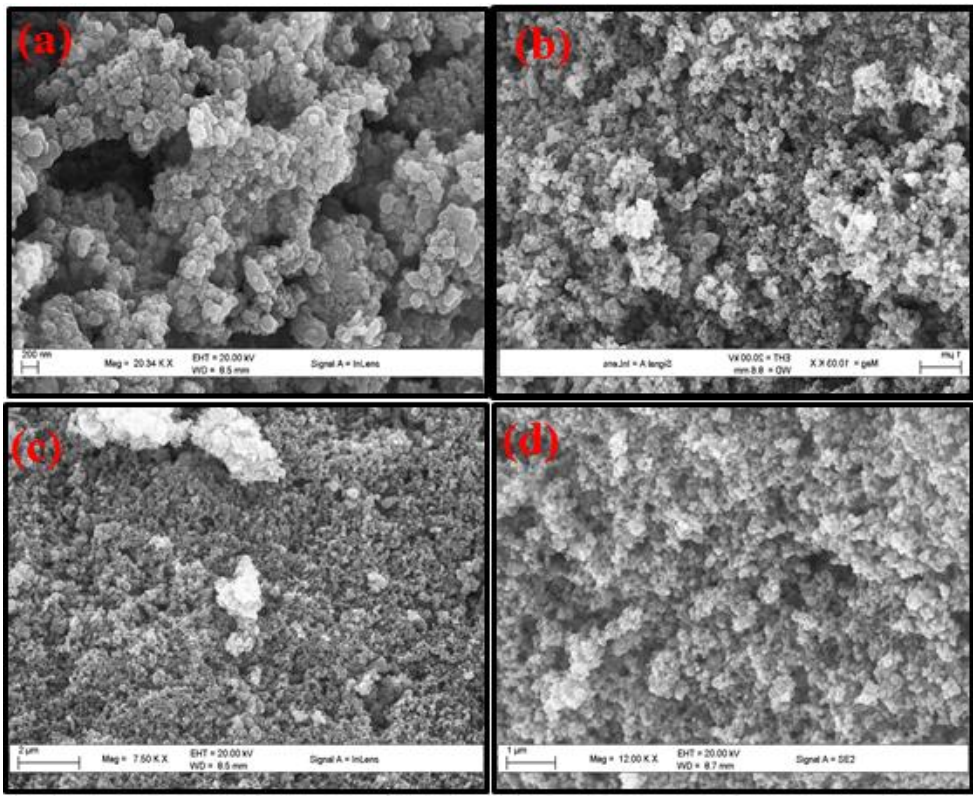

Figure.1 (a): SEM, (a) bare TiO_2 (b) 0.1% Ce-TiO_2 (c) 0.5% Ce-TiO_2 and (d) 1.0% Ce-TiO_2 as prepared material

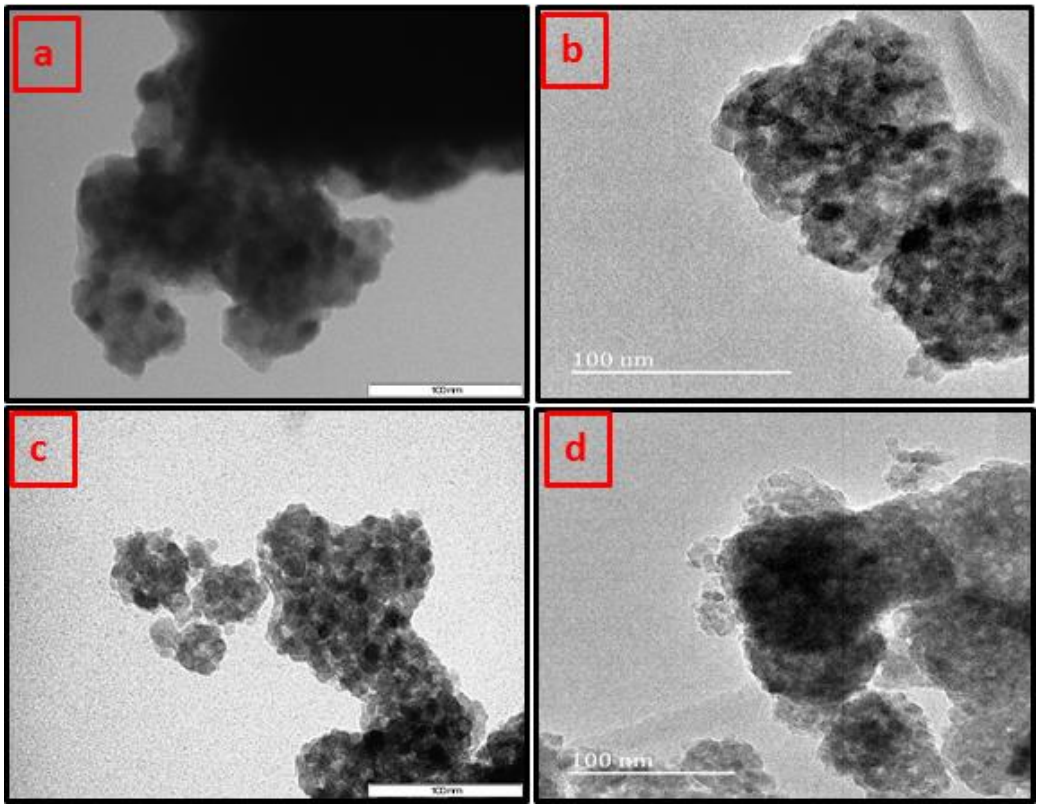

Figure 1 (b): TEM, (a) bare TiO_2 (b) 0.1% Ce-TiO_2 (c) 0.5% Ce-TiO_2 and (d) 1.0% Ce-TiO_2 as prepared material

3.2 Textural properties

N_2 sorption isotherm was used to evaluate the textural properties of the materials and is displayed in **figure 2**. The material was observed to be characteristics of the type IV isotherm with dual H1 hysteresis loops, which appears at 0.45–0.79 P/Po and 0.92–0.98 P/Po. The textural properties of the material obtained from N_2 sorption isotherm experiments are summarized in table.1. The hysteresis loop observed in the isotherm is caused by the presence of micropores, which are formed from inter-particle voids.

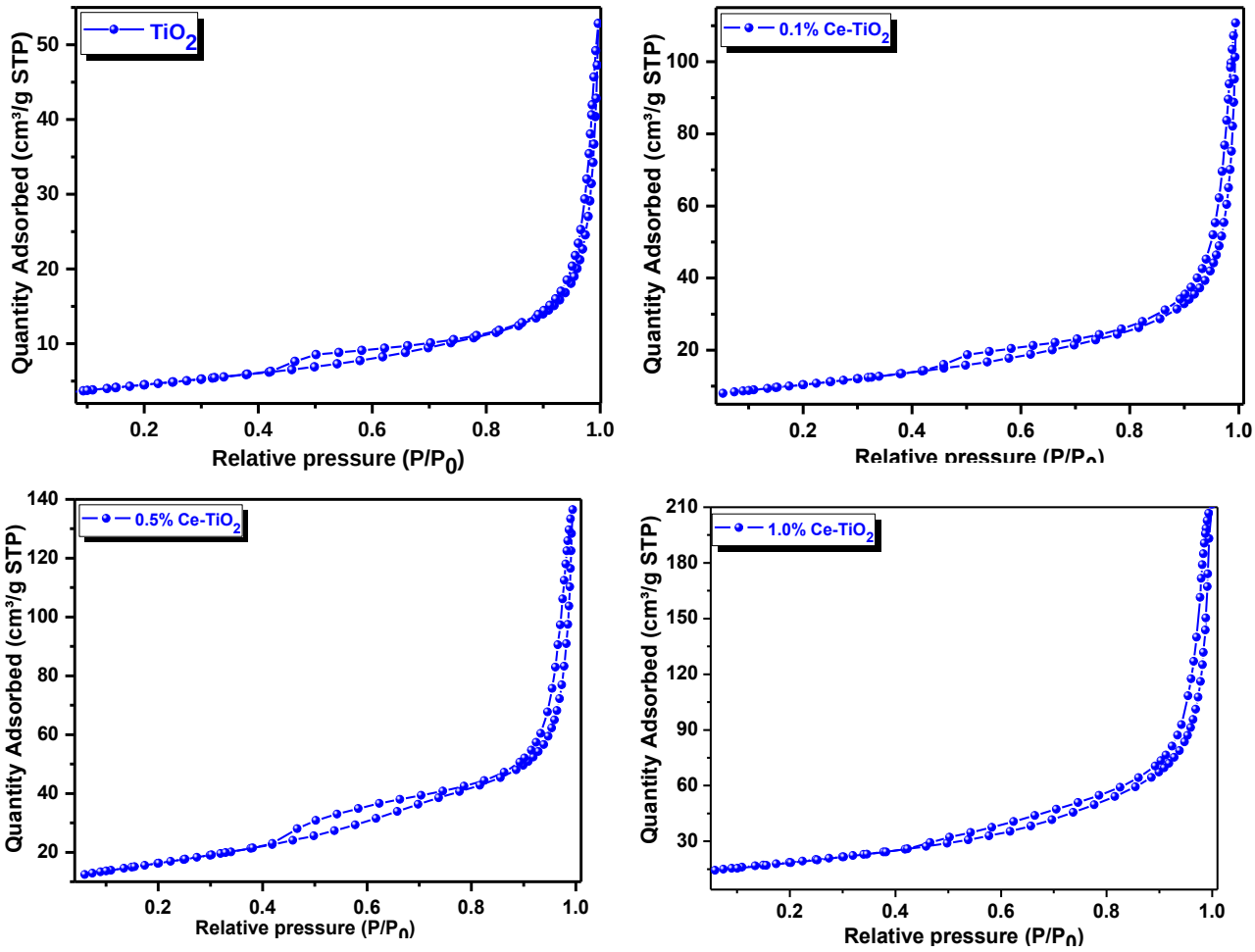

Figure 2: N_2 sorption isotherm of (a) bare TiO_2 (b) 0.1% Ce-TiO_2 (c) 0.5% Ce-TiO_2 and (d) 1.0% Ce-TiO_2 as prepared material

3.3 XRD analysis

Figure 3 displays the XRD pattern of Ce-TiO_2 nano-particles. Powder XRD was used to study information about the phase structure, and crystal size of the material. The sample consists of anatase as a single phase (JCPDS, No. 21-1272). No unanticipated phases were observed in XRD and there was no crystalline phase attributed to cerium oxides can be found. The average crystallite size for the anatase diffraction peak (101) was calculated using Debye–Scherrer formula and is shown in table 1.

$$D = \frac{K\lambda}{\beta \mathrm{Cos}\theta}$$

Where D is the crystallite size in nm, K is Scherrer's constant ≈ 0.9, λ is the wavelength of the X-ray radiation (CuK_α = 0.15406 nm). β is the corrected band broadening (full width at half-maximum (FWHM)) of the diffraction peak, and θ is the diffraction angle [20].

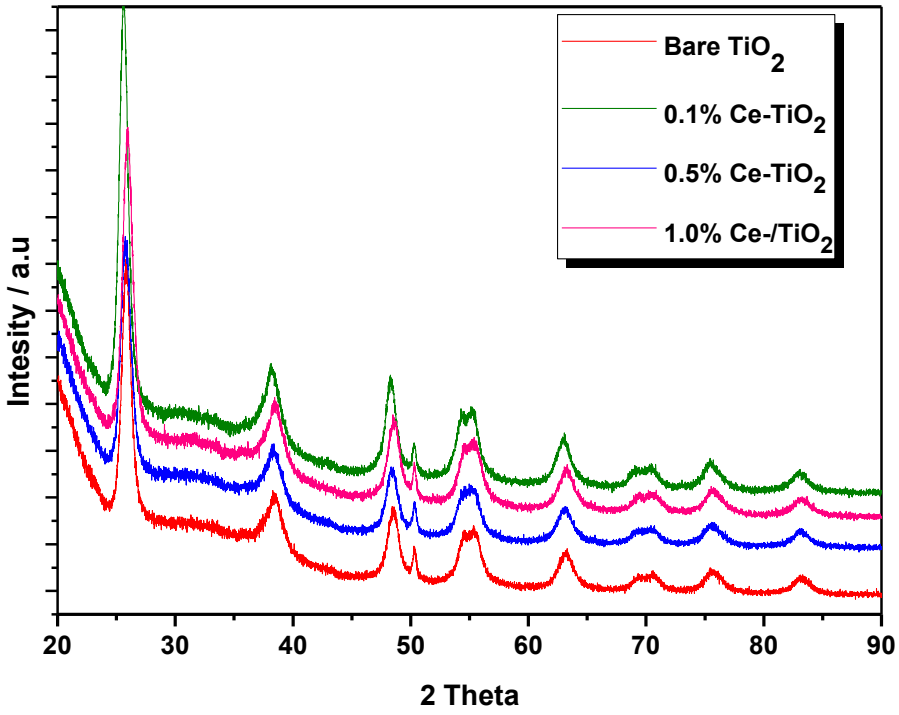

Figure 3: Powder XRD pattern of the as prepared material of (a) bare TiO_2 (b) 0.1% Ce-TiO_2 (c) 0.5% Ce-TiO_2 and (d) 1.0% Ce-TiO_2 as prepared material

Table1: Summary of the textural characterizations and XRD analysis for the prepared materials

Sample Wt%	BET Surface area/ $m^2 g^{-1}$	BJH adsorption pore volume/ $cm^3 g^{-1}$	BJH adsorption pore size / nm	FWHM (101) / rad	Anatase crystal size (101) / nm	EDX / Wt. %
Bare TiO_2	15.955	0.0841	18.012	0.01556	8.92	--
0.1% Ce/TiO_2	36.754	0.1762	17.232	0.01829	7.58	0.098
0.5% Ce/TiO_2	57.884	0.2229	12.613	0.01902	7.29	0.481
1.0% Ce/TiO_2	66.048	0.3342	16.475	0.01831	7.54	1.025

3.4 Catalytic ozonation

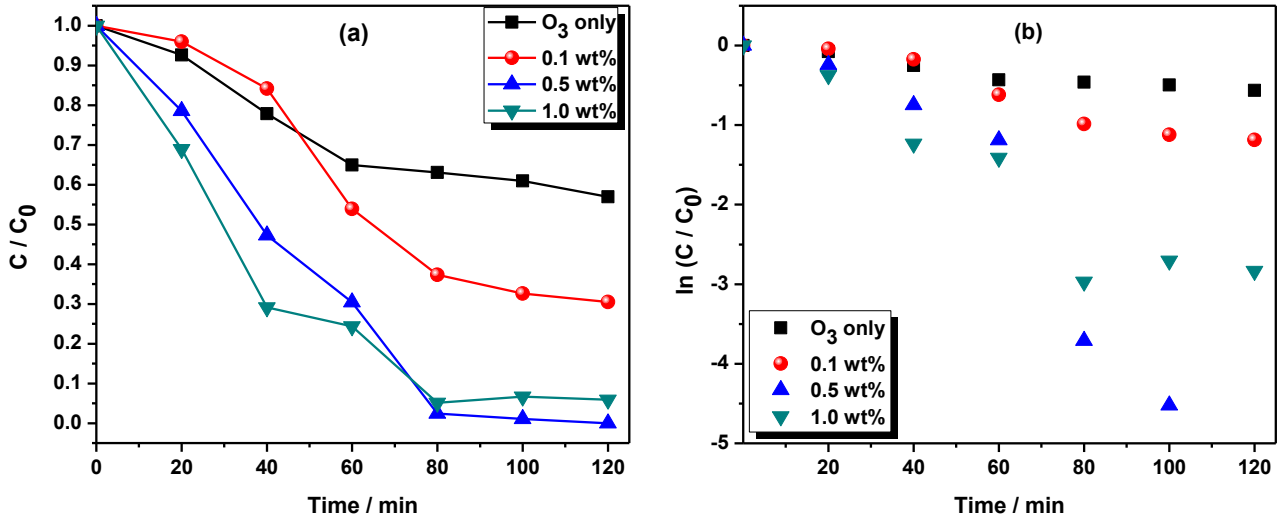

Figure 4: (a) Catalytic degradation of caffeine with Ce/TiO_2 and ozone only. **(b)** Kinetic of degradation of caffeine

Degradation studies of caffeine were evaluated using different methods are depicted in **figure 4**. A first order kinetic model was used to fit the obtained experimental data.

$$-\frac{dC_{Caffeine}}{dt} = k.\,C_{Caffeine} \qquad (1)$$

Where $C_{Caffeine}$ the concentration of caffeine and k is is the first order rate constant with respect to caffeine. Assuming $C_{Caffeine} = C_{Caffeine,0}$ when t = 0, integrating equation (1) gives

$$\ln\frac{C_0}{C} = kt \qquad (2)$$

Where C_0 is the initial concentration of caffeine when t = 0, C is caffeine concentration any time (t) during the reaction.

Using 2.5 mg/L of ozone yielded 47.5 % degradation efficiency in 120 minute. Combining ozone with catalyst is known to enhance the formation of hydroxyl radicals, which are required for catalytic ozonation of organic pollutant. The amount of loading used proved to influence degradation efficiency. This influence was observed when different loadings of Ce were tested in catalytic ozonation reaction. 0.1 wt% yielded the lowest efficiency of the three, with 70 % degradation efficiency. A, 0.5 wt % catalyst had 100 % degradation efficiency in the given time and 1.0 wt% had 99 % degradation efficiency. These results were expected, since it can be easily assumed that increasing catalyst loading leads to higher degradation efficiency. Ozone concentration was kept constant for the duration of the experiment. Catalysed ozonation is one of the most powerful oxidising methods among the advanced oxidation processes. It is characterised by production of highly reactive and non-selective hydroxy radicals. This was attributed to the formation of more hydroxyl radicals compared to catalyst and/or ozonation process alone. All these reactions were done in natural pH using caffeine as organic substrate.

Ozone and catalytic ozonation of caffeine occurs at liquid phase through direct and indirect mechanisms. Direct mechanism refers to the decomposition of ozone in water thereby generating hydroxyl radicals. Indirect mechanism is influenced by catalytic ozonation, whereby different pathways generate hydroxyl radicals [11, 21, 22].

3.5 Kinetics of degradation of caffeine

Figure 4.b shows the kinetics of degradation of caffeine obtained from the equation 2. From the obtained results, degradation of caffeine in all experiments followed a first-order kinetic model, as proposed in equation1. The first-order rate constant was obtained from the plots. The obtained rate constants and R^2 values are displayed in table 2. From the table, it was observed that there was an increase in rate constant with an increase in catalyst loading but, there was a decrease in 1.0 wt% Ce/TiO_2. The 0.5 wt% catalyst had the higher catalytic efficiency than the 1.0 wt%, this was the reason it had a decreased rate constant when compared to 0.5 wt%.

Table 2: Kinetics of degradation of caffeine

Catalyst	Rate constant, (k) / min^{-1}	R^2
Ozone only	0.0049	0.9278
0.1 wt %	0.0109	0.9418
0.5 wt %	0.0478	0.8796
1.0 wt %	0.0266	0.8981

3.6 Effect of Ozone concentration

Effect of ozone dose on catalytic ozonation of caffeine was tested by increasing the concentration of ozone. Increase in initial ozone concentration leads to faster consumption of caffeine (**figure** 5). Ozone concentration 2.5 mg/L gave 100 % degradation efficiency in 80 min. When O_3 concentration was increased to 5 mg/L, 100 % degradation was achieved in 60 min. A further increase in ozone concentration showed a better efficiency. This is to be expected, since during catalytic ozonation process, some of ozone is transformed into ozonide species ($O_3^{\bullet-}$), which is used to generate hydroxy radicals, which are highly reactive in degradation of caffeine. An increase in ozone concentration is assumed to be proportion with increase in ozonide species.

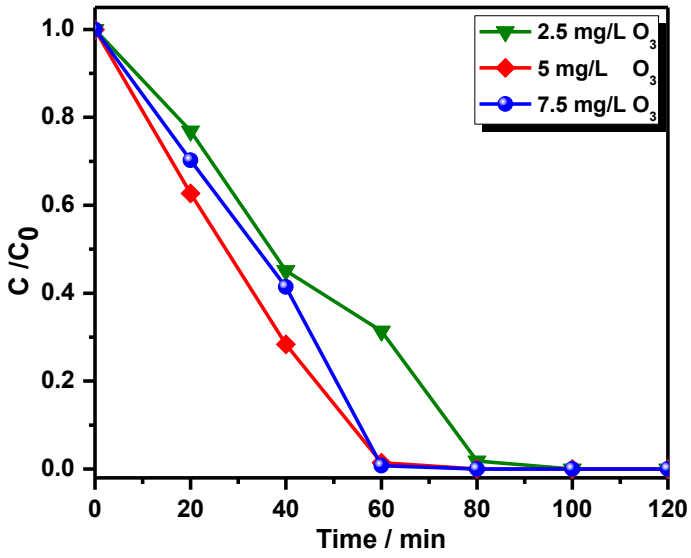

Figure 5. Effect of ozone dose on catalytic ozonation Ce/TiO_2 0.5%

3.7 Effect of pH

To investigate the effect of pH, the point of zero charge (PZC) of the material was determined. PZC of the catalyst was determined by a powder method. In a typical experiment,

0.2 g of the catalyst was added in 25 ml beaker containing 0.01 M sodium chloride solution. Several batches were carried out for various initial pH solutions. The pH was adjusted using 0.01 M HCl and 0.01 NaOH to desired pH. The electrolyte solution with catalyst was stirred for 48 h at room temperature. The final pH of each solution was then measured and plotted against initial pH, to determine the pH_{pzc} of the catalyst. The pH_{PZC} was extrapolated from the intersection point between pH_{final} and $pH_{initial}$.

Ce-TiO_2 exhibited pH_{PZC} of ≈ 6.5. This suggests that an electrostatic interaction between the catalyst and caffeine at pH less than its pH_{PZC}. The effect of pH on catalytic degradation of caffeine was evaluated by changing the initial pH of the solution from acidic to alkaline medium (pH = 2 – 10). It is known that the surface of the catalyst plays a vital role in degradation of organic pollutants in aqueous medium. An increase pH is known to increase the rate of decomposition of ozone in aqueous system, this then leads to enhanced ROS production in alkaline conditions consequently leading to higher removal of caffeine [23, 24].

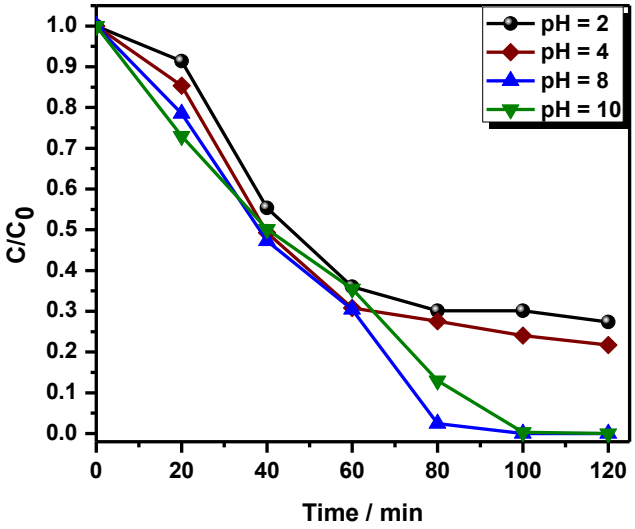

Figure.6: Effect of pH on catalytic ozonation Ce/TiO_2 0.5 wt%

Figure 6 displays the effect of pH solution in catalytic ozonation of caffeine. This was evaluated by performing catalytic ozonation at different pH values as displayed in **figure 6**. pH plays a vital role in formation of OH radicals which are an essential part of catalytic ozonation reactions. It is well known that an increase in pH will results in an increase in OH radicals since alkaline condition tend to favour the reaction. As displayed in the **figure**, at low pH values of 2 & 4 degradation of caffeine is low and not all caffeine was degraded. At high pH values 8 & 10, catalytic ozonation efficiency was increased. This was attributed to the generation of more OH radicals compared to lower pH values. It is worth noticing that high degradation efficiency was at pH 8 than pH 10. The important factor is the point of zero charge of the material, as in the case was determined to be 6.5, which is not surprising that pH 8 is favoured than pH 10.

3.8 Identification of degradation products

Identification of products was carried using LC-MS TOF. The analysis was run over a period of 5 minutes. A standard solution of pure caffeine was initially injected and was characteristic of a long intensity at m/z 194. The same conditions were used to identify product formed over time. Analysis was done by sampling after 20 minutes starting from pure caffeine. One intermediate was identified in the degradation of caffeine and one product (Supporting information). Scheme 1 depicts the proposed reaction mechanism using intermediates and product formed.

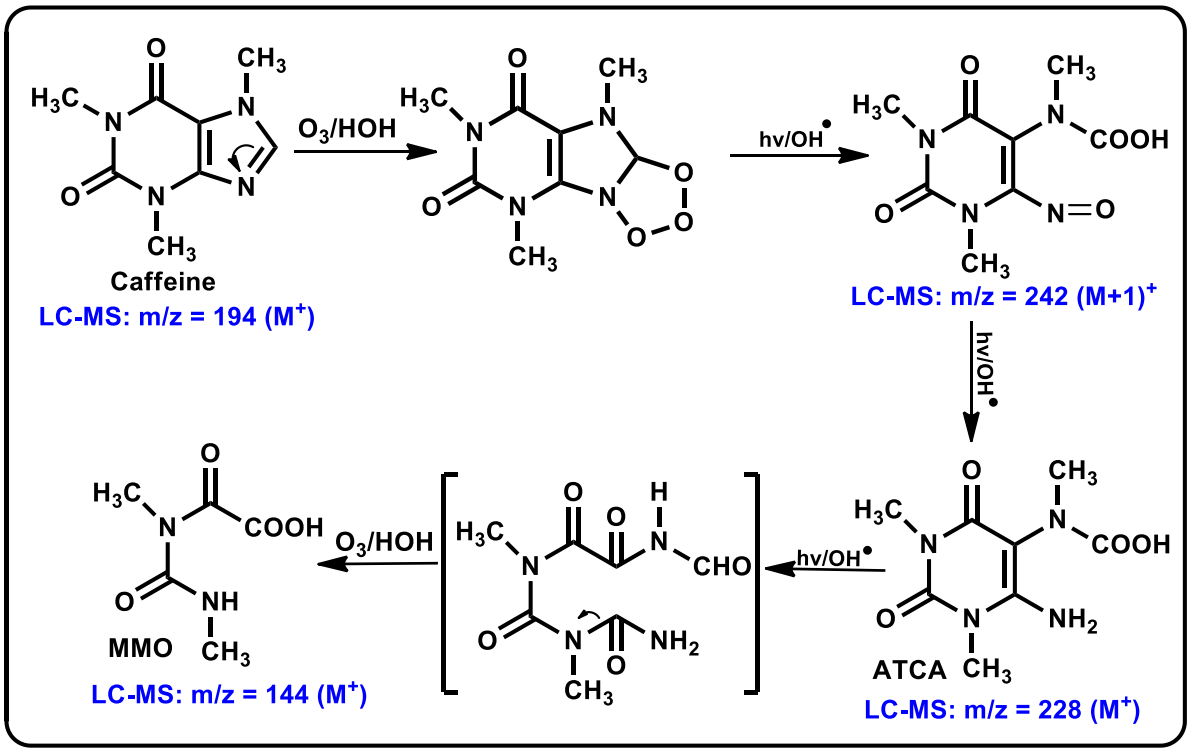

Scheme.1: Plausible reaction mechanism for catalytic ozonation of caffeine.

4 Conclusion

Extremely ordered CeO_2/TiO_2 was synthesized by a sol-gel process. The catalyst displayed the high catalytic activity for effective degradation of caffeine in ozonation process. The degradation experiments clearly indicate that catalytic ozonation has synergetic effect and higher degradation efficiency than the rest of other methods. CeO_2 doped TiO_2 significantly enhanced ozone decomposition into OH radicals in aqueous solution and concentrated ozone concentration in equilibrium. The oxidation mechanism of caffeine ensued through OH radicals. The recycled catalyst showed that CeO_2/TiO_2 retained a good catalytic activity and it was an auspicious catalyst for ozonation procedure.

Acknowledgements

The authors are thankful to the National Research Foundation (NRF) of South Africa, and University of KwaZulu-Natal, Durban, for financial support and research facilities.

References

[1] Y. Luo, W. Guo, H.H. Ngo, L.D. Nghiem, F.I. Hai, J. Zhang, S. Liang, X.C. Wang, A review on the occurrence of micropollutants in the aquatic environment and their fate and removal during wastewater treatment, Science of the Total Environment, 473 (2014) 619-641.

[2] C.G. Daughton, Chapter 1 Pharmaceuticals in the environment: sources and their management, in: M. Petrović, D. Barceló (Eds.) Comprehensive Analytical Chemistry, Elsevier2007, pp. 1-58.

[3] S.T. Glassmeyer, E.K. Hinchey, S.E. Boehme, C.G. Daughton, I.S. Ruhoy, O. Conerly, R.L. Daniels, L. Lauer, M. McCarthy, T.G. Nettesheim, K. Sykes, V.G. Thompson, Disposal practices for unwanted residential medications in the United States, Environment International, 35 (2009) 566-572.

[4] C.S. Wong, S.L. MacLeod, JEM Spotlight: Recent advances in analysis of pharmaceuticals in the aquatic environment, Journal of Environmental Monitoring, 11 (2009) 923-936.

[5] Q. Huang, Y. Yu, C. Tang, K. Zhang, J. Cui, X. Peng, Occurrence and behavior of non-steroidal anti-inflammatory drugs and lipid regulators in wastewater and urban river water of the Pearl River Delta, South China, Journal of Environmental Monitoring, 13 (2011) 855-863.

[6] S. Babic, D. Mutavdzic, D. Asperger, A.J.M. Horvat, M. Kastelan-Macan, Determination of veterinary pharmaceuticals in production wastewater by HPTLC-videodensitometry, Chromatographia, 65 (2007) 105-110.

[7] R.L. Oulton, T. Kohn, D.M. Cwiertny, Pharmaceuticals and personal care products in effluent matrices: A survey of transformation and removal during wastewater treatment and implications for wastewater management, Journal of Environmental Monitoring, 12 (2010) 1956-1978.

[8] M.M. Huber, S. Canonica, G.-Y. Park, U. von Gunten, Oxidation of pharmaceuticals during ozonation and advanced oxidation processes, Environmental Science & Technology, 37 (2003) 1016-1024.

[9] S. Palit, CHAPTER 14 Advanced environmental engineering separation processes, environmental analysis and application of nanotechnology: A far-reaching review, advanced environmental analysis: applications of nanomaterials, 1 (2017) 377-416.

[10] Q. Wang, Z. Yang, B. Chai, S. Cheng, X. Lu, X. Bai, Heterogeneous catalytic ozonation of natural organic matter with goethite, cerium oxide and magnesium oxide, RSC Advances, 6 (2016) 14730-14740.

[11] A. Hassani, A. Khataee, S. Karaca, M. Fathinia, Heterogeneous photocatalytic ozonation of ciprofloxacin using synthesized titanium dioxide nanoparticles on a montmorillonite support: parametric studies, mechanistic analysis and intermediates identification, RSC Advances, 6 (2016) 87569-87583.

[12] S. Ardizzone, G. Cappelletti, D. Meroni, F. Spadavecchia, Tailored TiO_2 layers for the photocatalytic ozonation of cumylphenol, a refractory pollutant exerting hormonal activity, Chemical Communications, 47 (2011) 2640-2642.

[13] F.J. Beltrán, F.J. Rivas, R. Montero-de-Espinosa, Ozone-Enhanced Oxidation of Oxalic Acid in Water with Cobalt Catalysts. 2. Heterogeneous Catalytic Ozonation, Industrial & Engineering Chemistry Research, 42 (2003) 3218-3224.

[14] Y. Liu, S. Wang, W. Gong, Z. Chen, H. Liu, Y. Bu, Y. Zhang, Heterogeneous catalytic ozonation of p-chloronitrobenzene (pCNB) in water with iron silicate doped hydroxylation iron as catalyst, Catalysis Communications, 89 (2017) 81-85.

[15] T. Zhang, W. Li, J.-P. Croué, Catalytic ozonation of oxalate with a cerium supported palladium oxide: an efficient degradation not relying on hydroxyl radical oxidation, Environmental Science & Technology, 45 (2011) 9339-9346.

[16] M. Sayed, L.A. Shah, J.A. Khan, N.S. Shah, J. Nisar, H.M. Khan, P. Zhang, A.R. Khan, Efficient photocatalytic degradation of norfloxacin in aqueous media by hydrothermally synthesized immobilized TiO_2/Ti Films with Exposed {001} Facets, The Journal of Physical Chemistry A, 120 (2016) 9916-9931.

[17] J. Lee, J. Kim, W. Choi, TiO_2 Photocatalysis for the redox conversion of aquatic pollutants, aquatic redox chemistry, American Chemical Society2011, pp. 199-222.

[18] S. Song, Z. Liu, Z. He, A. Zhang, J. Chen, Y. Yang, X. Xu, Impacts of morphology and crystallite phases of titanium oxide on the catalytic ozonation of phenol, Environmental Science & Technology, 44 (2010) 3913-3918.

[19] Z. He, Q. Cai, F. Hong, Z. Jiang, J. Chen, S. Song, Effective enhancement of the degradation of oxalic acid by catalytic ozonation with TiO_2 by exposure of {001} facets and surface fluorination, Industrial & Engineering Chemistry Research, 51 (2012) 5662-5668.

[20] K. Thamaphat, P. Limsuwan, B. Ngotawornchai, Phase characterization of TiO powder by XRD and TEM, Kasetsart J. (Nat. Sci.), 42 (2008) 357-361.

[21] A.C. Mecha, M.S. Onyango, A. Ochieng, C.J.S. Fourie, M.N.B. Momba, Synergistic effect of UV–vis and solar photocatalytic ozonation on the degradation of phenol in municipal wastewater: A comparative study, Journal of Catalysis, 341 (2016) 116-125.

[22] C.A. Orge, J.L. Faria, M.F.R. Pereira, Photocatalytic ozonation of aniline with TiO_2-carbon composite materials, Journal of Environmental Management.

[23] J.-C. Chou, L.P. Liao, Study on pH at the point of zero charge of TiO_2 pH ion-sensitive field effect transistor made by the sputtering method, Thin Solid Films, 476 (2005) 157-161.

[24] F. Loosli, P. Le Coustumer, S. Stoll, TiO2 nanoparticles aggregation and disaggregation in presence of alginate and Suwannee River humic acids. pH and concentration effects on nanoparticle stability, Water Research, 47 (2013) 6052-6063.

CHAPTER THREE

Photodegradation of caffeine by ceria doped TiO_2 under visible light in absence of added oxidants

Vuyolwethu O. Ndabankulu, Suresh Maddila and Sreekantha B Jonnalagadda*

*School of Chemistry & Physics, University of KwaZulu-Natal, Westville Campus, Chiltern Hills, Durban-4000, South Africa.

***Corresponding Author:** Prof. Sreekantha B. Jonnalagadda
School of Chemistry & Physics,
University of KwaZulu-Natal,
Durban 4000, South Africa.
Tel.: +27 31 2607325,
Fax: +27 31 2603091
E-mail: **jonnalagaddas@ukzn.ac.za**

Abstract

The photocatalytic activity of bare titania and ceria doped mesoporous titania (Ce/TiO_2) catalysts were evaluated for caffeine degradation under visible light illumination in absence of the oxidants. Different wt% metal loaded (bare, 0.1, 0.5 and 1.0) materials were synthesised by a sol-gel method using anionic surfactants. Various instrumentation techniques were used to characterise the prepared photo-catalysts such as BET, P-XRD, TEM, SEM-EDX, Raman, FT-IR, photoluminescence and UV-DRS spectroscopy. Ceria doped titania (0.5 wt.%) showed excellent efficiency in photo-degradation of caffeine in aqueous solution relative to all the other prepared heterogeneous catalysts. All materials showed good efficiency and were recyclable without loss of catalytic activity up to three times. Analysis of degradation products was carried with Liquid chromatograph-mass spectrometry (LC-MS)-TOF. Two reaction products 6-amino-1,3-dimethyl-2,4-dioxo-1,2,3,4-tetradropymidin-5-ly) (methyl)carbamic acid (ATCA) and *N*-methyl-N-(methylcarbomoyl)-2-oxoacetamide (MMO) were positively identified.

Keywords: Titania, Ceria, Visible light, Photocatalytic degradation, Hydroxyl radical, Caffeine

1. Introduction

The persistence of organic pollutants in water systems is one of the major concerns for the environmental protection and the entire world. Pharmaceutical compounds are a group of organic pollutants that have become an environmental topic of discussion. These are a class of micro-pollutants that have been recognised in the late 1990's, because the improvement in analytical techniques. Wastewater treatment plants (WWTP) and sewage treatment plants (STP) have been identified as major sources of environment discharge. This is because they are not designed to deal with this type of contaminants. As a result, pharmaceutical compounds have been detected in surface and ground waters and in sediments [1-4]. Pharmaceuticals may reach the aquatic environment through different pathways, i.e. from domestic wastewater from urban areas, effluent from pharmaceutical manufacturing industries, hospital disposal, and the disposal of unused medicine [5,6]. Residues of pharmaceutical chemicals in the environment and water systems have become a major issue for both consumers and producers. In view of this, it is prudent to improve technologies that promote the easy degradation of these organic compounds.

Semiconductor heterogeneous photocatalysis has been extensively been studied in the recent years for water purification and degradation of emerging contaminants in wastewater

[7,8]. Titanium dioxide (TiO_2) is one of the most investigated semiconductors that has been applied in the degradation of organic contaminates in aqueous system. Some of the attractive qualities of TiO_2 are its high activity, strong oxidizing power, chemical stability, robustness against photo-corrosion, low toxicity, eco-friendliness and cost-effectiveness [9,10]. It is well recognised that the surface-adsorbed water and OH groups can act as traps for photoexcited hole on the catalyst surface and produce $OH^{\cdot}$ radicals, which are powerful oxidants in degrading organics [11,12]. Photocatalysis using semiconductor is a three-step process. Light is used in the excitation of a semiconductor through the absorption of photons having energy greater than its band gap. This then leads to the excitation of an electron from the valence band to the conducting band, thereby creating an electron-hole pair, this then leads to the release of photon or heat which is due to the recombination of the photo-generated electrons and holes. Sometimes there is also a possibility of the migration of the photo-generated holes to move into the surface of the semiconductor [13,14]. There are some limitations with using TiO_2 as a photocatalyst, such as the large band gap energy (3.2eV) for anatase. This limits the use of TiO_2 in the ultraviolet region (< 380 nm), which is only about 5 % of the solar spectrum [15].

Some of the techniques that have been used to reduce the band gap energy to the visible region involves metal ion doping. Rare earth metals having empty 5d and incomplete 4d orbitals are ideal metals to serve as dopants and they promote photocatalysis [16,17]. Ceria has a good redox pair Ce^{3+}/Ce^{4+}, which plays a vital role as a catalyst, which led to its application as photocatalyst in degradation of dye [18]. Li *et al* has showed that doping TiO_2 with Ce increased its photocatalytic activity in degradation of 2-mercaptobenzothiazole (MBT) [19].

In this present work, we report ceria doped on TiO_2 photo catalysts in degradation of caffeine using visible light. Ceria is used as a metal dopant do reduce the band gap energy of anatase into visible region. Caffeine is used as a model compound, which among the pharmaceuticals is mostly found in wastewater treatment plant effluents.

2. Material and methods

Titanium (IV) isopropoxide (TIP) (MW = 284.22 97 %) (Sigma-Aldrich). Non-ionic surfactant (Pluronic F-127) (Sigma-Aldrich), Caffeine (Sigma-Aldrich), Absolute ethanol, Degussa P25 TiO_2 (Sigma-Aldrich), Cerium Acetylacetonate hydrate (Sigma-Aldrich), Hydrochloric acid, Sodium hydroxide. Surface morphology of the synthesised material were characterised by scanning electron microscope (ZEISS ULtralpus FEG-SEM). (JOEL JEM 1010) transmission electron microscope was used to obtain the physical structural characteristics. Bruker D2 phase Powder X-ray diffraction (PXRD) equipped with a Cu Kα

radiation (λ = 0.15401) was used to obtain diffractogram. The texture characterisation were determined using a micrometric flow 3030 instrument. All samples were degassed on micrometric flow prep (060) under nitrogen flow at 90 °C for 1 h then temperature was ramped to 200 °C for 12 h to allow the samples to degas before the textural analysis. Fourier Transmission Infrared (FTIR) spectrometer (Perkin Elmer spectrum 100 series with universal accessory) was used. Photoluminescence spectrum were determined using (Perkin Elmer LS 55 fluorescence spectrometer), materials were excited with high photon energy (310 nm). Raman spectroscopy (532^{TM} bench top spectrometer (Deltanu) was used to identify different phases in the synthesised material. UV-Vis diffuse reflectance spectra were obtained using an ocean optic high-resolution spectrometer (HR 2000+) equipped with a halogen light source (HL – 2000 – FHSA) and an integrating sphere accessory with $BaSO_4$ as a reference.

2.1. Catalyst synthesis

Sol-gel method was adopted for the synthesis for the ceria doped on titania (Ce/TiO_2) (wt% 0.1, 0.5, and 1.0) and bare TiO_2. For a typical synthesis, 60 ml of absolute ethanol was mixed with 2 g of Pluronic F-127 in a closed 400 ml Pyrex beaker, and placed under magnetic stirring for 4 h. In the resultant clear solution, 6 ml of TIP was added dropwise and stirred for 2 h. Then, 36 ml of deionised water was added dropwise into the solution and the solution changed colour from clear to white gel under continuous stirring for 24 h. The resulting mixture was aged overnight in the dark, at room temperature. Next, the gel was dried in an oven at 80 °C for overnight and the yellowish solid obtained was then calcined in the presence of air, at 450 °C for 4 h at the rate of 2 °C/min to obtain the white powder undoped TiO_2. Different wt% of the ceria doped on titania materials were synthesised following the similar protocol, but using 36 ml of water with requisite amounts cerium acetylacetonate hydrate precursor dissolved in it. The resultant catalyst materials were denoted as bare TiO_2, 0.1 wt% Ce/TiO_2, 0.5 wt% Ce/TiO_2 and 1.0 wt% Ce/TiO_2.

2.2. Photocatalysis experiments

Photodegradation experiments of caffeine were carried on lab scale using a 32 W / 480 Osram dulux F378 daylight – Compact fluorescence lamp. The lamp was fitted into a cylindrical Pyrex jacket used to cover the lamp. The reaction vessel was a 1 L Pyrex beaker, which was placed on a magnetic stirrer and lamp in the jacket was fitted in the reaction vessel. 300 ml of caffeine solutions containing 5, 10 or 15 mg/L were used in the experiments. In a typical run, 50 mg of catalyst was added to the caffeine solution. The solution was then sonicated for 10 min and stirred in the dark for another 60 min before the light illumination.

After 1 h, the solution was an irradiated with 32 W day light fluorescence lamp for 2 h. To monitor the progress of the reaction, 4 ml aliquots of reaction mixture was withdrawn at 20 min intervals. Samples were centrifuged using a Mikro 120 micro centrifuge for 2 min at 140 rpm and filtered using 0.45 micron. The change in absorbance of caffeine at wavelength 271 nm was measured using a UV-vis spectrophotometer to monitor the extent of degradation.

2.3. Products analysis

The product analysis was done using Shimadzu, LC-MS TOF mode. System was equipped with an electrospray ionization source ESI. An injection volume was kept at 10 µL. Isocratic elution using a reverse phase, in which mobile phase was made of 65 % v/v acetonitrile and 35 % v/v methanol. C18 analytical column of 3mm × 250 mm, 5 µm particle size (ZORBAX, SB-C18). While chromatogram was recorded for 15 min run, the product peaks appeared between retention times of 3 and 4 minutes. Samples were analysed by LC-Ms at 20 minutes intervals, starting from pure caffeine solution.

3. Results and Discussion

3.1. Catalyst characterisation

3.1.1. BET analysis

Figure.1 shows the N_2 adsorption-desorption isotherms of the prepared materials. The Brunauer–Emmett–Teller (BET) surface areas of the material are tabulated in Table 1. All the N_2 isotherms for the prepared material were observed to be type IV with H1 hysteresis loop [19]. Type IV isotherms are usually associated with mesoporous materials and H1 hysteresis loop is caused by agglomerates in the materials, it is also characteristic of material with high pore size uniformity. As shown in table 1, there is an increase in pore volume with the increase in metal dopant. The calculated BET surface area of all four catalysts also exhibited the similar pattern. This is commonly observed trend in doped materials, when the metal dopant possesses larger surface area than TiO_2.

Table 1: Summary of the textural characterizations, XRD and band gap analysis for the prepared materials

Sample Wt%	BET Surface area/ $m^2 g^{-1}$	BJH adsorption pore volume/ $cm^3 g^{-1}$	BJH adsorption pore size/ nm	FWHM (101) / rad	Anatase crystal size (101) / nm	Band gap energy / eV	EDX / Wt. %
Bare TiO_2	15.955	0.0841	18.012	0.01556	8.92	3.14	--
0.1% Ce/TiO_2	36.754	0.1762	17.232	0.01829	7.58	3.12	0.098
0.5% Ce/TiO_2	57.884	0.2229	12.613	0.01902	7.29	3.05	0.481
1.0% Ce/TiO_2	66.048	0.3342	16.475	0.01831	7.54	2.88	

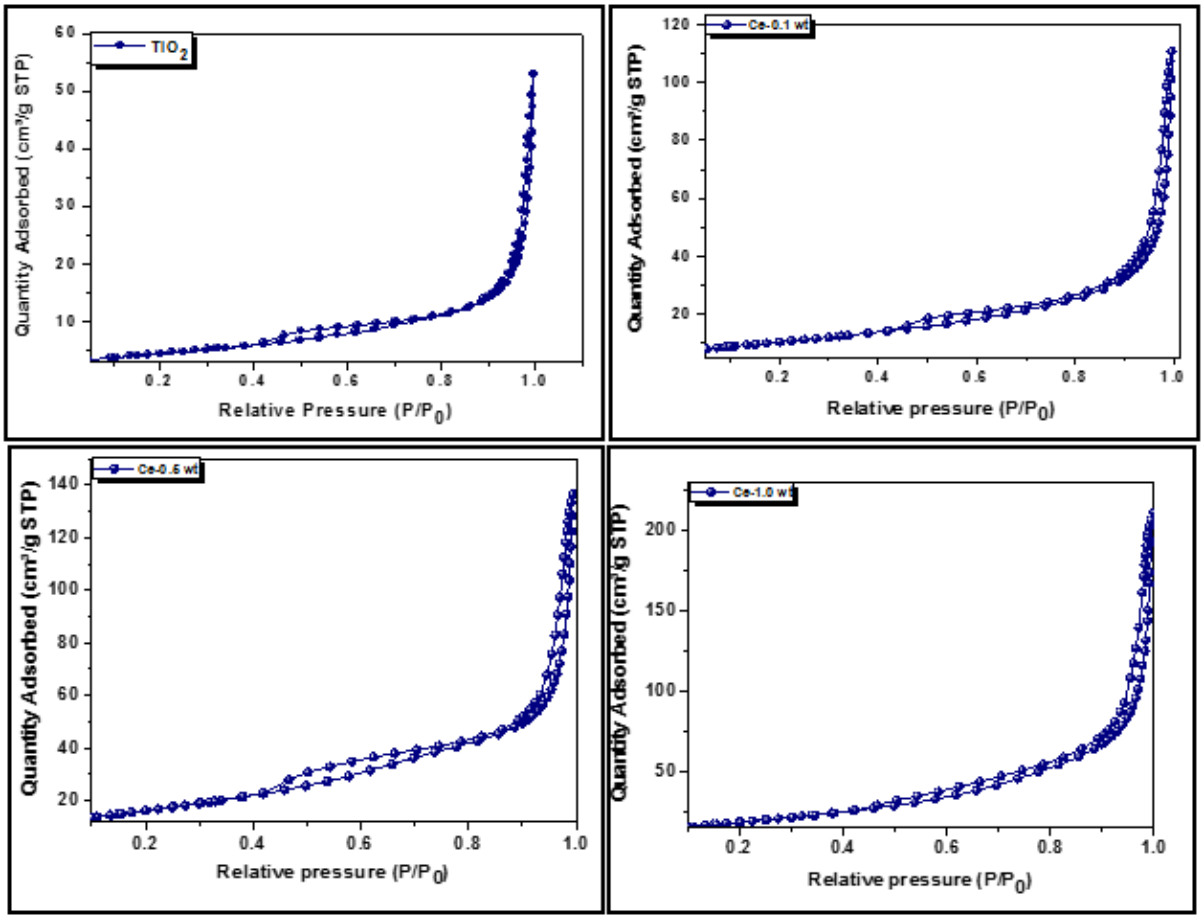

Figure 1: N_2 sorption/desorption isotherms of (a) bare TiO_2 (b) 0.1% Ce/TiO_2 (c) 0.5% Ce/TiO_2 and (d) 1.0% Ce/TiO_2 as prepared material

3.1.2. SEM & TEM analysis

SEM & TEM micrograph of (a) bare TiO_2, (b) 0.1% Ce/TiO_2 (c) 0.5% Ce/TiO_2 and (d) 1.0% Ce/TiO_2 are shown in the **figure** 2 and 3 below. An examination of the micrographs indicates that particles have irregular shapes and agglomerated. As a result of the agglomerates, inter-particle voids are generated. XRD spectra shows that ceria doping decreases the crystalline size by inhibiting growth, but this does not affect the morphology of the material. EDX analysis was performed for quantitative analysis of ceria in the prepared material. The results suggest that ceria is distributed throughout the TiO_2 surface. EDX revealed the presence of Ti, O and Ce.

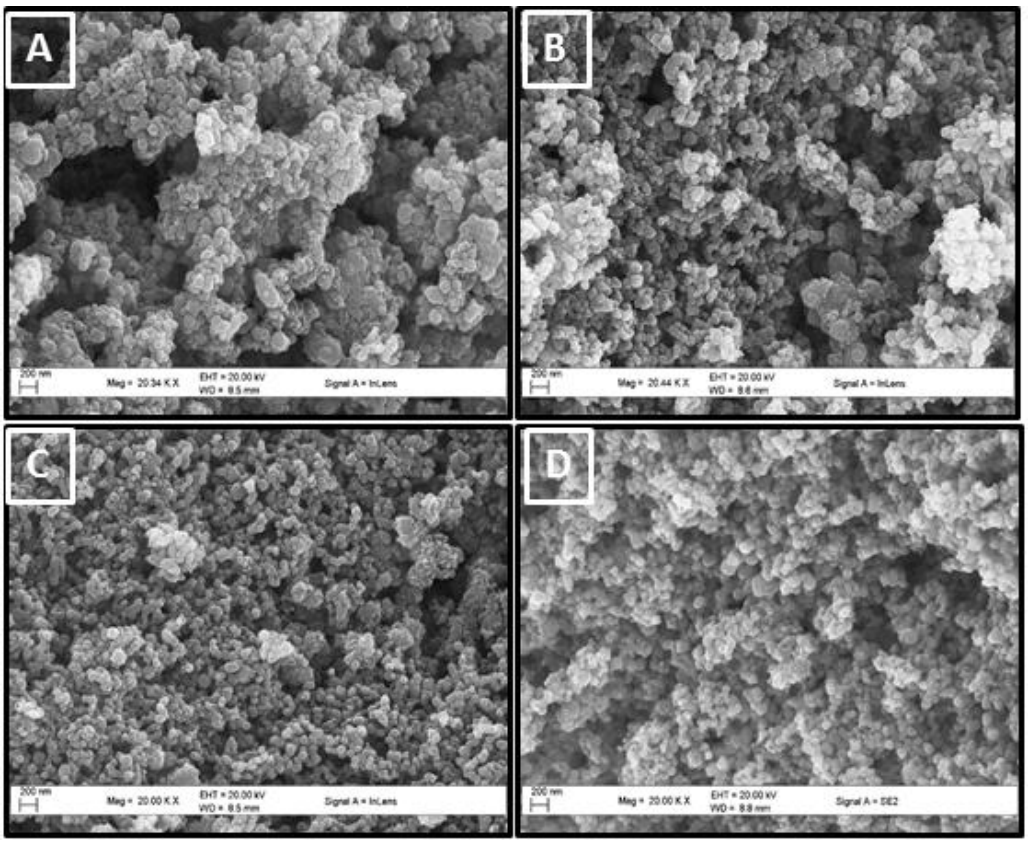

Figure 2: Scanning electron micrographs of (a) bare TiO_2 (b) 0.1% Ce/TiO_2 (c) 0.5% Ce/TiO_2 and (d) 1.0% Ce/TiO_2 as prepared material

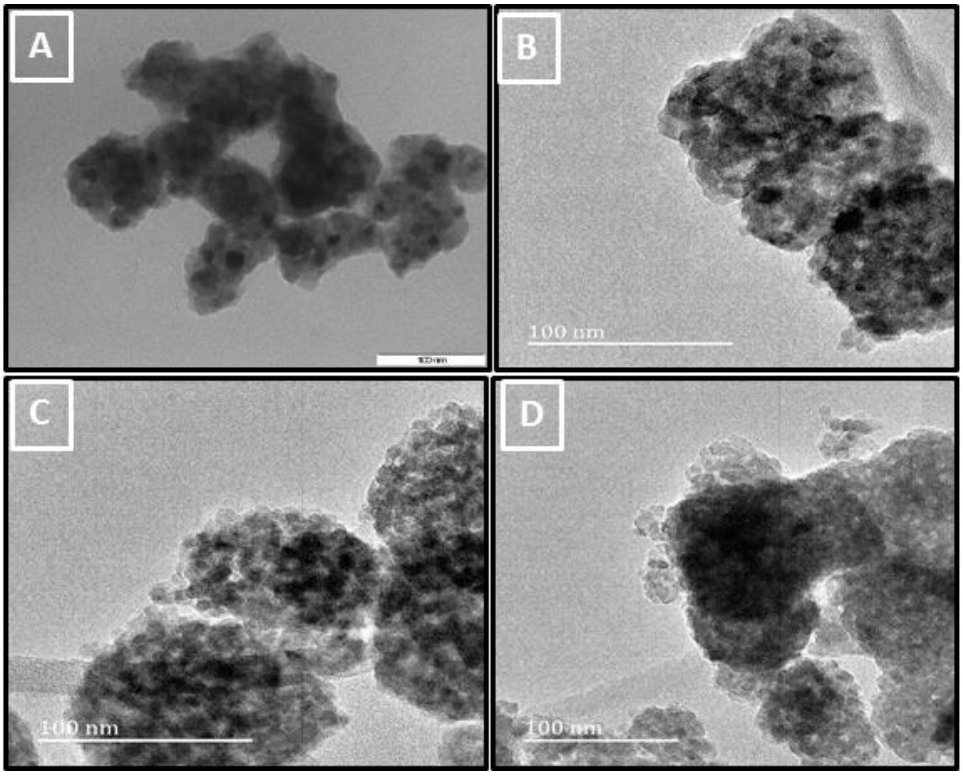

Figure 3: Transmission electron micrographs of (a) bare TiO_2 (b) 0.1% Ce/TiO_2 (c) 0.5% Ce/TiO_2 and (d) 1.0% Ce/TiO_2 as prepared material.

3.1.3. FT-IR analysis:

The FT-IR spectrum of different Ce/TiO_2 and bare TiO_2 are displayed **(figure** 4). The absorption bands found in the low range of 500–800 cm^{-1} for anatase are characteristic of Ti–O and Ti–O–Ce bands [20,21]. The broad peak appearing around 3300 cm^{-1} are due to the physisorbed OH group at the surface of the material [4]. The Ti–O–Ti bands are seen in the region of 380–1130 cm^{-1} [20]. The bands that appears in the range of 2200–2400 cm^{-1} are assumed to be due to Ce–O bands. There are no peaks attributed to organic compounds because of the fact that they were removed when the material was calcined. The peaks appeared at 1627 cm^{-1} at 3388 cm^{-1} are the characteristic of H_2O bending and vibration of hydroxyl groups [22-25].

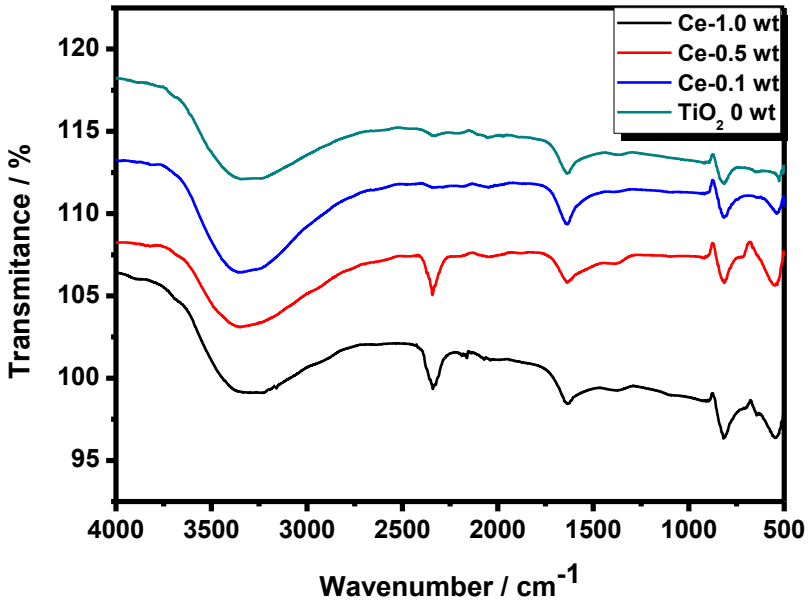

Figure 4: IR spectra of the prepared material

3.1.4. UV-DRS analysis

Figure 5 shows the optical absorption spectra of the synthesized catalyst materials. The results obtained indicate significant red shift in all doped samples. The red shift is caused by the dopant, ceria energy levels in the band gap [16]. This is attributed to charge transfer transition between the ceria electrons and the conducting/valance band of TiO_2 [17]. The optical band gap of the prepared material was calculated from the Tauc plot in **figure** 5 using this equation.

$$(\alpha h\nu)^2 = A\ (h\nu - E_g),$$

where hν is the photon energy, α is the absorption coefficient. $\alpha = \left(\frac{4\ \pi\ k}{\lambda}\right)$; k = absorption index/ absorbance; λ = wavelength; A = constant relative to the material, E_g = energy band

The calculated values from the Tauc plot display that all the catalyst materials had a reduced band gap compared to bare TiO_2 or commercial material, Degussa P25. It was seen that the band gap reduced with the increase in the metal loading of the dopant. Reduction in band gap suggest that e^- h^+ can be generated using visible light. The band gaps of different catalyst materials are summarised in table 1.

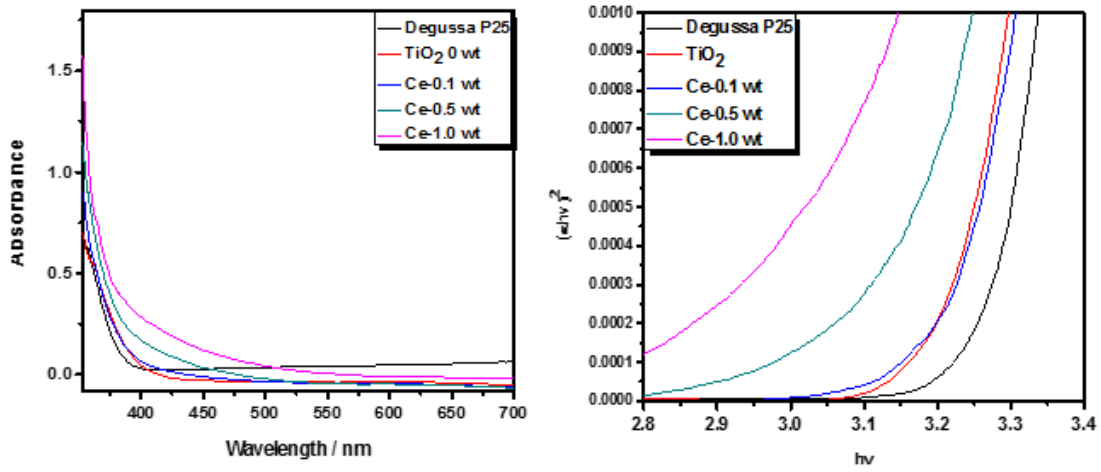

Figure 5: UV/ Vis – DRS and Tauc plot of the prepared material

3.1.5. XRD and Raman analysis:

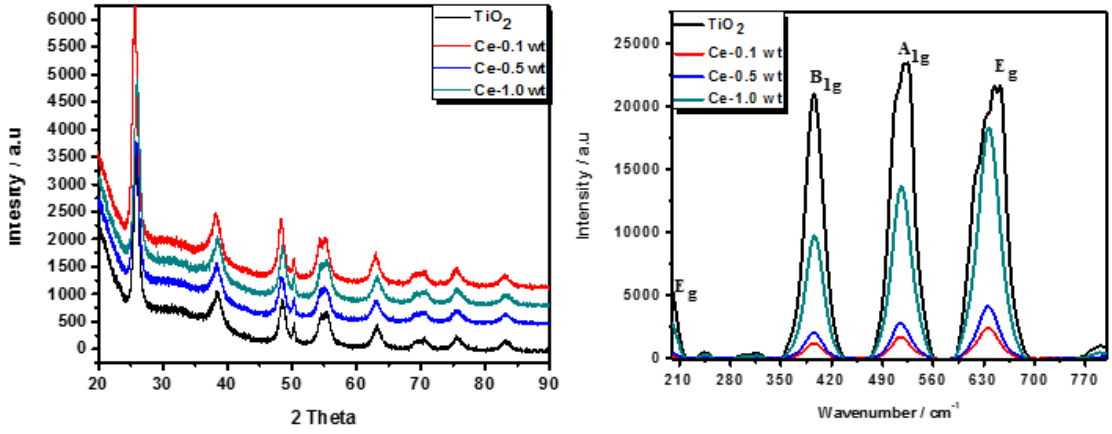

Figure 6: (a) X-ray diffraction and (b) Raman spectra

The XRD patterns and Raman spectra of the prepared materials are shown in **figure** 6. Spectra indicate that all the catalyst materials peaks characteristic of polycrystalline materials. **Figure** 6. (a) suggests that all the samples possess high crystallinity with anatase structure only (2θ = 25.2, 37.76, 48.02, 54.05, 55.03, 62.80, 68.85, 70.19 and 75.07) according to (JCPDS file no: 21-1272). No ceria diffraction peaks were observed in the spectra, which could be due to either CeO_2 is incorporated in the crystal structure of TiO_2 or it could be that the weight percentage of dopant is too small. From the diffraction patterns obtained it can be concluded that the incorporation of ceria ions in the crystal structure of TiO_2 did not cause significant structural changes and rather cause only slight shift in the diffraction peaks.

The average crystallite size for the anatase diffraction peak (101) was calculated using Debye–Scherrer formula [26].

$$D = \frac{K\lambda}{\beta Cos\theta}$$

where D is the crystallite size in nm, k is Scherrer's constant ≈ 0.9, λ is the wavelength of the X-ray radiation (Cu$K\alpha$ = 0.15406 nm). β is the corrected band broadening (full width at half-maximum (FWHM)) of the diffraction peak, and θ is the diffraction angle.

As shown in table 1, there is a decrease in crystalline size with addition of cerium dopant from 8.92 nm to 7.29 nm with the exception of 7.54 for ceria (1.0 wt%). This suggests that doping with ceria inhibits the growth of anatase crystallites to a certain extent.

Raman spectroscopy was used to examine the structural changes of all the prepared materials. According to symmetry group analysis anatase TiO_2 has six Raman mode of vibrations. Four of these modes are indicated in **figure** 6 (b). 146 (E_g), 197 (E_g), 399 (B_{1g}), 515 (A1g), 519 (B_{1g} is superimposed with the A_{1g} and), and 639 cm^{-1} (E_g) and the other three modes are IR active and one mode is inactive [27-29].

3.1.6. Photoluminescence analysis:

Photoluminescence (PL) is used to study ion-trapping, migration and the transfer of charge carriers and used in e^-h^+ pair relationship of the semiconductor [30]. The exciton emission detected suggests that the catalysts have large exciton binding energies and long exciton radiative lifetime [31-33]. PL study is used to understand the oxygen vacancy, surface state and defects of metal doping using ceria. From the results obtained in the **figure** 7, it is clearly seen that with increase in the weight composition of ceria, there is a decrease in the emission intensity compared with bare TiO_2. The decrease in emission intensity was attributed to oxygen vacancy or defects caused by the metal, which lead to an increase in optical properties. Emissions appearing at (376, 378, and 382 nm) are attributed to exciton recombination and emission band at 485 nm for self-trapped excitons and also peaks occurring at longer wavelengths are attributed to oxygen vacancies in the TiO_2 [23]. The signal seen around 530 nm is assumed to be caused by an increase in the amount of oxygen vacancies on the surface of the catalyst [31]. It was concluded that 0.1 wt% CeO_2/TiO_2 showed higher intensity compared to other catalysts.

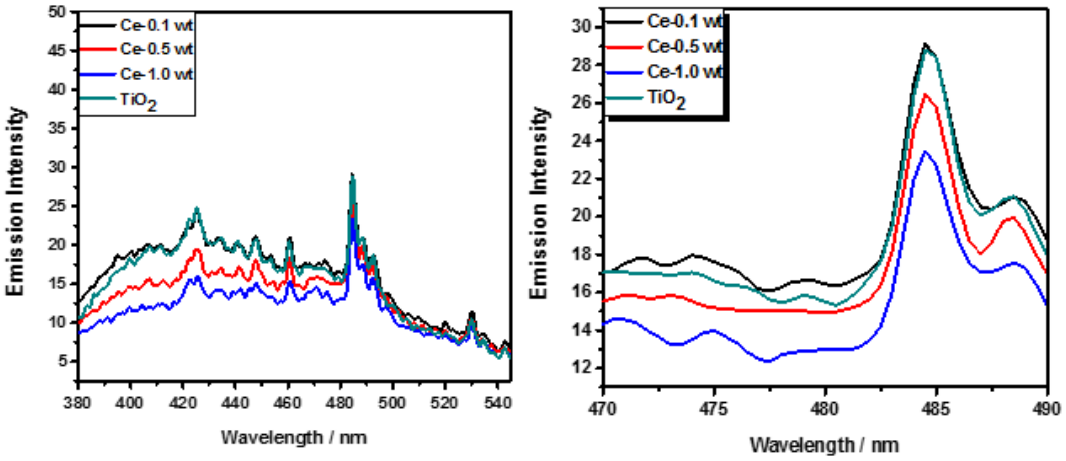

Figure 7: Photoluminescence spectra of the prepared material

3.2. Photocatalytic degradation of caffeine

Figure 8 shows degradation of CAF as a function of time using various synthesized materials and a commercial catalyst Degussa P25 under visible light after equilibrating in the dark for 60 min. Degradation of CAF was first done using a blank, in which light was used to degrade CAF without the catalyst. Assessing the obtained results, it is clear that BET surface area does not play much role in the current case of photo degradation of CAF. Although, 1.0% CeO_2/TiO_2 photocatalyst has the highest surface area and it had lower activity compared to 0.5% CeO_2/TiO_2, which possessed smaller surface area. The Tauc plot data shows that gap energy decreased with an increase in metal dopant. Further, there was no photodegradation observed in absence of any catalyst (**figure**. 8). This meant that visible light alone had no effect in degrading CAF. Better photocatalytic performance was observed with the commercial catalyst P25, which is assumed to contain both anatase and rutile phases of TiO_2. As shown in the **figure**, bare TiO_2 had low photocatalytic activity. However, the ceria doped TiO_2 demonstrated photo catalytic activity. This also suggests that though the prepared materials had reduced band gap compared to P25, their lower efficiency is due to the high electron – hole recombination rate. The increase in activity of ceria doped titania catalyst material compared to the undoped TiO_2, can be also attributed to the redox pair of ceria. It has been reported to act as an effective electron scavenger, which traps the bulk electrons from TiO_2, this leads to efficient adsorption of O_2 to generate superoxide (O^{2-}) radicals which increases photocatalytic activity [6,35].

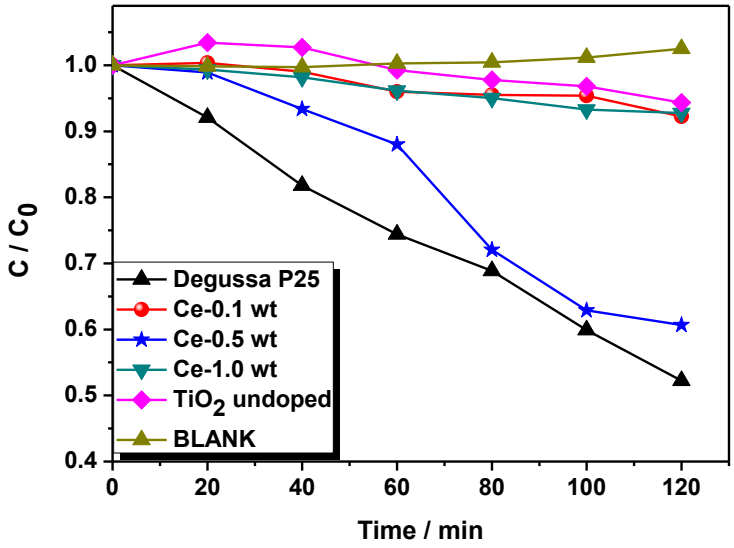

Figure 8: Photocatalytic degradation of caffeine

3.2.1. Effect of pH

Change in pH of the solution means an alteration of H^+ and OH^- ions in the reaction medium. Hydroxyl radicals are widely known to play a vital role in photocatalytic degradation studies. Hence, a change in pH to alkaline medium is expected to increase OH^- ions in the reaction medium, which will then be transferred into hydroxyl radicals [36]. However, caffeine is a weak base and it is more soluble in low pH medium than at high pH. In low pH solutions, caffeine exists completely as a protonated salt, thus making it more hydrophilic. In the aim of optimising the efficiency of Ce-0.5 wt. catalyst, degradation of caffeine was performed in different pH conditions and the results are displayed in **figure** 9. From the obtained results, it can be seen that degradation of caffeine is favoured in acidic conditions.

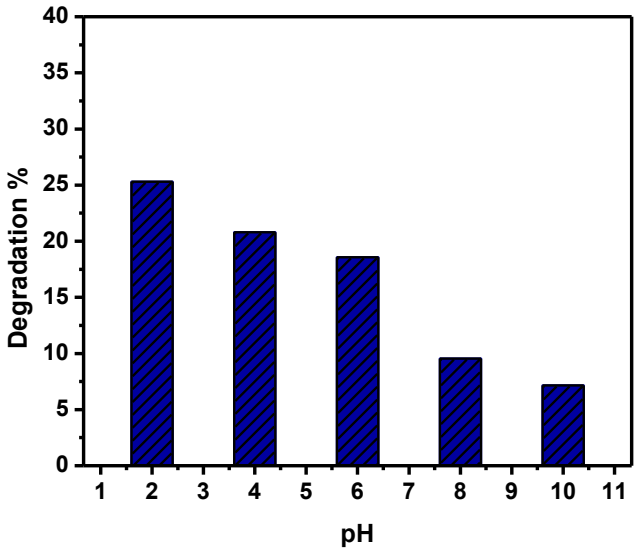

Figure 9: Effect of pH in degradation of caffeine over 120 min

3.2.2 Identification of degradation products

Identification of products was done using LC-MS TOF. The analysis was run over a period of 5 minutes. A standard solution of pure caffeine was initially injected and was characteristic of a long intensity at m/z 194. The same conditions were used to identify product formed over time. Reaction mixture was analysed by sampling at 20 min intervals starting from pure caffeine. One intermediates were identified in the degradation of caffeine and two products (ATCA and MMO). Scheme 1 depicts the proposed reaction mechanism using intermediates and product formed.

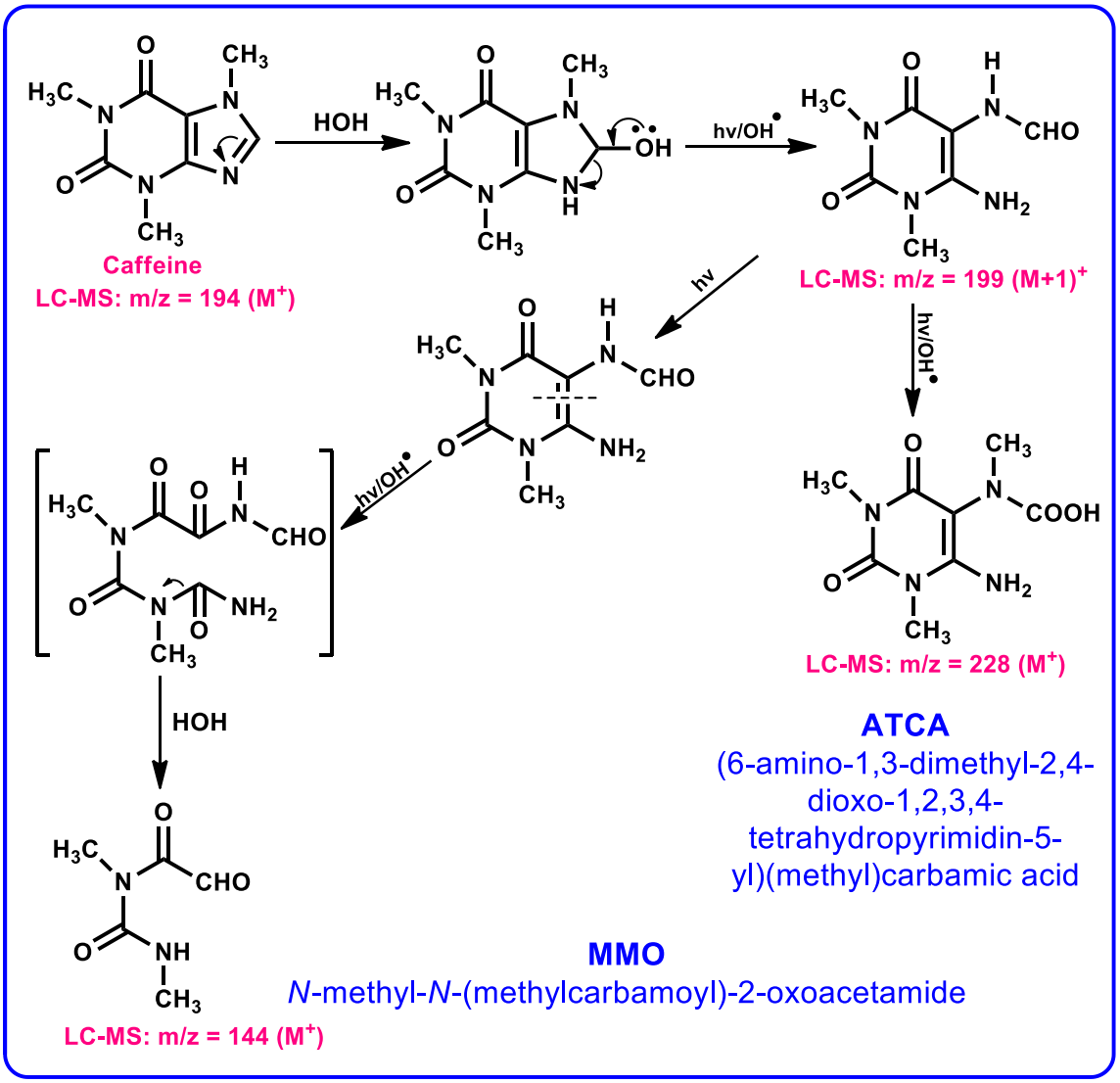

Scheme 1: Plausible reaction mechanism of photocatalytic degradation of caffeine under visible light using Ce/TiO_2.

4. Conclusion:

An efficient ceria doped TiO_2 nanoparticles were synthesised by sol gel method at room temperature. It was seen from nitrogen isotherms that all as prepared materials were mesoporous and exhibited type IV isotherms. Powder X-ray diffraction showed that all Ce doped TiO_2 were polycrystalline in nature and they were all anatase phase. All the catalyst materials showed good photocatalytic activity for degradation of caffeine under visible light whwn compared to the uncatalysed photo-degradation. The role of the pH of the solution in degradation of caffeine was evaluated and optimum pH conditions were established.

Acknowledgements:

The authors are thankful to the National Research Foundation (NRF) of South Africa, and University of KwaZulu-Natal, Durban, for financial support and research facilities.

References

[1] P. Emnet, S. Gaw, G. Northcott, B. Storey, L. Graham, Personal care products and steroid hormones in the Antarctic coastal environment associated with two Antarctic research stations, McMurdo Station and Scott Base, Environ. Res., 136 (2015) 331-342.

[2] A.M.P.T. Pereira, L.J.G. Silva, L.M. Meisel, C.M. Lino, A. Pena, Environmental impact of pharmaceuticals from Portuguese wastewaters: geographical and seasonal occurrence, removal and risk assessment, Environ. Res., 136 (2015) 108-119.

[3] S.L. Mumford, S. Kim, Z. Chen, R.E. Gore-Langton, D.B. Barr, G.M. Buck Louis, Persistent organic pollutants and semen quality: The LIFE Study, Chemosphere, 135 (2015) 427-435.

[4] C.S. Wong, S.L. MacLeod, JEM Spotlight: Recent advances in analysis of pharmaceuticals in the aquatic environment, Journal of Environmental Monitoring, 11 (2009) 923-936.

[5] O. Frederic, P. Yves, Pharmaceuticals in hospital wastewater: Their ecotoxicity and contribution to the environmental hazard of the effluent, Chemosphere, 115 (2014) 31-39.

[6] M. Magureanu, D. Piroi, N.B. Mandache, V. David, A. Medvedovici, V.I. Parvulescu, Degradation of pharmaceutical compound pentoxifylline in water by non-thermal plasma treatment, Water Res., 44 (2010) 3445-3453.

[7] A.B. Djurisic, Y.H. Leung, A.M.C. Ng, Strategies for improving the efficiency of semiconductor metal oxide photocatalysis, Mater. Horiz., 1 (2014) 400-410.

[8] A. Fujishima, T.N. Rao, D.A. Tryk, Titanium dioxide photocatalysis, J. Photochem. Photobiol., C, 1 (2000) 1-21.

[9] U.I. Gaya, A.H. Abdullah, Heterogeneous photocatalytic degradation of organic contaminants over titanium dioxide: A review of fundamentals, progress and problems, J. Photochem. Photobiol., C, 9 (2008) 1-12.

[10] R.R.N. Marques, M.J. Sampaio, P.M. Carrapico, C.G. Silva, S. Morales-Torres, G. Drazic, J.L. Faria, A.M.T. Silva, Photocatalytic degradation of caffeine: Developing solutions for emerging pollutants, Catal. Today, 209 (2013) 108-115.

[11] T. Sreethawong, S. Ngamsinlapasathian, S. Yoshikawa, Positive role of incorporating P-25 TiO_2 to mesoporous-assembled TiO_2 thin films for improving photocatalytic dye degradation efficiency, Journal of Colloid and Interface Science, 430 (2014) 184-192.

[12] R. Vijayalakshmi, V. Rajendran, Synthesis and characterization of nano-TiO_2 via different methods, Arch App Sci Res, 4 (2012) 1183-1190.

[13] J. Zhang, Y. Wu, M. Xing, S.A.K. Leghari, S. Sajjad, Development of modified N doped TiO_2 photocatalyst with metals, nonmetals and metal oxides, Energy Environ. Sci., 3 (2010) 715-726.

[14] D.H. Quinones, P.M. Alvarez, A. Rey, S. Contreras, F.J. Beltran, Application of solar photocatalytic ozonation for the degradation of emerging contaminants in water in a pilot plant, Chem. Eng. J. (Amsterdam, Neth.), 260 (2015) 399-410.

[15] H. Xu, P. Reunchan, S. Ouyang, H. Tong, N. Umezawa, T. Kako, J. Ye, Anatase TiO_2 Single Crystals Exposed with High-Reactive {111} Facets Toward Efficient H2 Evolution, Chemistry of Materials, 25 (2013) 405-411.

[16] M. Myilsamy, V. Murugesan, M. Mahalakshmi, Indium and cerium co-doped mesoporous TiO_2 nanocomposites with enhanced visible light photocatalytic activity, Appl. Catal., A, 492 (2015) 212-222.

[17] T. Tong, J. Zhang, B. Tian, F. Chen, D. He, M. Anpo, Preparation of Ce–TiO_2 catalysts by controlled hydrolysis of titanium alkoxide based on esterification reaction and study on its photocatalytic activity, Journal of Colloid and Interface Science, 315 (2007) 382-388.

[18] A.M.T. Silva, C.G. Silva, G. Drazic, J.L. Faria, Ce-doped TiO_2 for photocatalytic degradation of chlorophenol, Catal. Today, 144 (2009) 13-18.

[19] F.B. Li, X.Z. Li, M.F. Hou, K.W. Cheah, W.C.H. Choy, Enhanced photocatalytic activity of Ce^{3+}-TiO_2 for 2-mercaptobenzothiazole degradation in aqueous suspension for odour control, Appl. Catal., A, 285 (2005) 181-189.

[20] A.K. Tripathi, M.K. Singh, M.C. Mathpal, S.K. Mishra, A. Agarwal, Study of structural transformation in TiO_2 nanoparticles and its optical properties, Journal of Alloys Compound, 549 (2013) 114-120.

[21] J.T. Park, J.H. Koh, J.A. Seo, J.H. Kim, Formation of mesoporous TiO_2 with large surface areas, interconnectivity and hierarchical pores for dye-sensitized solar cells, Journal of Materials Chemistry, 21 (2011) 17872-17880.

[22] A. Rey, E. Mena, A.M. Chavez, F.J. Beltran, F. Medina, Influence of structural properties on the activity of WO_3 catalysts for visible light photocatalytic ozonation, Chem. Eng. Sci., 126 (2015) 80-90.

[23] Y. Zhao, C. Li, X. Liu, F. Gu, H. Jiang, W. Shao, L. Zhang, Y. He, Synthesis and optical properties of TiO_2 nanoparticles, Materials Letters, 61 (2007) 79-83.

[24] T. Zeng, Y. Chen, X. Su, Y. Li, Q. Feng, Hydrothermal steam induced crystallization synthesis of anatase TiO_2 nanoparticles with high photovoltaic response, Materials Letters, 119 (2014) 43-46.

[25] D. Liu, Y. Liu, Z. Wu, F. Tian, B.-C. Ye, X. Chen, Enhancement of photodegradation of Ce, N, and P tri-doped TiO_2/AC by microwave radiation with visible light response for naphthalene, Journal of the Taiwan Institute of Chemical Engineers, 68 (2016) 506-513.

[26] C. Burda, Y. Lou, X. Chen, A.C. Samia, J. Stout, J.L. Gole, Enhanced nitrogen doping in TiO_2 nanoparticles, Nano letters, 3 (2003) 1049-1051.

[27] A. Gajovic, M. Stubicar, M. Ivanda, K. Furic, Raman spectroscopy of ball-milled TiO2, J. Mol. Struct., 563-564 (2001) 315-320.

[28] T. Sekiya, S. Ohta, S. Kamei, M. Hanakawa, S. Kurita, Raman spectroscopy and phase transition of anatase TiO_2 under high pressure, Journal of Physics and Chemistry of Solids, 62 (2001) 717-721.

[29] W. Su, J. Zhang, Z. Feng, T. Chen, P. Ying, C. Li, Surface phases of TiO_2 nanoparticles studied by UV raman spectroscopy and FT-IR Spectroscopy, The Journal of Physical Chemistry C, 112 (2008) 7710-7716.

[30] L. Kernazhitsky, V. Shymanovska, T. Gavrilko, V. Naumov, L. Fedorenko, V. Kshnyakin, J. Baran, Photoluminescence of Cr-doped TiO_2 induced by intense UV laser excitation, Journal of Luminicences., 166 (2015) 253-258.

[31] E.O. Oseghe, P.G. Ndungu, S.B. Jonnalagadda, Photocatalytic degradation of 4-chloro-2-methylphenoxyacetic acid using W-doped TiO_2, Journal Photochemistry. Photobiology, A, 312 (2015) 96-106.

[32] D. Reyes-Coronado, G. Rodríguez-Gattorno, M. Espinosa-Pesqueira, C. Cab, R.d. de Coss, G. Oskam, Phase-pure TiO_2 nanoparticles: anatase, brookite and rutile, Nanotechnology, 19 (2008) 145605.

[33] S. Mathew, A. kumar Prasad, T. Benoy, P.P. Rakesh, M. Hari, T.M. Libish, P. Radhakrishnan, V.P.N. Nampoori, C.P.G. Vallabhan, UV-Visible Photoluminescence of TiO_2 nanoparticles prepared by hydrothermal method, Journal of Fluorescence, 22 (2012) 1563-1569.

[34] M.M. Khan, S.A. Ansari, D. Pradhan, M.O. Ansari, D.H. Han, J. Lee, M.H. Cho, Band gap engineered TiO_2 nanoparticles for visible light induced photoelectrochemical and photocatalytic studies, J. Mater. Chem. A, 2 (2014) 637-644.

[35] J. Zhang, Y. Nosaka, Mechanism of the OH radical generation in photocatalysis with TiO_2 of different crystalline types, J. Phys. Chem. C, 118 (2014) 10824-10832.

[36] Y. Nosaka, A. Nosaka, Understanding hydroxyl radical (.bul.OH) generation processes in photocatalysis, ACS Energy Lett., 1 (2016) 356-359.

CHAPTER FOUR

Synthesis of lanthanide doped TiO_2 nanoparticles and their photocatalytic activity under visible light

Vuyolwethu O. Ndabankulu, Suresh Maddila and Sreekantha B Jonnalagadda*

*School of Chemistry & Physics, University of KwaZulu-Natal, Westville Campus, Chiltern Hills, Durban-4000, South Africa.

***Corresponding Author:** Prof. Sreekantha B. Jonnalagadda
School of Chemistry & Physics,
University of KwaZulu-Natal,
Durban 4000, South Africa.
Tel.: +27 31 2607325,
Fax: +27 31 2603091
E-mail: **jonnalagaddas@ukzn.ac.za**

Abstract:

Four different lanthanide (Ce, Dy, Lu & Sm) doped TiO_2 mesoporous materials were synthesised using sol gel method with titanium (IV) isopropoxide as precursor. All the synthesized materials were characterised using various analytical techniques with BET, PXRD, TEM, SEM-EDX, Raman, FT-IR, Photoluminescence and UV-DRS spectroscopy. Photocatalytic activity and efficacy of the materials in degradation of Caffeine in aqueous solutions was investigated under visible light illumination. Ce doped TiO_2 exhibited better activity than the rest of the prepared materials. High photoactivity of the catalysts were attributed to the presence of lanthanides to the ability to generate ions that are electron scavengers thereby enhancing photo-degradation of caffeine under visible light. All materials proved good and recyclable as catalysts without loss of activity up to three times. One intermediate [*N*-1,3,6-trimethyl-2,4-dioxo-1,2,3,4-tetrahydropyrimidin-5-yl)formamide] (TDTF) and two products (6-amino-1,3-dimethyl-2,4-dioxo-1,2,3,4-tetradropymidin-5-ly)(methyl)carbamic acid (ATCA) and *N*-methyl-*N*-(methylcarbomoyl)-2-oxoacetamide (MMO) were analysed and identified by the LC-MS spectra.

Keywords: TiO_2, lanthanides, visible light, photocatalytic degradation, hydroxyl radical, caffeine.

1. Introduction:

Pharmaceutical compounds (PC) are a class of emerging contaminates, that found widely in the environment [1,2]. PCs have been recurrently detected in wastewater treatment plants (WWTP), surface water, ground water around residential, industrial areas and sometimes in drinking water at levels (rang from 0.1 – 20 ppb) [3,4]. Due to their high stability in water, these substances are persistent in the environment and they possess poor biodegradability. Pharmaceutical compounds identified in water includes nonsteroidal anti-inflammatory drug (NAID), endocrine disruptors (EDs) and stimulants like caffeine [5]. Caffeine is the most used legal stimulant and it is metabolised by humans. It is found in the environment due to caffeinated drinks and unconsumed coffee. Because of the potential risk in aquatic and other living organisms associated with the presence of such substances in the environment, this has led to a demand for an efficient method for the remediation of such substances [6].

Advanced oxidation processes (AOPs) have been found to be one of the powerful methods in removal of organic contaminates in aqueous solution. Heterogeneous photo-catalysis is one of the important AOPs applied in the degradation of organic contaminants such as pesticides, dyes, chlorinated aromatics and pharmaceuticals. AOPs

involves the use of a heterogeneous photo-catalyst such as titania, assisted with either Ultra-violet or visible light (TiO_2/light) [7]. Recently, photo-catalysts have received high attention, due to high stability, extended activity, recovery and reusability. It has proven to be as an efficient process because of the use of oxygen as oxidant, and the mainly the generation of hydroxyl radicals for photooxidation of the organic compounds. Depending on the pH of the solution in most cases super-oxides are also produced which assist in the process [8].

Titania is widely used this is owing to its advantages such as photocatalytic activity, non-toxicity, low cost, high performance in degrading organic compounds. Anatase being the most active phase of TiO_2 with wide band gap (E_g = 3.2 eV, anatase) is one of the limitations facings its application, because it cannot be used efficiently under visible light, but rather performs better under ultra-violate radiation [8,9]. High carrier charge recombination is also a limiting factor with using TiO_2 as a photocatalyst. Doping with metal or non-metal ion is one of the methods used to retard the carrier charge recombination so to increase photocatalytic efficiency. Oseghe et.al., have reported manganese doped TiO_2 showed better photocatalytic efficiency in degrading methyl blue under visible light, when compared with bare TiO_2. Manganese was said to act as an electron trap, there by provoking a red shift allowing the catalyst to absorb light in the visible spectrum [10]. Doping titania with rare-earth metals has received attention in the recent past and doping with lanthanide with 4f electrons will reduce the charge recombination rate significantly and showing the absorption in longer wavelengths [11]. Xiao et al. reported a significant red shift, which extended the photocatalytic response into longer wavelength because of doping TiO_2 with samarium [12]. Our previous work involved the degradation of different pesticides and dyes, using AOPs, the ozone facilitated dechlorination of tetrachloro-o-benzoquinone using cesium doped mixed oxides, chloronitrophenol using Ce-V doped mixed metal oxides as catalysts and photocatalytic degradation of 4-chloro-2-methylphenoxyacetic acid using W-doped TiO_2 [13-15].

In this communication, we report the synthesis of different lanthanide doped TiO_2 materials, their characterization and potential as photocatalysts in degradation of model compound, caffeine under visible light and aqueous conditions.

2. Experimental Section:

Titanium (IV) isopropoxide (TIP) (MW = 284.22 97 %), non-ionic surfactant (Pluronic F-127), Caffeine (Sigma-Aldrich), Degussa P25 (TiO_2) were supplied by Sigma-Aldrich. Cerium acetylacetonate hydrate, dysprosium oxide, lutetium oxide and samarium acetylacetonate hydrate were of analytical grade and purchased from Sigma-Aldrich.

Hydrochloric acid, absolute ethanol and sodium hydroxide were purchased from Promark chemicals in analytical grade.

2.1 Catalyst synthesis

Sol gel method adopted for the synthesis the material used. For a typical synthesis, 2 g of Pluronic F-127 was dissolved in absolute ethanol (60 ml) under continuous stirring for 4 h. To the resultant clear solution, 6 ml of TIP was added dropwise and stirring was continued for another 2 h. Then, 36 ml of deionised water with lanthanide precursor was added dropwise to the solution. For the completion of addition, the solution changes colour from clear to white gel. The stirring of the gel suspension was continued for another 24 h and the resulting mixture was aged overnight in the dark at room temperature. After aging the gel separated from the solvent by decantation of the solvent. The resulting precipitate was filtered and washed thrice with deionized water and dried at 80-90 °C for overnight. The dried precipitate was calcined at 450 °C for 4 h, in the presence of air, (ramp rate = 2 °C/ min) to obtain the wt.% (0.5) of Ce/Sm/Lu or Dy doped TiO_2 materials.

2.2 Product characterisation

Surface morphology of the synthesised material were characterised by use of Scanning electron microscope (ZEISS ULtralpus FEG-SEM). (JOEL JEM 1010) transmission electron microscope to obtain the physical structural characteristics. Bruker D2 phase Powder X-ray diffraction (PXRD) equipped with a Cu – Kα radiation (λ = 0.15401) was used to obtain diffractogram. The texture characterisation were determined using a micrometric flow 3030 instrument. All samples were degassed on micrometric flow prep (060) under nitrogen flow at 90 °C for 1 h then temperature was ramped to 200 °C for 12 h to allow the samples to degas before the textural analysis. The Fourier Transmission Infrared (FT-IR) spectrum for the samples was established using a Perkin Elmer Perkin Elmer Precisely 100 FT-IR spectrometer at the 400-4000 cm^{-1} area. Photoluminescence spectra were obtained using (Perkin Elmer LS 55 fluorescence spectrometer) and materials were excited with high photon energy (310 nm). Raman spectroscopy (532^{TM} bench top spectrometer (Deltanu) was used to identify different phases in the synthesised material. UV-Vis diffuse reflectance spectra were obtained using an Ocean Optic High Resolution Spectrometer (HR 2000+) equipped with a halogen light source (HL – 2000 – FHSA) and an integrating sphere accessory with $BaSO_4$ as a reference.

2.3 Hydroxyl radical generation test

To detect and quantify the hydroxyl radical formation and concentrations, Dosimetry method was employed. In a routine run, 100 mg/L of photocatalyst was suspended to a 250 mL

of the 0.1 mM terephthalic acid solution prepared in 2 mM NaOH solution. Then, the solution was irradiated with a 26 W/480 Osram dulux F378 daylight compact fluorescence lamp (CFL). Samples for analysis were collected in 20 min intervals. The collected sample was centrifuged for 2 min at 14000 r/min and it was further filtered with 0.45 micron before it was analysed using a PerkinElmer LS 55 fluorescence spectrophotometer. Product (2-hydroxyterephthalic acid) formation was identified at 425 nm wavelength using an excitation wavelength of 310 nm.

2.4 Photocatalytic experimental

Photo-degradation experiments of caffeine in the laboratory were conducted using CFL as light source. The lamp was fitted into a cylindrical Pyrex jacket to cover the lamp. The reaction vessel was a 1 L Pyrex beaker, which was placed on a magnetic stirrer and lamp in the jacket was fitted in a reaction vessel. 300 mL of caffeine solution was used in each experiment. For optimization experiments, 15, 10, and 5 mg/L of caffeine was used. In a typical degradation experiment, 50 mg of catalyst was added into caffeine solution and the solution was then sonicated for 10 min and stirred in the dark for 1 h before light illumination. Dark experiment was performed to establish adsorption–desorption equilibrium. Then, the solution was the irradiated with 26 W day light fluorescence lamp for 2 h. Samples were taken at 20 minute intervals starting from t = 0. Further, 4 mL sample solution was centrifuged using with micro centrifuge (Mikro 120) for 2 min at rpm of 14000. Samples were then analysed using a double beam Shimadzu UV-Vis spectrophotometer. Photocatalytic degradation observed by monitoring the change in absorbance of caffeine at wavelength 271 nm.

In order to identify the intermediates / product of Caffeine degradation, UPLC-ESI–MS analysis in the negative mode was used to obtain the mass spectra with an injection volume of 10 µL. Waters Aquity UPLC with BEH C18 (1.7 mm, 2.1 mm, 100 mm,35 ^{o}C) column was used. The mobile phase (flow rate 0.15 mL.min^{-1}) was a composed of acetonitrile and water acidified using 0.1% acetic acid (1:1, v/v).

3 Results and discussion:

3.1 Transmission electron microscope

HRTEM micrographs at the same magnification are illustrated in **figure 1**, for all the four materials synthesised (a) Ce-TiO_2, (b) Dy-TiO_2, (c) Lu-TiO_2, and (d) Sm-TiO_2. Continuous lattice was used to confirm the crystalline nature of the as prepared materials. Lattice fringes were observed in all images indicating the anatase crystallographic plane. It was

noted that d spacing increases with the ionic radius of the metal ion doped in TiO_2. The HRTEM suggests that the particles were agglomerates and aggregates and then dispersed.

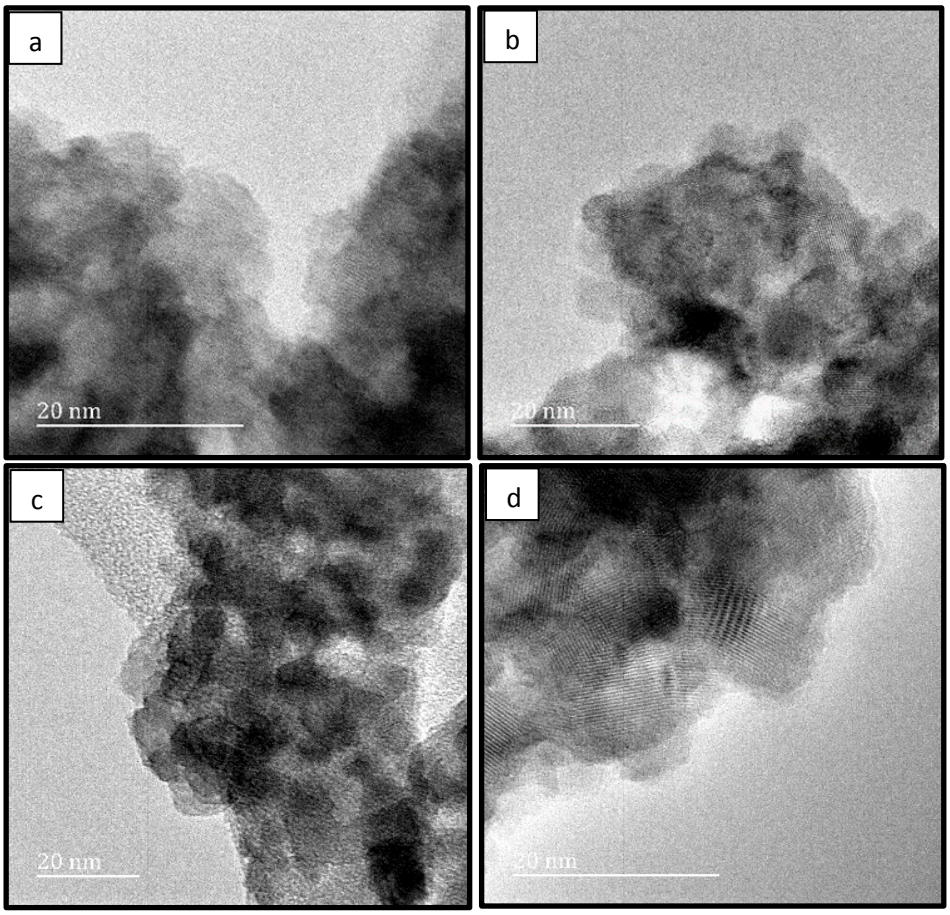

Figure.1: HRTEM micrographs of (0.5 wt%) (a) Ce (b) Dy (c) Lu and (d) Sm doped TiO_2 prepared materials

3.2 Scanning electron microscope

Figure 2(a) displays SEM micrographs of as prepared materials, (a) Ce-TiO_2, (b) Dy-TiO_2, (c) Lu-TiO_2, and (d) Sm-TiO_2. A perusal of the images displayed, suggests that all as prepared materials showed agglomerated irregular shaped particles with inter-particle voids, which is associated with loose particle aggregates. Cerium doped material had reduced particle size compared to the rest, this was attributed to the crystallinity of the material. The EDX analysis results evidently specify the presence of respective lanthanide species on the surface of titania as all dopants (**figure 2(e)**).

3.3 BET N_2 – sorption / desorption studies

N_2 sorption - desorption isotherms were used to determine the textural properties of the lanthanide doped materials and are displayed in **figure 3**. All the obtained isotherms can be classified as type IV isotherms according to IUPAC with distinct hysteresis loop type III. This was not a surprising, since all materials were mesoporous (2 – 50 nm).

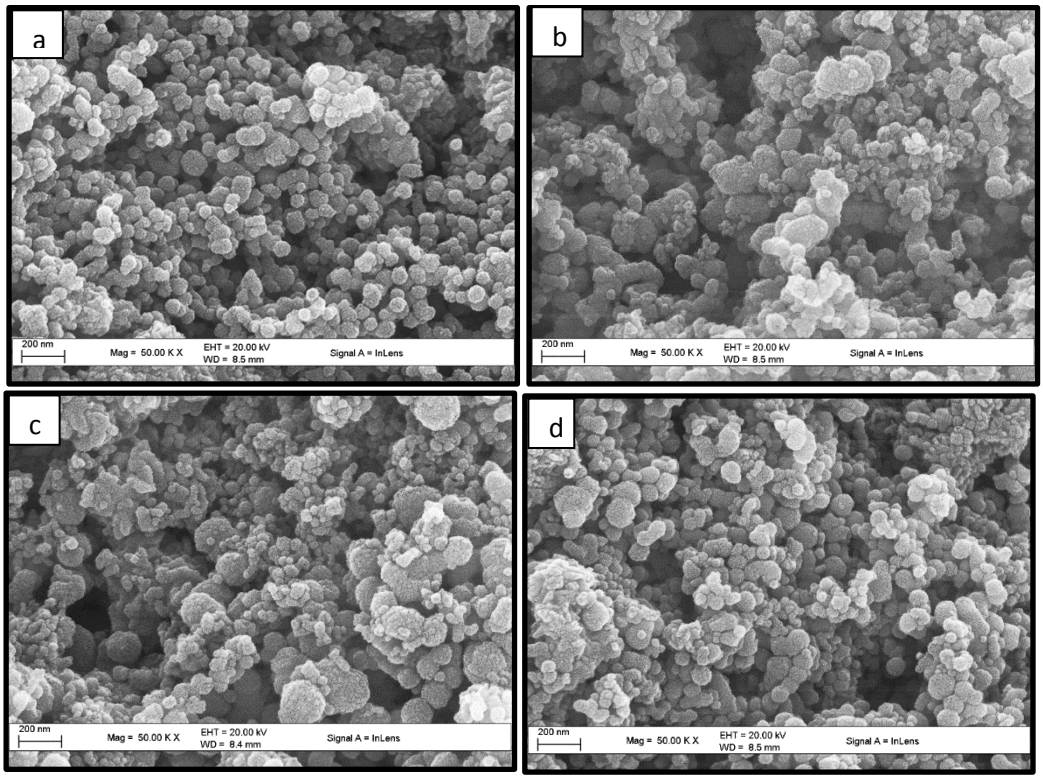

Figure.2: SEM micrographs of (0.5 wt%) (a) Ce (b) Dy (c) Lu and (d) Sm doped TiO_2 as prepared material

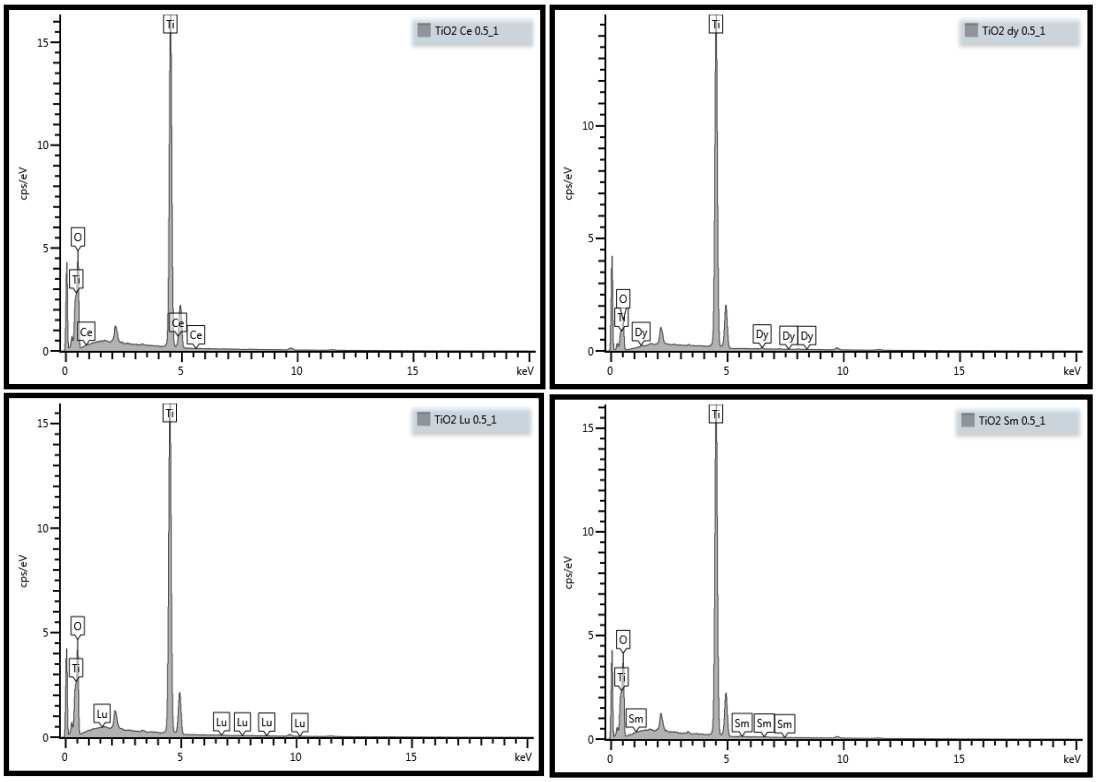

Figure.2 (e). EDX spectrum of lanthanide doped TiO_2.

Results summarised in table1 suggest that loaded metal play a crucial role in the surface area and pore volume of the material. Depending on the metal ion used, different values were obtained (**Table 1**). The increase in BET surface area and pore volume may imply enhanced capability for organic pollutant adsorption, which could lead to the improvement of photocatalytic activity of the as prepared materials.

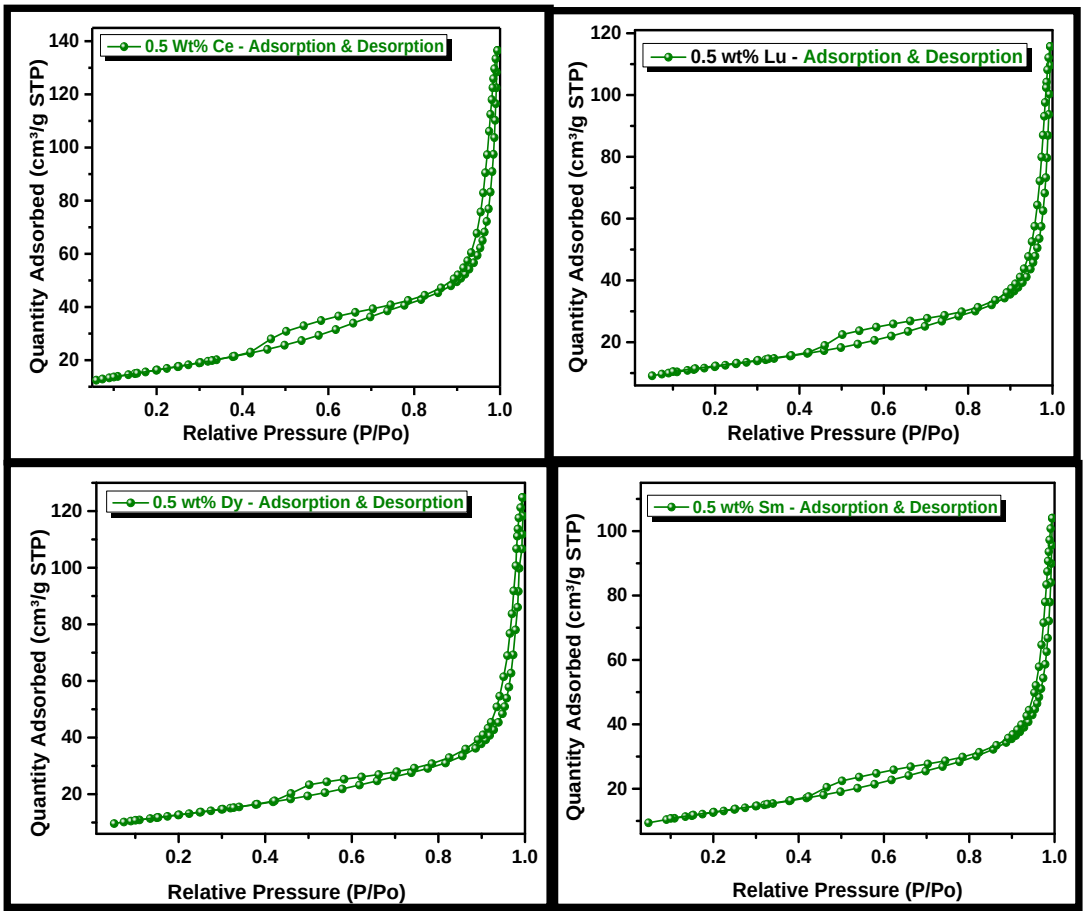

Figure.3: N_2 sorption and desorption isotherms of 0.5 wt%) (a) Ce (b) Dy (c) Lu and (d) Sm doped TiO_2 as prepared material

Table 1: Summary of the textural characterizations, XRD and band gap analysis for the prepared materials

Sample	BET Surface area/ m^2g^{-1}	BJH adsorption pore volume/ cm^3g^{-1}	BJH adsorption pore size/ nm	FWHM (101) / rad	Anatase crystal size (101) / nm	Band gap energy/ eV
Ce-0.5 wt.	57.884	0.2229	12.613	0.0190	7.29	3.08
Dy-0.5 wt.	45.687	0.2003	15.968	0.0178	7.79	3.19
Lu-0.5 wt.	43.561	0.1841	15.565	0.0148	9.35	3.14
Sm-0.5 wt.	45.555	0.1654	13.888	0.0176	7.86	3.09

3.4 XRD analysis

Figure 4 shows the XRD diffraction patterns of lanthanide doped titania (0.5%) powder samples calcined at 450 °C. All doped TiO_2 exhibit similar XRD pattern that were all attributed to anatase phase according to (JCPDS file No: 21-1272), 2θ = 25.28° (101), 36.95°, 48.05°, 55.06°, 62.69°, 70.91°. The only difference was with respect to the diffraction peaks; they were slightly shifted relative to one another. There were no new peaks, which meant that there were no impurities that were detected. From this, it was concluded that all dopants were inside crystal lattice, since no metal ion peaks were observed. In addition, the dopant concentration was also small to be strikingly noticed by the instrument. The average crystallite size for the anatase diffraction peak (101) was calculated using Debye–Scherrer formula and are shown in table 1

$$D = \frac{K\lambda}{\beta \mathrm{Cos}\theta}$$

Where D is the crystallite size in nm, k is Scherrer's constant ≈ 0.9, λ is the wavelength of the X-ray radiation (Cu$K\alpha$ = 0.15406 nm). β is the corrected band broadening (full width at half-maximum (FWHM)) of the diffraction peak, and θ is the diffraction angle. All the La-doped materials were polycrystalline in nature and their crystalline sizes are tabulated in table.1.

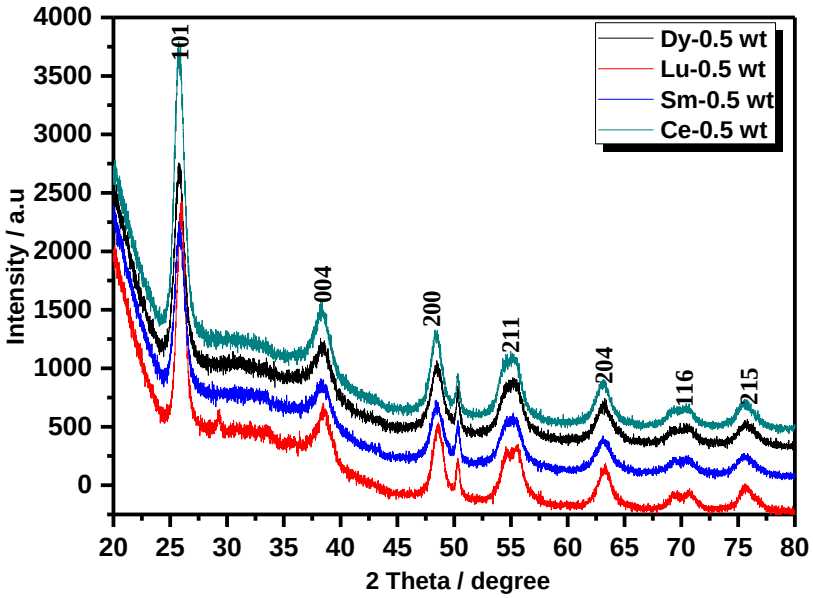

Figure.4: X-ray diffraction of the as prepared material

3.5 Raman analysis

Raman spectroscopy was used to examine structural changes of the as prepared TiO_2 material. Anatase TiO_2 crystal has six Raman active modes of vibrations and three are IR active. These active bands are found at approximate wavenumbers, 146 (E_g), 197 (E_g), 409 (B_{1g}) at 515 (A_{1g}) which is superimposed at 519 (B_{1g}) and 639 cm^{-1} (E_g) [16-19]. Not all of the bands are observed in the given **figure**. All the materials showed the same pattern, with an exception of a band broadening that was observed for cerium doped materials. This observation was attributed to structural changes occurring when Ce ions doped in the lattice structure of TiO_2.

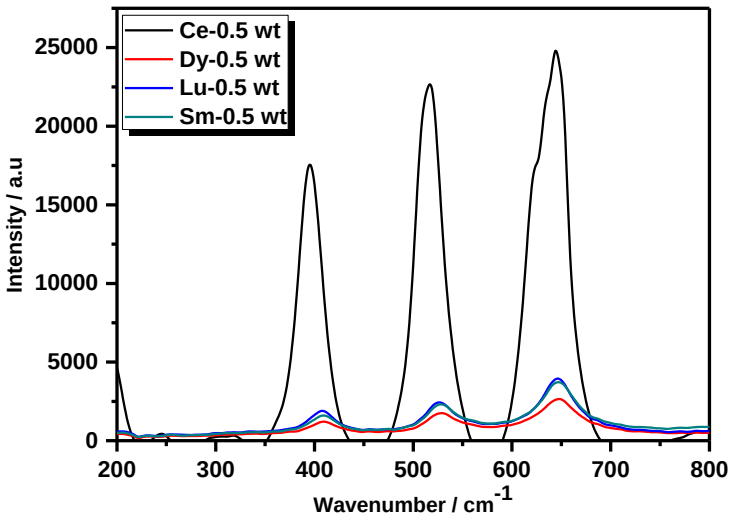

Figure.5: Raman spectra of Lanthanide doped TiO_2

There were no new bands observed in all the materials, this was assumed to be as results of successful doping or due to low concentrations of dopants which were not detected by the instrument. The crystallinity in the as prepared TiO_2 materials was seen using Raman bands, since Raman lines become weak and broad when the material exhibit local lattice defects [20]. As seen in **figure 5**. Raman bands of all dopants are broad and have overlapping feature which implies nanocrystals are imperfect. This was also confirmed by powder XRD measurements since it was determined that all the materials are polycrystalline in nature.

3.6 FT-IR analysis

Figure 6 shows FTIR of Ce, Dy, Lu and Sm doped TiO_2. TiO_2 with high specific surface area is known to absorb water molecules on the active sites on its surface and form Ti^{4+} - OH_2 on the surface [21]. The presence of physisorbed water molecule is determined by the appearance of absorption band around 1630 cm^{-1} [22], this band appears in all the as prepared materials. Studies shows that the water molecule plays an important role in phase transformation of anatase to rutile. The broad band around 3400 cm^{-1} is ascribed to hydroxyl group [23]. The absorption band around 400 – 800 cm^{-1} is attributed to the anatase TiO_2 skeletal to O – Ti – O and Ti – O bonds. The band at 1400 is due to Ti – O – Ti vibration [14,24].

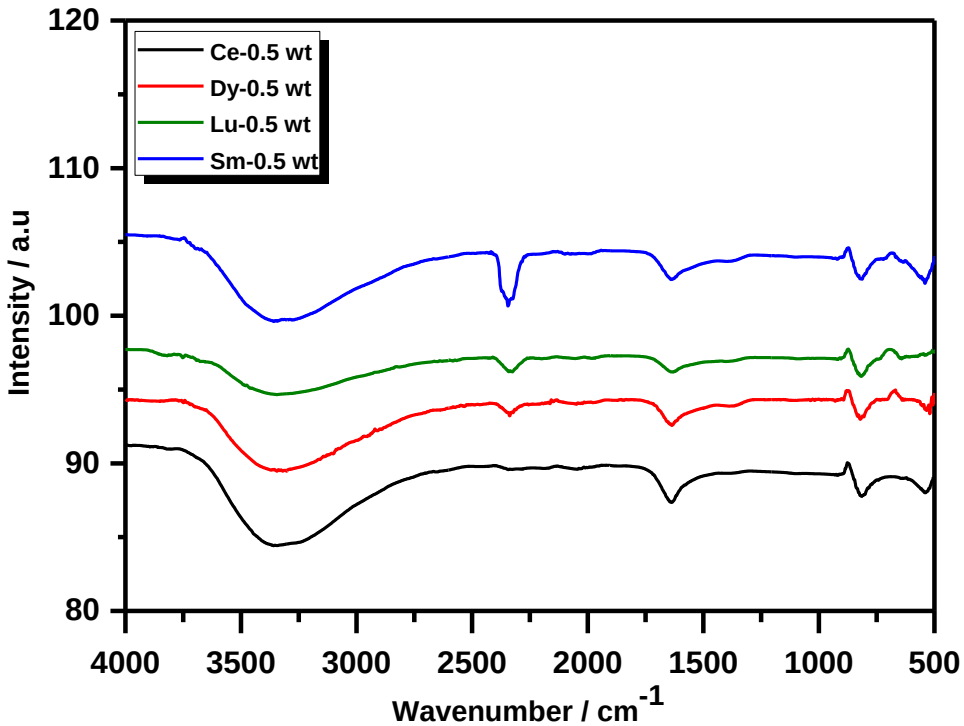

Figure.6: IR spectra of Lanthanide doped TiO_2 materials

3.7 UV-DRS analysis

UV-Visible DRS of all the as prepared materials are depicted in **figure 7**. From the spectrum, it can be seen that for all materials the absorption was shifted towards the longer wavelength, i.e. a typical a redshift can be observed. Ceria doped TiO_2 exhibited highest redshift compared with others and Dy had the lowest. The typical red shift is attributed to charge-transfer transition between the electrons of rare earth metal ion and TiO_2 conduction or valence band [25]. Ce has an unpaired electron in its orbital, that creates new filled energy levels with TiO_2, which results in covalent bonding of Ce on the TiO_2 surface and this leads to an enhanced red shift compared to other metal ions [26].

The optical band gap of the prepared material was calculated from the Tauc plot in **figure** 7 (b).

$$(\alpha h\nu)^2 = A\,(h\nu - E_g)$$

where $h\nu$ is the photon energy, α is the absorption coefficient, $\alpha = (\frac{4\pi k}{\lambda})$, k = absorption index/ absorbance, λ = wavelength and A = a constant relative to the material. In all prepared materials, there was a reduction in band gap and this was attributed to the presence of metal ion in the lattice structure of TiO_2. Dy doped TiO_2 had the lowest band gap reduction with 3.19 eV, followed by Lu with 3.14 eV, Sm^{3+} 3.09 eV and the highest band reduction was that Ce with 3.08 eV. From the obtained results, it can be expected that under visible light cerium doped TiO_2 to be the most effective.

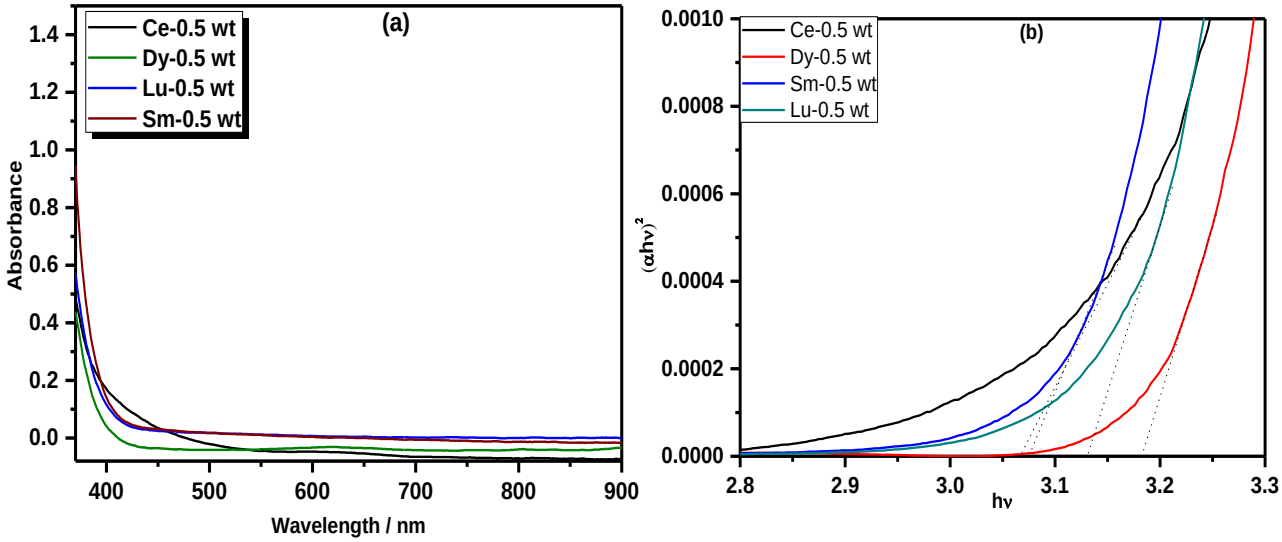

Figure.7: UV-Visible diffuse reflectance (a) and Tauc plot of the as prepared materials (b)

3.8 Photoluminescence analysis

Photoluminescence is used in determining the effectiveness of charge transfer, migration, and trapping of charge carriers [27,28]. **Figure 8** displays the PL emission spectra of Ce, Dy, Lu, and Sm doped TiO_2. It is seen that the Dy – TiO_2 had the highest intensity and Ce has the lowest, this suggests that Ce doped TiO_2 will have the highest photocatalytic performance. PL emission is caused by the recombination of the excited electron and generated hole; thus, low PL means slow rate of recombination.

The characteristic peaks of TiO_2 were found between 350 and 540 nm. PL of TiO_2 anatase is attributed to three types of phenomenon, Oxygen vacancies, surface state defects and self-trap excitons [29-31]. Peaks appearing at shorter wavenumbers (360 – 380 nm) are attributed to exciton recombination. The decrease in emission intensity was attributed to oxygen vacancy or defects caused by the metal which lead to an increase in optical properties [21,32,33]. The peaks observed at 410 nm at 470 nm are attributed to band-edge free exciton and bound exciton luminesces respectively [34,35]. The dominant peaks between 480 nm and 530 are due to self-trap exciton and oxygen vacancies. An examination of the spectra illustrated in **figure** 7 shows that there is varied decrease in band gap depending on the metal ion used. Cerium shows the lowest intensity in the PL spectrum with the shortest band gap while dysprosium doped TiO_2 showed the highest intensity with the longest band gap. The results summarised in **figure** 8 suggests that Ce/TiO_2 will exhibit higher photocatalytic activity compared with other metal ions.

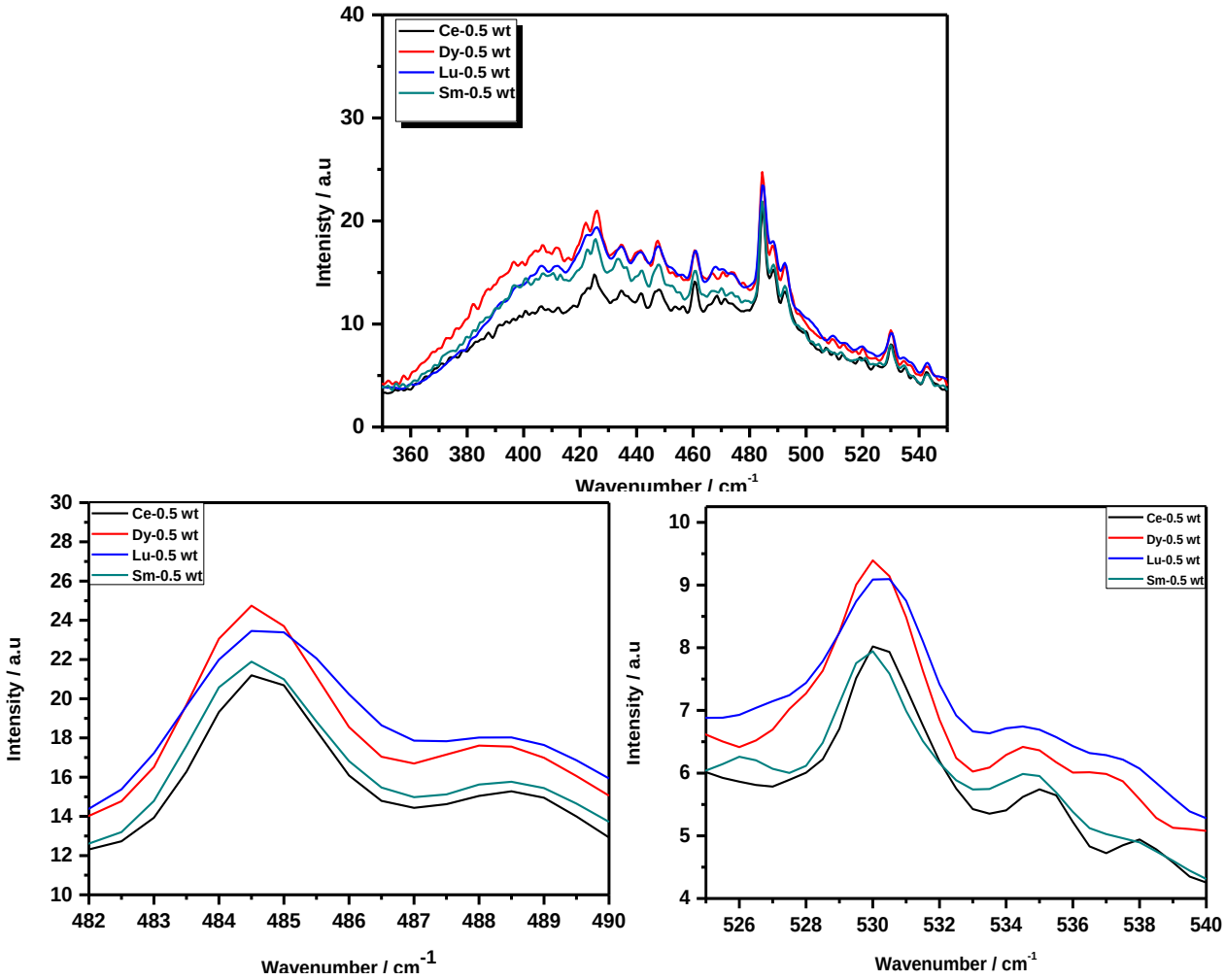

Figure.8: Photoluminescence of Lanthanide doped titania materials

3.8 Photocatalytic experiments

3.8.1 OH, radical generation experiment

Aqueous solution of terephthalic acid is the standard chemical used as sensitive chemical Dosimetry system in radiation chemistry [36]. Dosimetry analysis was employed to estimate the formation of OH radicals from the as-prepared photocatalyst. The as prepared materials were illuminated in terephthalic acid solution (0.1 mM) under visible light 28 W (CFL). **Figure 9(a)** displays the PL spectra of 2-hydrxyterephthalic acid obtained, when terephthalic acid was reacted with Ce doped TiO_2 for 120 min. The product formation was followed monitoring the absorbance at 425 nm. While the light intensity was kept constant, the fluorescence intensity was observed to increase over time. Since the resultant spectra are identical in shape to that of 2-hydroxyterephthalic acid, it was assumed that the product formed as results of Ce doped TiO_2 photocatalysis is caused by the reaction of OH radicals and terephthalic acid. The amount of OH radicals formed by the photocatalyst is directly dependent on the visible light absorbed by the catalyst. Although, terephthalic acid can directly reacts

with photogenerated holes, to give the hydroxyl added product by radical cation, it is known that aromatic compounds are easily oxidised by OH radicals compared with TiO_2 photogenerated hole [37].

Figure 9(b) shows the relative efficiency of different of as-prepared catalysts, in the formation of 2-hydroxyterephthalic acid with time. The obtained results showing Ce doped material with good efficiency relative to others are in agreement with with prediction based on the reduced band gap Ce doped TiO_2 (**figure** 7 (b)). This means that charge recombination in Ce-TiO_2 has retarded, compared with other prepared materials.

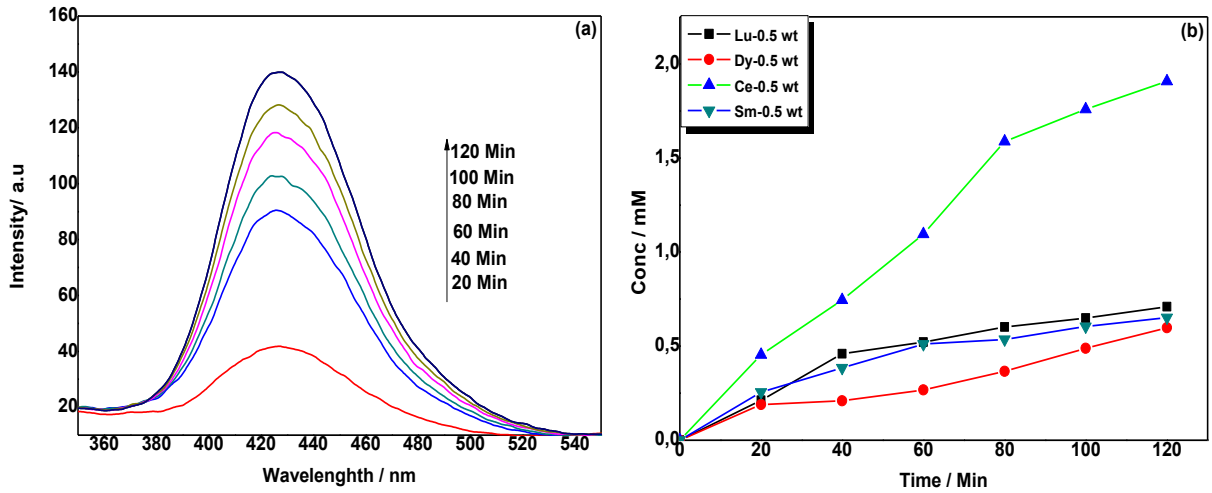

Figure.9: Photoluminescence for the formation of 2-hydroxyterephthalic acid generated by Ce doped TiO_2 in 120 minutes (a) and comparison of product formation using different catalyst (b) OH radical generation by 100 mg/L of catalysts in 200 mL 0.1 mM terephthalic acid solution irradiated with 28 W daylight CFL.

3.8.2 Photocatalytic degradation of caffeine

Caffeine is one of the most commonly consumed pharmaceutical and is frequently detected in wastewater. **Figure 10** displays the photocatalytic degradation of caffeine as a function of time in the presence of different lanthanide doped TiO_2 used as photocatalysts under otherwise similar conditions. It is well known that dopants are required to enhance the space charge region potential of TiO_2 [38,39]. Charge carrier recombination plays a crucial role in TiO_2 photocatalysis, the type of metal dopant used is responsible for the process. In lanthanide doped TiO_2, it has been reported that lanthanide-ions could act as electron scavengers which trap electrons from the CB of TiO_2, this is assumed to occur when lanthanide ions are acting as Lewis acids because they are better than O_2 molecule in trapping CB electrons [40].

From the degradation profiles of caffeine illustrated in **figure** 10, it can be observed that cerium doped TiO_2 exhibits better photocatalytic activity than all other as prepared materials. These results are in agreement with earlier observations, where Ce/TiO_2 showed a greater red-shift compared to other dopants. Red-shift allows the photocatalyst to absorb photons in longer wavelength, thereby increasing the photocatalytic activity of the catalyst. This leads to formation of more hydroxyl radicals for degradation of caffeine in presence of visible light.

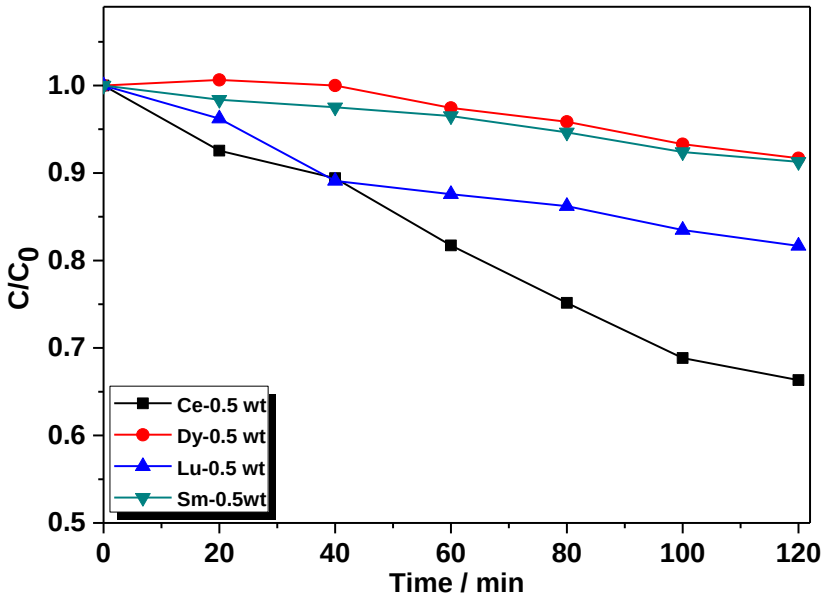

Figure.10: Photocatalytic degradation curves of caffeine over 120 min of irradiation with visible light

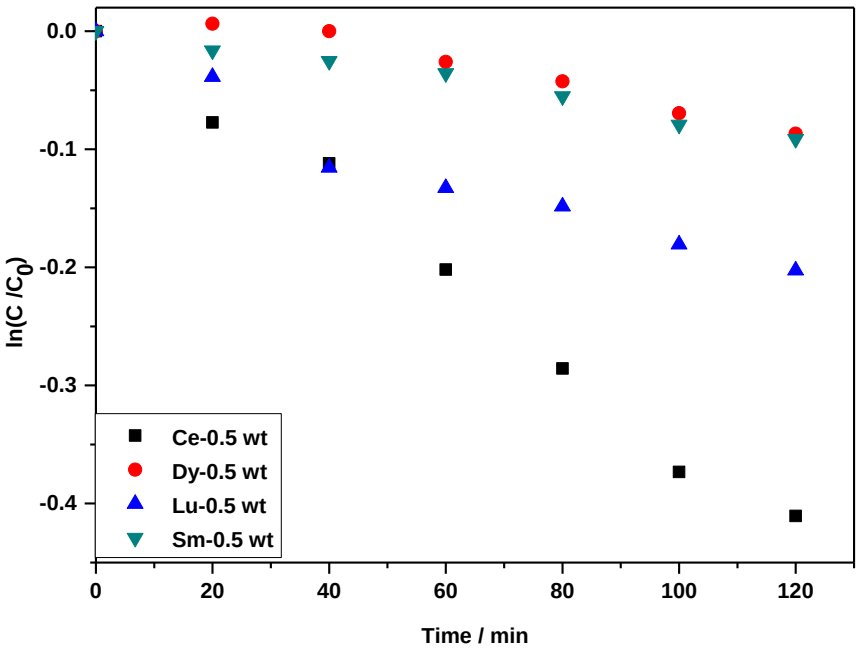

Figure.11: First order degradation of caffeine curves

The kinetic data was analysed the ln [caffeine] versus time plots gave good straight lines as displayed in **figure**.11 suggesting the degradation of caffeine follow a pseudo first-order kinetics. The rate constants and R^2 values are shown in **table 2**. Cerium doped catalyst had the highest rate constant of 3.0×10^{-3} min^{-1}. The photogenerated holes play a vital role in degradation process, when charge separation is preserved, the electron and hole migrate to the photocatalyst surface where they participate in redox reactions with the adsorbed molecule. The respective rate constants and half-lives for the four photocatalysts were evaluated (**figure. 10 and 11**) and results are summarised in Table 2.

Table.2: Degradation kinetics of caffeine

Sample	Rate constant (k) / min × 10^{-3}	Half-life / min	R^2
Ce-TiO_2	3.00	231.05	0.9896
Dy-TiO_2	0.80	866.43	0.9244
Lu-TiO_2	1.70	407.73	0.9412
Sm-TiO_2	0.80	866.43	0.9804

3.8.3 Identification of intermediates and products

The intermediates and products were analyzed with Shimadzu, LC-MS TOF mode. Analysis was done over the period of 15 minutes with the retention time between 3 to 4 minutes. Analysis was done by sampling after 20 minutes starting from pure caffeine. From the degradation, one intermediate [*N*-1,3,6-trimethyl-2,4-dioxo-1,2,3,4-tetrahydropyrimidin-5-yl)formamide] (TDTF) and two products (6-amino-1,3-dimethyl-2,4-dioxo-1,2,3,4-tetradropymidin-5-ly)(methyl)carbamic acid (ATCA) and *N*-methyl-*N*-(methylcarbomoyl)-2-oxoacetamide (MMO) were identified (Scheme 2) after 120 minutes of irradiation and they eluted in the retention time 3.47 minutes. All the identified products are shown in the supporting information (**S1**).

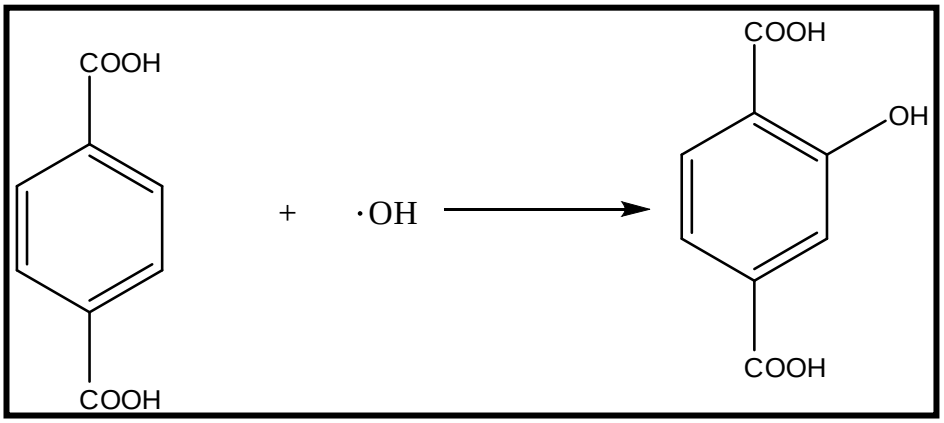

Scheme 1: Formation of 2-hydroxyterephthalic acid

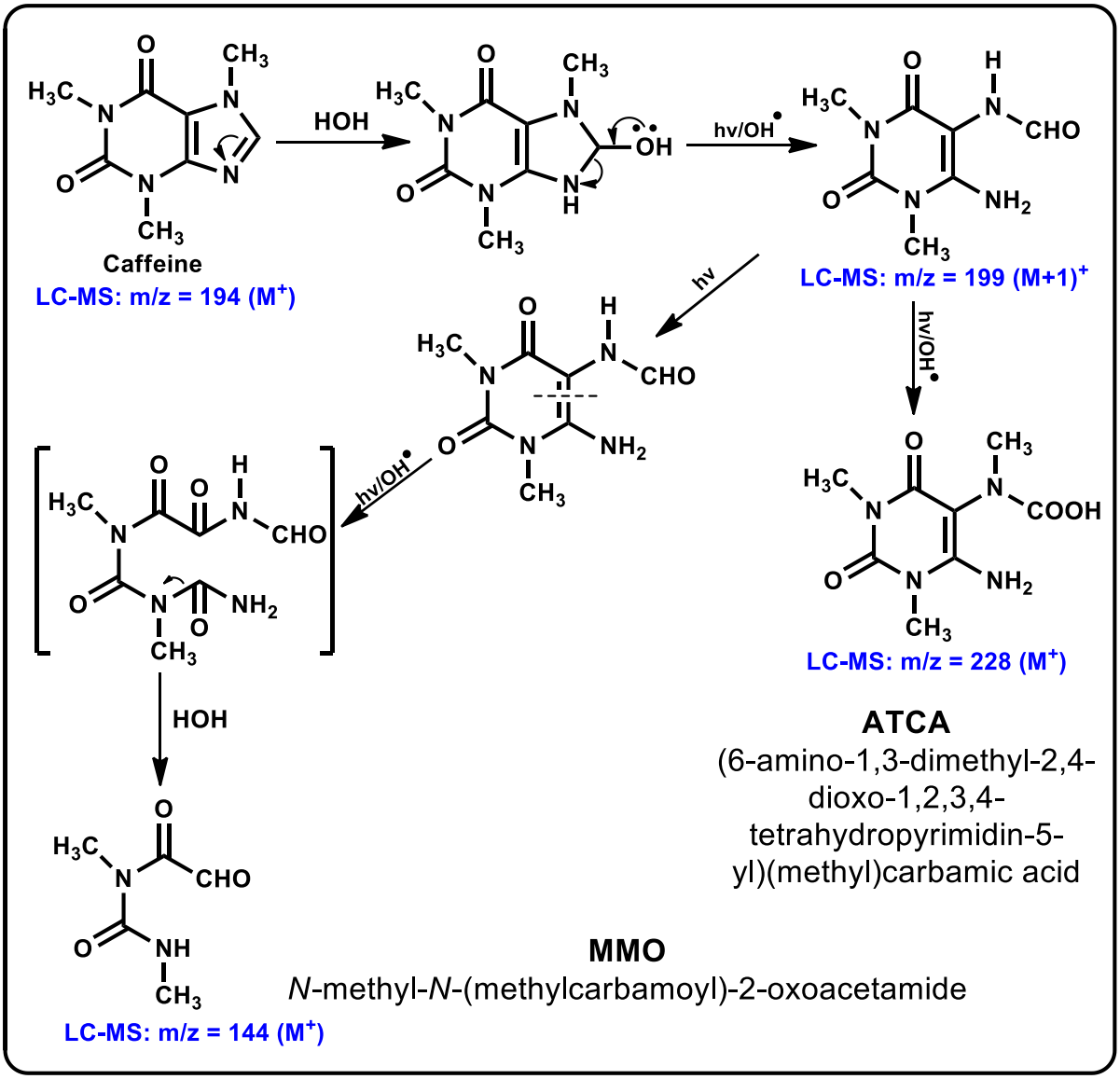

Scheme 2: Possible reaction mechanism

4 Conclusion

Four lanthanide doped TiO_2 mesoporous materials were synthesised and were characterised using different techniques. From the XRD pattern that was obtained it was observed that all the as prepared materials were polycrystalline in nature. All the as prepared materials showed a redshift, towards longer wavelength and their photo-activity was assessed under visible light. Hydroxyl radicals have been generated from each of the as prepared materials. Ce doped TiO_2 showed far better activity than the rest of the catalysts. High photoactivity of the catalysts were attributed to the presence of lanthanides to the ability to

generate ions that are electron scavengers thereby enhancing photo-degradation of caffeine under visible light.

Acknowledgement

The authors are thankful to the National Research Foundation (NRF) of South Africa, and University of KwaZulu-Natal, Durban, for financial support and research facilities.

References

[1] Y. He, N.B. Sutton, H.H.H. Rijnaarts, A.A.M. Langenhoff, Degradation of pharmaceuticals in wastewater using immobilized TiO_2 photocatalysis under simulated solar irradiation, Applied Catalysis B: Environmental, 182 (2016) 132-141.

[2] J. Nawrocki, B. Kasprzyk-Hordern, The efficiency and mechanisms of catalytic ozonation, Applied Catalysis B: Environmental, 99 (2010) 27-42.

[3] A.G. Trovó, T.F.S. Silva, O. Gomes Jr, A.E.H. Machado, W.B. Neto, P.S. Muller Jr, D. Daniel, Degradation of caffeine by photo-Fenton process: Optimization of treatment conditions using experimental design, Chemosphere, 90 (2013) 170-175.

[4] R. Rosal, A. Rodríguez, J.A. Perdigón-Melón, A. Petre, E. García-Calvo, M.J. Gómez, A. Agüera, A.R. Fernández-Alba, Degradation of caffeine and identification of the transformation products generated by ozonation, Chemosphere, 74 (2009) 825-831.

[5] R. Broséus, S. Vincent, K. Aboulfadl, A. Daneshvar, S. Sauvé, B. Barbeau, M. Prévost, Ozone oxidation of pharmaceuticals, endocrine disruptors and pesticides during drinking water treatment, Water Research, 43 (2009) 4707-4717.

[6] M. Huerta-Fontela, M.T. Galceran, F. Ventura, Occurrence and removal of pharmaceuticals and hormones through drinking water treatment, Water Research, 45 (2011) 1432-1442.

[7] A. Zarubica, M. Vasić, M.D. Antonijevic, M. Ranđelović, M. Momčilović, J. Krstić, J. Nedeljković, Design and photocatalytic ability of ordered mesoporous TiO_2 thin films, Materials Research Bulletin, 57 (2014) 146-151.

[8] J. Hensel, G. Wang, Y. Li, J.Z. Zhang, Nano Lett., 10 (2010) 478-483.

[9] S. Naraginti, T.V.L. Thejaswini, D. Prabhakaran, A. Sivakumar, V.S.V. Satyanarayana, A.S. Arun Prasad, Enhanced photo-catalytic activity of Sr and Ag co-doped TiO_2 nanoparticles for the degradation of Direct Green-6 and Reactive Blue-160 under UV & visible light, Spectrochimica Acta, Part A, 149 (2015) 571-579.

[10] E.O. Oseghe, P.G. Ndungu, S.B. Jonnalagadda, Photocatalytic degradation of 4-chloro-2-methylphenoxyacetic acid using W-doped TiO_2, The Journal of Photochemistry and Photobiology A, 312 (2015) 96-106.

[11] E.O. Oseghe, P.G. Ndungu, S.B. Jonnalagadda, Synthesis of mesoporous Mn/TiO_2 nanocomposites and investigating the photocatalytic properties in aqueous systems, Environmental Science and Pollution Research, 22 (2015) 211-222.

[12] J. Reszczynska, T. Grzyb, J.W. Sobczak, W. Lisowski, M. Gazda, B. Ohtani, A. Zaleska, Visible light activity of rare earth metal doped (Er3+, Yb3+ or Er3+/Yb3+) titania photocatalysts, Applied Catalysis B Environmental, 163 (2015) 40-49.

[13] Q. Xiao, Z. Si, Z. Yu, G. Qiu, Sol-gel auto-combustion synthesis of samarium-doped TiO_2 nanoparticles and their photocatalytic activity under visible light irradiation, Materials Science Engineering, B, 137 (2007) 189-194.

[14] S. Maddila, V.D.B.C. Dasireddy, S.B. Jonnalagadda, Ce-V loaded metal oxides as catalysts for dechlorination of chloronitrophenol by ozone, Applied Catalysis B: Environmental, 150–151 (2014) 305-314.

[15] S. Maddila, V.D.B.C. Dasireddy, S.B. Jonnalagadda, Dechlorination of tetrachloro-o-benzoquinone by ozonation catalyzed by cesium loaded metal oxides, Applied Catalysis B: Environmental, 138–139 (2013) 149-160.

[16] S. Kelly, F.H. Pollak, M. Tomkiewicz, Raman Spectroscopy as a Morphological Probe for TiO_2 Aerogels, The Journal of Physical Chemistry B, 101 (1997) 2730-2734.

[17] A. Gajovic, M. Stubicar, M. Ivanda, K. Furic, Raman spectroscopy of ball-milled TiO_2, Journal of Molecular Structure, 563-564 (2001) 315-320.

[18] V. Jabbari, M. Hamadanian, M. Shamshiri, D. Villagran, Band gap and Schottky barrier engineered photocatalyst with promising solar light activity for water remediation, RSC Advances, 6 (2016) 15678-15685.

[19] C. Xiang, M. Li, M. Zhi, A. Manivannan, N. Wu, Reduced graphene oxide/titanium dioxide composites for supercapacitor electrodes: shape and coupling effects, Journal of Materials Chemistry, 22 (2012) 19161-19167.

[20] B. Choudhury, A. Choudhury, Local structure modification and phase transformation of TiO_2 nanoparticles initiated by oxygen defects, grain size, and annealing temperature, International Nano Letters, 3 (2013) 1-9.

[21] A.K. Tripathi, M.K. Singh, M.C. Mathpal, S.K. Mishra, A. Agarwal, Study of structural transformation in TiO_2 nanoparticles and its optical properties, J. Alloys Compd., 549 (2013) 114-120.

[22] Y. Zhao, C. Li, X. Liu, F. Gu, H. Jiang, W. Shao, L. Zhang, Y. He, Synthesis and optical properties of TiO_2 nanoparticles, Mater. Lett., 61 (2007) 79-83.

[23] J.T. Park, J.H. Koh, J.A. Seo, J.H. Kim, Formation of mesoporous TiO_2 with large surface areas, interconnectivity and hierarchical pores for dye-sensitized solar cells, Journal of Materials Chemistry, 21 (2011) 17872-17880.

[24] E.O. Oseghe, P.G. Ndungu, S.B. Jonnalagadda, Photocatalytic degradation of 4-chloro-2-methylphenoxyacetic acid using W-doped TiO_2, Journal of Photochemistry and Photobiology A: Chemistry, 312 (2015) 96-106.

[25] C.F.B. Dias, J.C. Araujo-Chaves, K.C.U. Mugnol, F.J. Trindade, O.L. Alves, A.C.F. Caires, S. Brochsztain, F.N. Crespilho, J.R. Matos, O.R. Nascimento, I.L. Nantes, Photo-induced electron transfer in supramolecular materials of titania nanostructures and cytochrome c, RSC Advances, 2 (2012) 7417-7426.

[26] N. Yan, Z. Zhu, J. Zhang, Z. Zhao, Q. Liu, Preparation and properties of Ce-doped TiO_2 photocatalyst, Materials Research Bulletin, 47 (2012) 1869-1873.

[27] Z.-L. Shi, C. Du, S.-H. Yao, Preparation and photocatalytic activity of cerium doped anatase titanium dioxide coated magnetite composite, Journal of the Taiwan Institute of Chemical Engineers., 42 (2011) 652-657.

[28] X. Wang, Z. Feng, J. Shi, G. Jia, S. Shen, J. Zhou, C. Li, Trap states and carrier dynamics of TiO_2 studied by photoluminescence spectroscopy under weak excitation condition, The Journal of Physical Chemistry, 12 (2010) 7083-7090.

[29] J. Yan, G. Wu, N. Guan, L. Li, Z. Li, X. Cao, Understanding the effect of surface/bulk defects on the photocatalytic activity of TiO_2: anatase versus rutile, Physical Chemistry Chemical Physics, 15 (2013) 10978-10988.

[30] M.M. Khan, S.A. Ansari, D. Pradhan, M.O. Ansari, D.H. Han, J. Lee, M.H. Cho, Band gap engineered TiO_2 nanoparticles for visible light induced photoelectrochemical and photocatalytic studies, Journal of Materials Chemistry A, 2 (2014) 637-644.

[31] J.S. Roy, T. Pal Majumder, R. Dabrowski, Photoluminescence behavior of TiO_2 nanoparticles doped with liquid crystals, Journal of Molecular Structure, 1098 (2015) 351-354.

[32] M. Rajabi, S. Shogh, A. Iraji zad, Defect study of TiO_2 nanorods grown by a hydrothermal method through photoluminescence spectroscopy, Journal of Luminescence, 157 (2015) 235-242.

[33] L. Kernazhitsky, V. Shymanovska, T. Gavrilko, V. Naumov, L. Fedorenko, V. Kshnyakin, J. Baran, Photoluminescence of Cr-doped TiO_2 induced by intense UV laser excitation, Journal of Luminescence, 166 (2015) 253-258.

[34] L. Hu, H. Song, G. Pan, B. Yan, R. Qin, Q. Dai, L. Fan, S. Li, X. Bai, Photoluminescence properties of samarium-doped TiO_2 semiconductor nanocrystalline powders, Journal of Luminescence, 127 (2007) 371-376.

[35] H. Nakajima, T. Mori, Q. Shen, T. Toyoda, Photoluminescence study of mixtures of anatase and rutile TiO_2 nanoparticles: Influence of charge transfer between the nanoparticles on their photoluminescence excitation bands, Chemical Physics Letters, 409 (2005) 81-84.

[36] C.R.S. Matos, M.J. Xavier, L.S. Barreto, N.B. Costa, I.F. Gimenez, Principal Component Analysis of X-ray Diffraction Patterns To Yield Morphological Classification of Brucite Particles, Analytical Chemistry, 79 (2007) 2091-2095.

[37] M. Myilsamy, V. Murugesan, M. Mahalakshmi, Indium and cerium co-doped mesoporous TiO_2 nanocomposites with enhanced visible light photocatalytic activity, Applied Catalysis A: General, 492 (2015) 212-222.

[38] F.B. Li, X.Z. Li, M.F. Hou, K.W. Cheah, W.C.H. Choy, Enhanced photocatalytic activity of Ce^{3+}-TiO_2 for 2-mercaptobenzothiazole degradation in aqueous suspension for odour control, Applied Catalysis A, 285 (2005) 181-189.

[39] K.E. Karakitsou, X.E. Verykios, Effects of altervalent cation doping of titania on its performance as a photocatalyst for water cleavage, The Journal of Physical Chemistry, 97 (1993) 1184-1189.

[40] A.M.T. Silva, C.G. Silva, G. Dražić, J.L. Faria, Ce-doped TiO_2 for photocatalytic degradation of chlorophenol, Catalysis Today, 144 (2009) 13-18.

CHAPTER FIVE

Conclusions:

The aim of this work was to synthesise mixed metal oxides, with good activity to act as recyclable heterogeneous catalysts and/or photocatalysts in advanced oxidation processes, for degradation of the selected organic substrate, caffeine in aqueous systems, and to fully characterise the catalyst materials and oxidative degradation products.

The use of external oxidant source, such as ozone in wastewater treatment is one of the vastly used methods in advanced oxidation processes. In this work, catalytic ozonation was tested for the degradation of caffeine using Ce doped on titania as catalyst. In the experiments, three different oxidation methods were used, which were (i) the use ozone only and (ii) the combination of both (ozone and catalyst). This study showed that ozone is a powerful oxidant, which in water produce hydroxy radicals that enhance the degradation of caffeine. The ozone concentration plays a vital role in production of hydroxy radicals and degradation efficiency is directly proportional to the ozone concentration. Another finding was the effect of water pH on catalytic ozonation of caffeine. The studies on catalysed ozonation of substrate at different pH ranges showed optimum rate at its point of zero charge (pH_{PZC}), 6.2 of caffeine. The lower degradation of caffeine at higher pH (10) is justified by it. The caffeine degradation products were identified and plausible mechanism was elucidated.

Synthesis of mesoporous TiO_2 nanoparticles Ce/TiO_2 was achieved using non-ionic surfactant, using different ceria loadings (0.0, 0.1, 0.5 and 1.0 wt%) and their efficiency was evaluated in degradation of caffeine under visible light without the use of external oxidants. Based on the characterisation data of the catalyst materials, it was seen that the BET surface area increases with an increase in loading. All materials were found to be polycrystalline. 0.5wt% Ce/TiO_2 showed optimum caffeine degradation efficiency, compared to other materials. SEM and TEM micrographs of the prepared material showed that all the catalysts had aggregated particles, which was caused by agglomeration. All Ce/TiO_2 catalysts showed a huge redshift with a reduced energy band gap when compared to bare TiO_2.

A comparison study was done to evaluate four different lanthanide metals doped on TiO_2, (Ce, Sm, Dy, and Lu) with the same metal loading (0.5 wt%). Characterisation showed that all materials were polycrystalline using XRD. Ce/TiO_2 had the lowest band energy and highest BET surface are compared to other materials. Ce/TiO_2 showed better activity under visible light this was observed using Dosimetry analysis for the quantification of OH radicals

generated by each metal ion dopant. The photocatalytic activity of the as prepared materials was assessed by studying degradation of caffeine in aqueous system. Probable mechanism consistent with reaction product isidentification is proposed.

Recommendations:

The research outcomes from this work have shown that there are areas of the study that needs to be improved for the future work.

1. One of the areas to be investigated is the finding an improved route for synthesis of uniform TiO_2 nanoparticles. Although, sol-gel method is one of the mostly used method, nanoparticles formed have irregular shapes due agglomerates that are formed during synthesis, which may hinder the catalyst activity. The investigations in to the use of different pH conditions to synthesize the catalyst during the hydrolysis stage, might lead to change the pH_{PZC} of the catalyst, which will allow it to be applicable in a range of pH conditions
2. The use of more instrumental techniques to study of the catalyst such as X-ray photoelectron spectroscopy (XPS) which will tell us about the state of dopant inside the crystal lattice of the material.
3. Developing and applying models that would identify independent or synergistic properties of a photo-catalyst responsible for its performance. The model will help understand and compare the photocatalytic efficiency of different sets of catalysts.
4. Application of the photocatalytic experimental setup in this study to different classes of organic pollutants is important. This will help assert the efficiency of photo-catalysts across various classes of organic pollutants.